THE CONSERVED PCH2 GENE ACTS TO REGULATE DNA DOUBLE-STRAND BREAK REPAIR IN SACCHAROMYCES CEREVISIAE MEIOSIS

by Sarah Elizabeth Zanders

THE CONSERVED *PCH2* GENE ACTS TO REGULATE DNA DOUBLE-STRAND BREAK REPAIR IN *SACCHAROMYCES CEREVISIAE* MEIOSIS

A Dissertation

Presented to the Faculty of the Graduate School

of Cornell University

In Partial Fulfillment of the Requirements for the Degree of

Doctor of Philosophy

by

Sarah Elizabeth Zanders

August 2010

THE CONSERVED *PCH2* GENE ACTS TO REGULATE DNA DOUBLE-STRAND BREAK REPAIR IN *SACCHAROMYCES CEREVISIAE* MEIOSIS

Sarah Elizabeth Zanders, Ph. D.

Cornell University 2010

In the first chromosome division of meiosis (MI), homologous chromosome pairs are separated, allowing for the production of fertile haploid gametes from diploid progenitor cells. Proper MI segregation of homologous chromosomes in most eukaryotic organisms requires that at least one programmed DNA double-strand break (DSB) per pair of homologous chromosomes is repaired as a crossover. These crossover events tether homologous chromosomes together, which allows for the generation of a bipolar spindle to separate the homologous chromosomes. The widely conserved *PCH2* gene of *Saccharomyces cerevisiae* is involved in regulating the repair of meiotic DSBs. First, Pch2 promotes the use of the homologous chromosome, instead of the sister chromatid, as a DSB repair template. Second, Pch2 regulates the fate of DSBs that are repaired using the homologous chromosome by limiting gene conversion and by promoting crossover interference. *pch2*Δ mutants repair a greater proportion of meiotic DSBs using the sister chromatid than wild-type cells, but the majority of DSBs are still repaired using the homologous chromosome. The DSBs that are repaired using the homologous chromosome in *pch2*Δ mutants have a higher likelihood to be associated with gene conversion events and to be repaired as crossovers, as opposed to noncrossovers. The distribution of crossover events observed in *pch2*Δ also demonstrates a significant reduction in crossover interference in these mutants. I hypothesize that a single Pch2-dependent role in meiotic

chromosome axis organization inhibits intersister DSB repair, limits gene conversion tract length, and promotes the interference regulation of interhomolog DSB repair.

BIOGRAPHICAL SKETCH

Sarah Elizabeth Zanders is the daughter of Darrold and Suzanne Nord. Sarah grew up the youngest of five children in the small town of Glenwood, located in the beautiful loess hills of southwest Iowa. Sarah graduated from Glenwood High School in 2001 and then moved to the eastern side of the state to attend the University of Iowa. At Iowa, Sarah majored in Biology and was fortunate to be introduced to both genetics and the study of meiosis by her mentor Dr. Robert E. Malone. After graduating from Iowa with honors and highest distinction in 2005, Sarah married her high school sweetheart Patrick and came to Cornell University to pursue a Ph.D. in Genetics. Sarah joined the lab of Dr. Eric Alani where she studied DNA mutagenesis and meiotic recombination. Now that Sarah has completed her dissertation, she plans to continue and expand her studies of meiosis in the lab of Dr. Harmit Malik at the Fred Hutchinson Cancer Research Center.

To Patrick

ACKNOWLEDGMENTS

I want to first thank my advisor Eric Alani. I have learned a lot from Eric and greatly appreciate his guidance and support. I especially want to thank Eric for challenging my thinking and giving me the freedom to both make mistakes and try out new ideas. Also, I want to thank Eric for the significant amount of cloning he did to assist my projects in the lab. I would also like to thank my committee members Tom Fox and Dan Barbash for their support throughout my time here.

I was fortunate to be a part of two collaborations during my time at Cornell. First, I would like to thank Jennifer Wanat, Megan Sonntag, Keun Kim, Romain Kozul, Beth Weiner, and Nancy Kleckner for letting me join in on their studies of the role of *CSM4* in meiosis. Second, I would like to thank Ann Demogines, Maria Ma, Arindam RoyChoudury, Ryan Hernandez, Brandon Barker, Zhenglong Gu, and Carlos Bustamante for their efforts on our long, drawn out project identifying a novel mutational hotspot.

I am also grateful for the enjoyable environment in the Alani lab created by all of its members throughout my years here. Specifically, I would like to thank Jennifer Surtees, Ann Demogines, Amy Lyndaker, Jen Wanat, and Megan Sonntag.

I want to give a special thanks to my classmates and Heather Flores and Maho Shibata, whose friendship greatly enriched my years in Ithaca.

Finally, I want to thank my parents, siblings and husband for their love, support, and unwavering confidence in my abilities.

TABLE OF CONTENTS

LIST OF FIGURES

LIST OF TABLES

CHAPTER 1

Introduction to meiosis and meiotic recombination mechanisms

Meiosis is a specialized form of cell division that generates haploid gametes from diploid progenitor cells, thus permitting eukaryotes to reproduce sexually while maintaining a stable genome size [1]. Meiosis consists of one round of DNA replication, followed by two rounds of chromosome segregation. In the first meiotic division (MI) homologous chromosome pairs are separated or disjoined. Because the reduction in cell ploidy from diploid to haploid occurs at this division, it is also known as the "reductional division." The second meiotic division (MII) is similar to mitosis because it is an equational chromosome division in which sister chromatids are disjoined [1]. Chromosome missegregation (nondisjunction) in either MI or MII can lead to the production of aneuploid gametes which can lead to infertility or conditions like Down syndrome and Edwards syndrome in humans [2].

An elaborate series of meiosis-specific events occur prior to the MI division to ensure reductional chromosome segregation. For proper MI disjunction to occur, the spindle apparatus must attach to the individual chromosomes of a homologous pair and pull them towards opposite spindle poles. This is a major challenge because, with two centromeres per replicated homolog, there are numerous possible spindle-chromosome orientations. Four meiosis-specific processes help promote MI reductional division in budding yeast (reviewed in [3]). First, homologous chromosomes are physically tethered together at the sites of genetic exchanges between chromosome arms, or crossovers (COs). Crossovers serve to hold homologs together because of sister chromatid cohesion centromere-distal from the crossover site. Second, a single kinetochore assembles at the centromeres of sister chromatid pairs to ensure the sisters are disjoined from their homolog as a unit at anaphase of MI. Third, sister chromatid cohesion is lost in a step-wise fashion. In anaphase of MI, most sister chromatid cohesion is lost to allow homologs joined by COs to separate, but cohesion is protected around the centromeres to keep sister chromatids joined until

anaphase of MII [3]. The spindle checkpoint apparatus can sense that homologous chromosome pairs are attached to opposite poles when there is tension resisting pole-directed forces ([4]; Figure 1-1). Homologous chromosome pairs lacking crossover connections cannot generate tension across the spindle apparatus and therefore often fail to segregate properly at MI [1]. Chromosome nondisjunction can also result if crossovers are present, but not properly placed on chromosomes and/or if sister chromatid cohesion is prematurely disrupted [5-8]. Finally, an inefficient last-resort backup system (sometimes called distributive pairing) involving recombination-independent centromere pairing can promote MI disjunction of chromosomes that fail to receive a crossover [9-12].

Models of meiotic double-strand break repair. Meiotic recombination occurs in prophase I and in budding yeast begins with the formation of ~170 programmed DNA double-stranded breaks (DSBs) by a group of ten proteins [1, 13, 14]. Spo11 is thought to be the catalytic component of this complex because it is covalently attached to the DNA ends during break formation [15]. After DSB formation, the short oligo-nucleotide with attached Spo11 is removed by Mre11-Rad50-Xrs2 and Sae2 and the 5' of the DNA ends are resected by Exo1 to expose a 3' single-stranded DNA overhang with an average length of around 800 nucleotides [16, 17]. This single-stranded DNA can then invade a homologous sequence on either the sister chromatid (~10-30% of breaks) or the homologous chromosome (~70-90%) and be repaired by homologous recombination (see Chapter 3; [18-21]). Both intersister and interhomolog DSB repair events can be resolved as crossovers or noncrossovers in which chromosome/chromatid arms are not exchanged. All types of DSB repair events can also be associated with gene conversion events in which the allele at the DSB site is changed due to copying information from the repair template. Because intersister events are in the minority, unless otherwise specified, crossover,

Figure 1-1. Interhomolog crossovers and sister chromatid cohesion contribute to proper chromosome segregation in meiosis.

A model of meiosis depicting one pair (red and blue lines) of homologous chromosomes is shown [3]. The centromeres are represented by the circles. After undergoing pre-meiotic DNA synthesis, the two sister chromatids comprising each homologous chromosome are held together throughout their lengths by sister chromatid cohesion, represented here by the light horizontal lines between chromatids. Crossovers serve to tether homologs together prior to the MI division because of the crossover-distal sister chromatid cohesion. When the individual chromosomes of a homologous pair are attached to MI spindles from opposite poles, pole directed forces will be resisted, generating tension. This tension signals proper spindle attachment. Sister chromatid cohesion is then removed along the chromosome arms and homologs are separated at MI. The centromeric sister chromatid cohesion is protected until anaphase of MII. In budding yeast, the four meiotic products are packaged together in a tetrad.

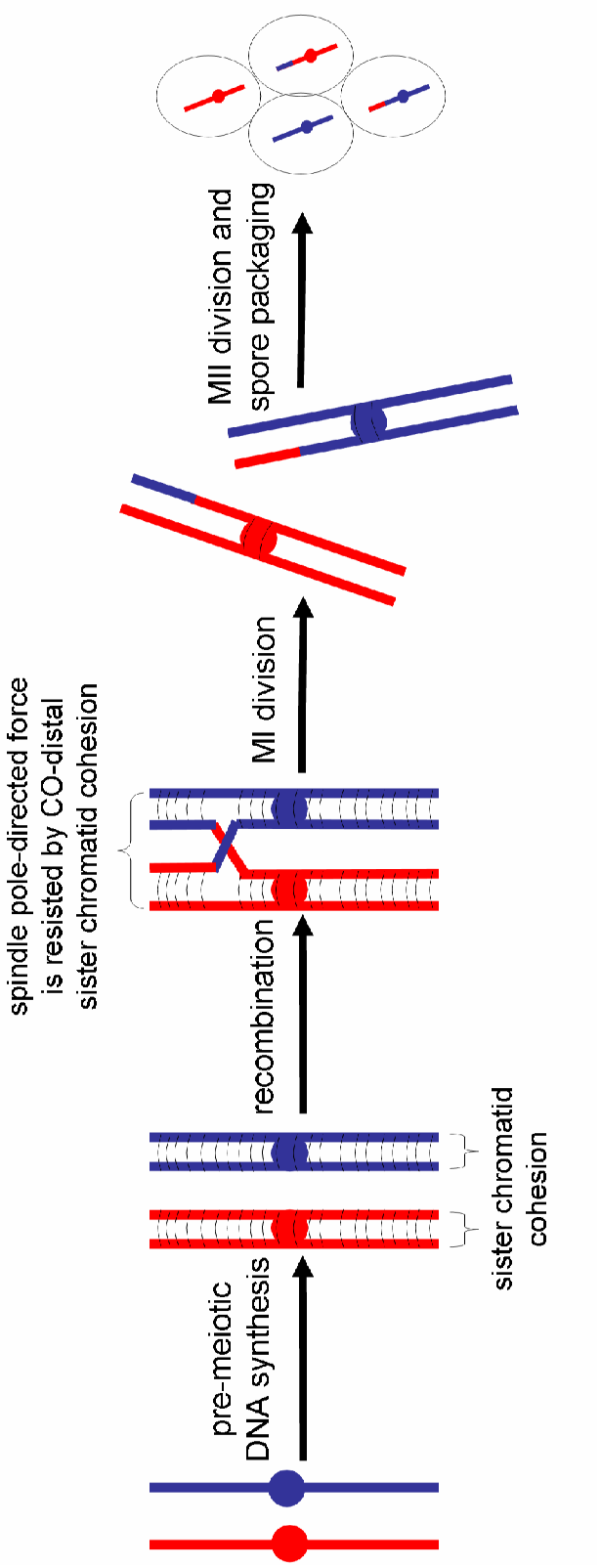
pre-meiotic
DNA synthesis
sister chromatid
cohesion
recombination
spindle pole-directed force
is resisted by CO-distal
sister chromatid cohesion
MI division
MII division and
spore packaging

noncrossover, and gene conversions usually refer to products of interhomolog DSB repair products.

The meiotic DSB repair utilizing the sister chromatid as a template is thought to proceed via a homologous recombination pathway similar to the one which repairs DSBs incurred during vegetative growth [22]. This repair pathway, which utilizes the Rad51-Rad54 recombinase to mediate intersister strand exchange, does not promote MI disjunction, and is therefore actively inhibited in meiosis ([18, 20, 21, 23-29]; see Chapter 3).

The ~90 interhomolog crossovers (COs) per meiosis are formed via two main pathways in budding yeast ([30-34]; Figure 1-2). The crossovers formed by the first pathway (Figure 1-2B), are said to be "interfering" because they display crossover interference; the COs are more uniformly spaced than if placed at random ([34]; see Chapter 2). In this pathway, the Rad51 loads the Dmc1-Rdh54 complex onto the exposed 3' overhangs of DSBs which then promote invasion of the single-stranded DNA into the homologous chromosome to create what is known as a D-loop (Figure 1-2A, B; [28, 29, 35-37]. These nascent D-loops can mature into stable structures known as single-end invasions (SEIs) (Figure 1-2B; [38]). SEIs are thought to be stabilized by the Msh4-5 complex, which counteracts the SEI disruptive function of the Sgs1helicase [39]. SEIs mature into double Holiday junctions (dHJs) [38, 40, 41]. Although a dHJ could theoretically be resolved to form a CO or NCO, evidence suggests they are resolved primarily into crossovers ([38, 40-42]; Figure 1-2B).

The COs formed via the second major pathway (Figure 1-2D) are also thought to begin with Dmc1-Rdh54 mediated strand exchange, but D-loops do not mature into SEIs and dHJs (Figure 1-2A, D). Little is known about the intermediates that form in this latter pathway, but the prevalent model posits that single or half Holiday junctions form and are resolved by the Mms4-Mus81 nuclease pair ([32, 33, 43, 44]; Figure 1-

Figure 1-2. Models for different interhomolog DSB repair pathways.

Two of the four homologous chromatids present in meiotic prophase I are shown. Each chromatid is composed of two lines which represent the Watson and Crick strands of the DNA. (A) The red chromatid incurs a DSB which is processed to reveal single-stranded 3' ends. One of these ends then invades the homologous chromosome. Following the nascent strand invasion event, the DSB repair pathways are thought to branch apart. The break can be repaired using the "interfering" CO pathway (B), the NCO pathway (C), or the "non-interfereing CO pathway (D). The scissors represent sites of endonuclease DNA cutting. See text for additional details.

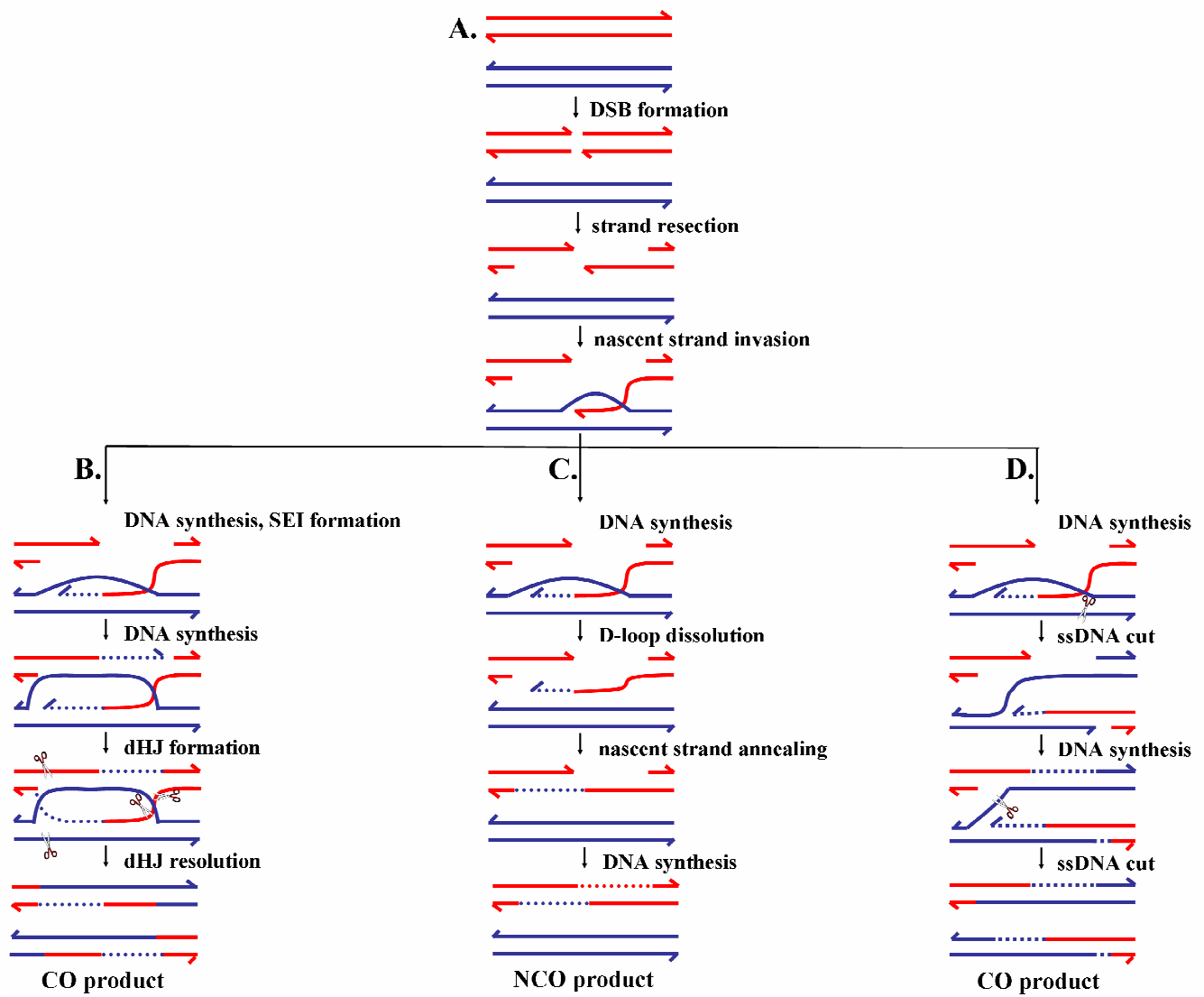
A.
DSB formation
strand resection
nascent strand invasion
B.
DNA synthesis, SEI formation
DNA synthesis
dHJ formation
dHJ resolution
CO product
C.
DNA synthesis
D-loop dissolution
nascent strand anncaling
DNA synthesis
NCO product
D.
DNA synthesis
ssDNA cut
DNA synthesis
ssDNA cut
CO product

2D). The crossovers formed in this pathway are said to be "non-interfering" because the do not display crossover interference [34].

In all eukaryotes where meiotic DSB and crossover levels have been analyzed, there is an excess of DSBs over the number of crossovers formed [13, 14, 45-47]. Some of these extra breaks are repaired using the homolog, but result in noncrossover formation. Noncrossovers are thought to form via a synthesis-dependent strand annealing pathway (SDSA) [48]. Like CO formation, SDSA begins with a Dmc1-Rdh54 catalyzed strand invasion event (Figure 1-2A, C). The 3' end of the invading strand is then used to prime DNA synthesis using the DNA from the homolog as a template. After this DNA synthesis extends beyond the site of the initial break formation, the D-loop can be dissolved and the invading strand can bridge the DSB site by annealing back to the broken chromosome ([48]; Figure 1-2C). The mechanisms regulating whether a meiotic DSB is repaired as a CO or NCO are discussed in Chapter 2.

Meiotic recombination occurs within a highly complex and dynamic chromosomal context. Meiotic prophase is subdivided into five stages (leptotene, zygotene, pachytene, diplotene, and diakinesis) based on the progressive condensation of chromosomes and the changing morphology of the zipper-like structure linking homologous chromosomes known as the synaptonemal complex (SC; Figure 1-3; Reviewed in [49]). In leptotene, the Hop1 and Red1 proteins load along each pair of sister chromatids to form what are called "axial elements" [50-53]. Mature SC formation begins in zygotene when the Zip1-containing SC central element connects the axial elements, which are now termed "lateral elements" [54-56]. The first crossover-specific recombination intermediates, SEIs, are also first detectable in zygotene. SC formation is completed by the pachytene and all recombination intermediates are resolved by the end of this stage. The SC disassembles in diplotene

Figure 1-3. Meiotic recombination occurs in a complex and dynamic chromosomal context.

The events of meiotic prophase from leptotene to diplotene are shown in temporal order from left to right. The top images depict the telomere led chromosome movements. A grey yeast cell with a blue nucleus, two pink chromosomes, and green telomeres is shown. The telomeres attach to the nuclear envelope, transiently cluster near the spindle-pole body at the leptotene-zygotene transition, and then move rapidly and dramatically throughout pachytene. The DNA processing steps of the "interfering crossover" repair pathway are shown in the center of the image. The bottom images are typical mouse meiocyte spreads from the given stages to illustrate the steps of synaptonemal complex construction. See text for details. Figure kindly provided by Jennifer Wanat.

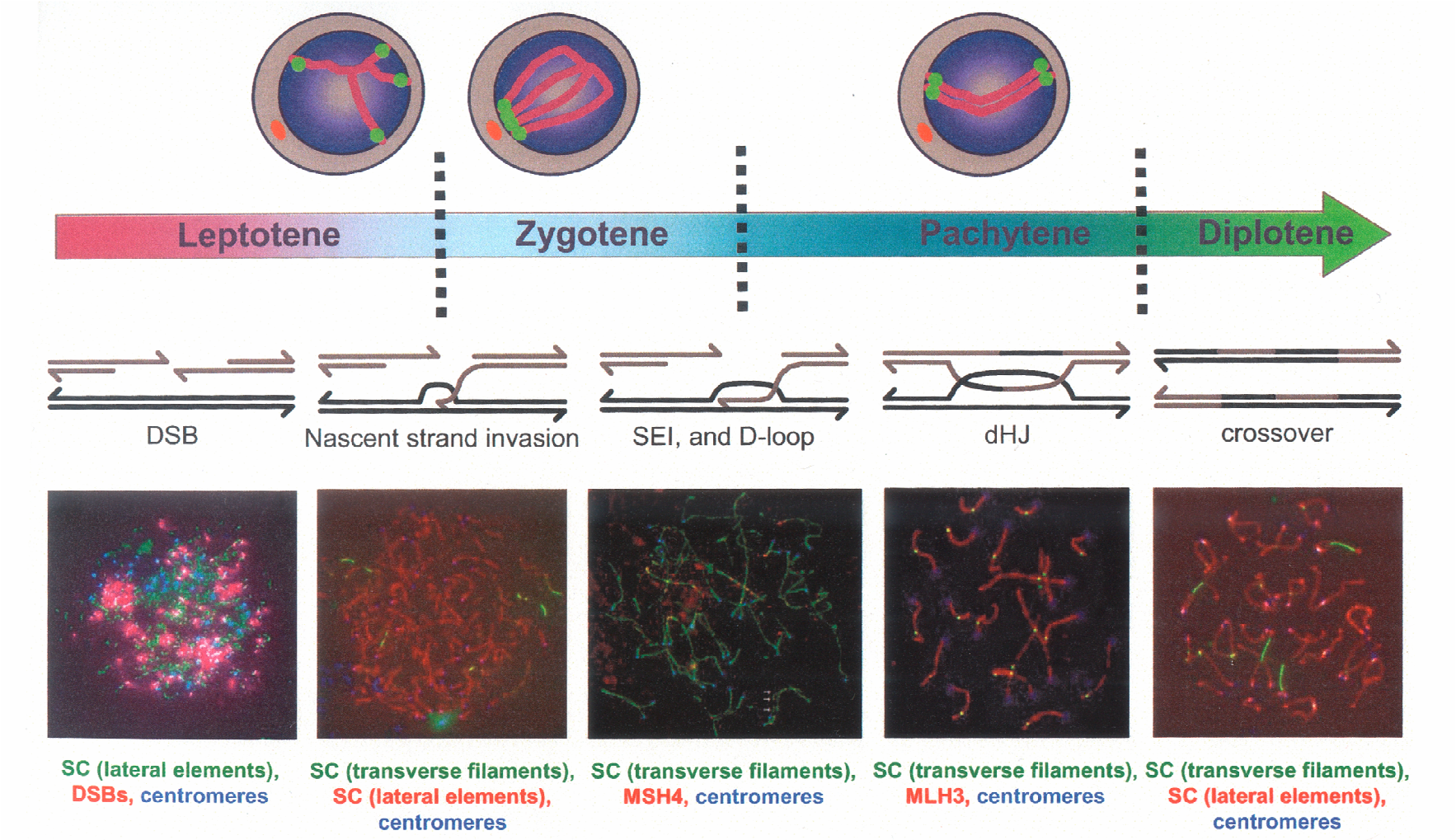
Leptotene
Zygotene
Pachytene
Diplotene
DSB
Nascent strand invasion
SEI, and D-loop
dHJ
crossover
SC (lateral elements), DSBs, centromeres
SC (transverse filaments), SC (lateral elements), centromeres
SC (transverse filaments), MSH4, centromeres
SC (transverse filaments), MLH3, centromeres
SC (transverse filaments), SC (lateral elements), centromeres

and throughout diplotene and diakinesis chromosomes continue condensing prior to metaphase I [49].

In addition to progressive condensing and packaging into the SC, meiotic chromosomes are also subject to dramatic telomere-led movements that, like meiotic recombination, begin at the leptotene-zygotene transition and end at the end of pachytene [57-62]. Although the relationships between the events of prophase I are not fully understood, they are clearly interconnected. For example, recombination is required for SC formation and SC formation is required for completion of recombination [1]. Additionally, two of the structural components of the SC axial/lateral elements, Red1 and Hop1, are required for wild-type levels of DSB formation and to inhibit intersister DSB repair [24-27, 63, 64]. The SC central element protein, Zip1, promotes: homologous pairing prior to DSB formation, interhomolog CO formation, and MI disjunction of non-exchange chromosomes [9-11, 41, 55]. Chromosome motion in prophase has been shown to regulate chromosome pairing and DSB repair outcomes, as well as promote to timely progression through prophase [57-62].

The meiotic recombination checkpoint ensures completing of DSB repair prior to the MI division. It is important that one stage of meiosis is complete before cells progress to the next stage. Just as in the mitotic cell cycle, the order of meiotic events is ensured by several known checkpoints. A suite of checkpoints is thought to monitor the recombination events of meiotic prophase to ensure that no broken DNA persists when cells proceed to the MI division [65]. The best studied of these checkpoints is the "recombination checkpoint," which is also known as the "pachytene checkpoint." In mutants that are unable (i.e. *dmc1*Δ) or slow (i.e. *ndj1*Δ) to complete meiotic recombination, the recombination checkpoint is activated and cell cycle progression is delayed or arrested at pachytene [66-68]. The lesion recognized by the

recombination checkpoint may be Rad51 and/or Dmc1-coated ssDNA. This checkpoint requires Mec1, Rad24, Rad17, Ddc1, and Mec3, which are also used in the mitotic DNA damage checkpoint [65, 67]. If any of these checkpoint factors are mutated, recombination deficient mutants, such as *dmc1*Δ, progress through the MI division with broken chromosomes and produce inviable gametes [67].

*zip1*Δ mutants also arrest or delay in pachytene, depending on the strain background [54, 55]. Like many of the mutants that trigger meiotic recombination checkpoint arrest, *zip1*Δ mutants have trouble completing recombination and accumulate unresolved double Holliday junctions [41, 69]. Many of the same components required for the recombination checkpoint have been shown to be required for the *zip1*Δ checkpoint [65]. However, the checkpoint triggered in the *zip1*Δ mutant is currently considered distinct from the recombination checkpoint because the consensus opinion in the field is that the *zip1*Δ checkpoint requires the protein Pch2 (see below), whereas the recombination checkpoint does not [65].

The *PCH2* gene is reported to be a meiotic checkpoint signaling factor. The function of an additional meiosis-specific factor, Pch2, in the recombination checkpoint has been disputed. *PCH2* (*Pachytene CHeckpoint 2*) was first identified in yeast as a recombination checkpoint factor because a *pch2* mutation was seen to suppress the meiotic arrests of both *dmc1*Δ and *zip1*Δ recombination defective mutants in the BR strain background [70]. Although the ability of a *pch2* mutation to suppress the meiotic arrest or delay (in the SK1 strain background) of *zip1*Δ mutants has been confirmed, the phenotype of *pch2*Δ *dmc1*Δ mutants is disputed ([70-73]; A. Hochwagen personal communication). One group supported the initial observation of meiotic progression in a *pch2*Δ *dmc1*Δ double mutant, whereas others have been unable to replicate this result [72, 73]. Additionally, unlike other recombination checkpoint factors, the *pch2*Δ mutation is unable to suppress the meiotic arrest/delay

phenotypes of other mutants (*csm4*Δ, *ndj1*Δ and *mnd1*Δ) known to trigger the recombination checkpoint ([72, 74]; SZ unpublished data). These results prompted the hypothesis that Pch2 is not required for the recombination checkpoint. Instead, it was proposed that *zip1*Δ triggers a Pch2-dependent "synapsis checkpoint" that recognizes defects in SC formation and halts defective recombination intermediates and prevents progression to the MI division [69, 74, 75].

In support of a synapsis checkpoint role for Pch2, the gene is conserved in organisms that construct a synaptonemal complex in meiosis, but not in organisms in which SC formation has been lost, such as *Schizosaccharomyces pombe* [74]. Additionally, the synapsis checkpoint signaling role proposed for budding yeast Pch2 has been reported to be conserved in *C. elegans* [75]. Unlike budding yeast, *C. elegans* homologous chromosomes contain sequences known as pairing centers which allow homologs to pair and construct SC independently of recombination [76]. In hermaphrodites heterozygous for a pairing center deletion on the X chromosome, the X chromosomes fail to synapse and trigger a Pch2-dependent checkpoint that causes apoptosis [75, 76].

Not all data, however, is consistent with the existence of a conserved Pch2-dependent "synapsis checkpoint." In budding yeast, most mutants that are unable to make SC do not trigger a checkpoint to delay meiosis; in fact, they go through meiosis faster (i.e. [77]). Additionally, the Pch2-dependent checkpoint that has been described in *D. melanogaster* is triggered by mutations in genes required for crossover formation, not all of which have synapsis defects [78].

Despite Pch2's classification as a checkpoint factor in three organisms with dramatically different meioses, several phenotypes of *pch2* mutants appear inconsistent with loss of checkpoint regulation. In checkpoint arrested cells, Pch2 accumulates in the nucleolus, which houses the rDNA, and is unable to promote

checkpoint arrest in *sir2*Δ or *dot1*Δ mutants in which Pch2 fails to localize to the nucleolus [70, 79]. Pch2 also acts to inhibit DSB formation near, and gene conversion within, the rDNA repeats ([70]; A Hochwagen personal communication). It is unclear why nucleolar localization and anti-recombinase functions would be seen in a signaling factor required for a checkpoint that recognizes lesions that can occur anywhere in the genome. In addition, *PCH2* is required for the proper organization of meiotic chromosomes. In *pch2*Δ mutants, the SC is longer and the alternating organization of Hop1 and Zip1 proteins is lost, thus allowing both proteins to localize along the entire length of the SC [69, 80]. Mutants of the mouse ortholog of *PCH2*, *Trip13*$^{-/-}$, display a similar disruption of the reciprocal organization of the HORMAD proteins (Hop1 homologs) and the mouse SC central element protein SYCP1, suggesting the chromosome organizational role of *PCH2* is conserved between yeast and mouse [81].

Finally, evidence for increased intersister DSB repair has been observed in some *pch2*Δ double mutants. In a physical analysis of DSB repair, Borner *et al.* [69] saw an increase in intersister DSB repair products in *pch2*Δ *zip1*Δ mutant. Genetic analyses done by Wu and Burgess showed that the spore inviability of a *pch2*Δ *rad17*Δ could be suppressed by a *spo13*Δ mutation [74]. *spo13* mutants undergo one meiotic division in which chromosomes can divide reductionally (like MI) or equationally (like MII and mitosis) [82, 83]. Because equational divisions do not require crossovers to ensure proper chromosome disjunction, *spo13* mutants can produce viable spores if no DSBs are formed or if DSBs are repaired in ways that do not form COs [25, 50, 52, 84]. Therefore, the high spore viability of the *pch2*Δ *rad17*Δ *spo13*Δ mutant could be explained by an increase in intersister DSB repair in *pch2*Δ *rad17*Δ [74].

Outline of experiments presented in this thesis. The experiments described in this thesis were designed to develop a deeper understanding of the mechanisms regulating meiotic DSB repair. This aim was achieved by examining the role the widely-conserved *PCH2* gene of budding yeast in the regulation of meiotic recombination. Chapter 2 presents experiments designed to assay the role of Pch2 in interhomolog DSB repair. These experiments confirmed the finding of others that the *pch2*Δ mutant has wild-type spore viability, despite exhibiting a delay in completing meiosis [69, 70, 74]. Although initial reports concluded that Pch2 has no role in recombination, I discovered that *pch2*Δ mutants displayed a dramatic increase in interhomolog crossover frequencies on chromosome XV [70]. Further investigation revealed a similar increase in crossing over on large and medium chromosomes (VII and VIII), but no increase on a small chromosome (III). Unlike crossovers, an elevated level of gene conversion of all markers on all chromosomes was observed in the *pch2*Δ mutant.

The increases in both crossover frequencies and gene conversion events in the *pch2*Δ mutant could be explained by an increase in DSB formation. Wu and Burgess assayed DSB frequencies at a known DSB hotspot on chromosome III and found DSB levels were not altered at this site in *pch2*Δ. However this analysis was done in the *sae2*Δ mutant background in which DSBs are not processed or repaired, but sub-maximal levels of DSBs are likely formed [13, 14, 74]. DSB levels have also been assayed utilizing a less sensitive genome-wide approach in *pch2*Δ and no change in DSB frequencies were observed, other than an increase in DSB formation near the rDNA repeats on chromosome XII (A. Hochwagen Personal communication). I confirmed that *pch2*Δ does not increase DSB levels by analyzing the DSB frequencies in both the *dmc1*Δ mutant background, in which maximal levels of DSBs are thought to form, and the *rad50S* strain background, which is similar to *sae2*Δ [13, 14, 85]. My

findings demonstrate that the crossover and gene conversion phenotypes observed in *pch2*Δ are not due to changes in DSB formation, but are rather due to differences in DSB repair.

One class of mutants, consisting of *ndj1*Δ and *csm4*Δ, are also known to have increased crossover frequencies, although the increase is less dramatic than that observed in *pch2*Δ [59, 60, 86, 87]. Evidence suggests that the excess crossovers produced in *ndj1*Δ (and likely *csm4*Δ) are produced by the non-interfering Mus81-Mms4-dependent crossover pathway, not the interfering Msh4-Msh5-dependent pathway [88]. To test if a similar mechanism led to the increased COs observed in *pch2*Δ, I assayed the recombination frequencies in both *pch2*Δ *mms4*Δ and *pch2*Δ *msh5*Δ double mutants. Unlike *ndj1*Δ, I found that both known crossover pathways contributed to the excess crossovers produced in *pch2*Δ mutants as the *pch2*Δ *mms4*Δ had higher CO frequencies than *mms4*Δ and *pch2*Δ *msh5*Δ had higher CO frequencies than *msh5*Δ.

I also found that crossover interference is significantly reduced in *pch2*Δ mutants, suggesting that Pch2 promotes the nonrandom distribution of crossovers. Consistent with this, I observed that combining the *pch2*Δ mutation with *spo11* hypomorphs resulted in synthetic losses of spore viability due to MI nondisjunction events. I hypothesize that Pch2 limits gene conversion, crossing over and promotes crossover interference via a common mechanism.

My discovery that Pch2 regulates interhomolog DSB repair and the intersister DSB repair phenotypes described above seemed inconsistent with Pch2's characterization as a checkpoint signaling factor. This motivated me to hypothesize that the phenotypes observed in *pch2*Δ mutants were due to errors in DSB repair, not checkpoint function. To test my hypothesis, I reexamined the role of Pch2 in the checkpoint arrest and delay phenotypes of *dmc1*Δ and *zip1*Δ mutants, respectively

[70]. I confirmed that the *pch2*Δ mutation partially suppresses both the *dmc1*Δ arrest and the *zip1*Δ delay. I also observed that the *pch2*Δ *dmc1*Δ arrest bypass phenotype is very sensitive to slight changes in strain background and temperature, possibly explaining the discrepancies in the literature regarding this phenotype. Unexpectedly, I found that the *dmc1*Δ arrest could be suppressed by *spo11* hypomorphs which decrease DSB levels. This suggests that the extent of the recombination checkpoint is sensitive to the level of unrepaired DSBs. This is a stark contrast to the mitotic DNA damage checkpoint that can trigger cell-cycle arrest in response to a single unrepaired DSB [89].

Although I observed checkpoint bypasses in *pch2*Δ mutants, my data from genetic and physical assays monitoring DSB repair are inconsistent with a checkpoint signaling role for the Pch2 protein. I add genetic support for physical analyses concluding that *pch2*Δ *zip1*Δ mutants have increased intersister repair by demonstrating that the synthetic spore inviability of *pch2*Δ *zip1*Δ can be suppressed by the *spo13* mutation. Similar analyses in the *spo13* strain background show that checkpoint bypass in *pch2*Δ *dmc1*Δ mutants is also due to increased levels of DSB repair. The sporulation and spore viability (of *spo13* derivatives) in *pch2*Δ *dmc1*Δ is Rad54-dependent, suggesting the repair is intersister homologous recombination.

Previously, increased intersister repair in *pch2*Δ *rad17*Δ and *pch2*Δ *zip1*Δ has been interpreted to result from lack of Pch2-dependent checkpoint signaling in response to lesions accrued in *rad17*Δ or *zip1*Δ mutants [69, 74]. I propose that the "checkpoint signaling" phenotypes of *pch2*Δ are explained by a larger portion of DSBs being repaired using the sister chromatid. This repair decreases the number of checkpoint eliciting lesions below the threshold required for checkpoint activation, leading to checkpoint bypass in the *pch2*Δ *dmc1*Δ and *pch2*Δ *zip1*Δ and *pch2*Δ *rad17*Δ mutants.

Although Pch2's role in limiting intersister recombination is most easily observed in mutants defective for interhomolog recombination, I utilized two independent experiments to show that Pch2 inhibits intersister recombination in wild-type meiosis as well. First, *pch2*Δ *rad54*Δ double mutants display a synthetic spore inviability phenotype, suggesting *pch2*Δ mutants are more reliant upon Rad54-dependendent intersister recombination. Second, I used a genetic reporter assay to show an increased in intersister DSB repair in *pch2*Δ as compared to wild-type. These experiments confirm my hypothesis that Pch2 is a recombination, not a checkpoint protein.

Together, Chapters 2 and 3 demonstrate that Pch2 contributes to the regulation of both major DSB repair decisions in meiosis: 1) sister vs. homolog repair template choice and 2) the CO vs. NCO interhomolog repair decision. I propose a model in which a common Pch2-dependent chromosome organization both inhibits intersister DSB repair and regulates the interhomolog crossover vs. noncrossover decision. The possibility that the function of Pch2 is conserved, and that the protein is not a checkpoint factor in any organism is explored.

Finally, Chapter 4 presents a separate project unrelated to Pch2 or meiosis. This project utilized whole-genome sequencing of diploid wild-type and mismatch repair deficient temperature-sensitive mutants (*mlh1-7*) allowed to accumulate mutations for 160 generations [90]. This project was a collaboration with Xin Ma, Arindam RoyChoudury, and Carlos Bustamante and required the development of a method to detect heterozygous mutations using short-read whole genome sequencing data. After identifying and verifying a set of heterozygous mutations, we were able to identify a novel mutational phenotype in which insertion/deletion mutations within homopolynucleotide (HP) tracts are more likely to occur in genomic regions containing additional HP tracts in *S. cerevisiae*.

REFERENCES

1. Roeder GS (1997) Meiotic chromosomes: it takes two to tango. Genes Dev 11: 2600-21.

2. Hassold T, Hall H, Hunt P (2007) The origin of human aneuploidy: where we have been, where we are going. Hum Mol Genet 16 Spec No. 2: R203-8.

3. Sakuno T, Watanabe Y (2009) Studies of meiosis disclose distinct roles of cohesion in the core centromere and pericentromeric regions. Chromosome Res 17: 239-49.

4. Watanabe Y (2005) Shugoshin: guardian spirit at the centromere. Curr Opin Cell Biol 17: 590-5.

5. Buonomo SB, Clyne RK, Fuchs J, Loidl J, Uhlmann F, et al. (2000) Disjunction of homologous chromosomes in meiosis I depends on proteolytic cleavage of the meiotic cohesin Rec8 by separin. Cell 103: 387-98.

6. Bickel SE, Orr-Weaver TL, Balicky EM (2002) The sister-chromatid cohesion protein ORD is required for chiasma maintenance in *Drosophila* oocytes. Curr Biol 12: 925-9.

7. Hodges CA, Revenkova E, Jessberger R, Hassold TJ, Hunt PA (2005) SMC1beta-deficient female mice provide evidence that cohesins are a missing link in age-related nondisjunction. Nat Genet 37: 1351-5.

8. Rockmill B, Voelkel-Meiman K, Roeder GS (2006) Centromere-proximal crossovers are associated with precocious separation of sister chromatids during meiosis in *Saccharomyces cerevisiae*. Genetics 174: 1745-54.

9. Tsubouchi T, Roeder GS (2005) A synaptonemal complex protein promotes homology-independent centromere coupling. Science 308: 870-3.

10. Newnham L, Jordan P, Rockmill B, Roeder GS, Hoffmann E The synaptonemal complex protein, Zip1, promotes the segregation of nonexchange chromosomes at meiosis I. Proc Natl Acad Sci U S A 107: 781-5.

11. Gladstone MN, Obeso D, Chuong H, Dawson DS (2009) The synaptonemal complex protein Zip1 promotes bi-orientation of centromeres at meiosis I. PLoS Genet 5: e1000771.

12. Stewart MN, Dawson DS (2008) Changing partners: moving from non-homologous to homologous centromere pairing in meiosis. Trends Genet 24: 564-73.

13. Buhler C, Borde V, Lichten M (2007) Mapping meiotic single-strand DNA reveals a new landscape of DNA double-strand breaks in *Saccharomyces cerevisiae*. PLoS Biol 5: e324.

14. Blitzblau HG, Bell GW, Rodriguez J, Bell SP, Hochwagen A (2007) Mapping of meiotic single-stranded DNA reveals double-stranded-break hotspots near centromeres and telomeres. Curr Biol 17: 2003-12.

15. Keeney S, Giroux CN, Kleckner N (1997) Meiosis-specific DNA double-strand breaks are catalyzed by Spo11, a member of a widely conserved protein family. Cell 88: 375-84.

16. Neale MJ, Pan J, Keeney S (2005) Endonucleolytic processing of covalent protein-linked DNA double-strand breaks. Nature 436: 1053-7.

17. Zakharyevich K, Yi-Hwa, P, Hunter, N (Submitted) Temporally and biochemically distinct activities of Exo1 during meiosis promote double-strand-break resection and resolution of double-Holliday junctions into crossovers.

18. Jackson JA, Fink GR (1985) Meiotic recombination between duplicated genetic elements in *Saccharomyces cerevisiae*. Genetics 109: 303-32.

19. Game JC, Sitney KC, Cook VE, Mortimer RK (1989) Use of a ring chromosome and pulsed-field gels to study interhomolog recombination, double-strand DNA breaks and sister-chromatid exchange in yeast. Genetics 123: 695-713.

20. Schwacha A, Kleckner N (1994) Identification of joint molecules that form frequently between homologs but rarely between sister chromatids during yeast meiosis. Cell 76: 51-63.

21. Goldfarb T, Lichten, M (Submitted) The sister chromatid is frequently and efficiently used for DNA double-strand break repair during budding yeast meiosis.

22. Krogh BO, Symington LS (2004) Recombination proteins in yeast. Annu Rev Genet 38: 233-71.

23. Schwacha A, Kleckner N (1997) Interhomolog bias during meiotic recombination: meiotic functions promote a highly differentiated interhomolog-only pathway. Cell 90: 1123-35.

24. Wan L, de los Santos T, Zhang C, Shokat K, Hollingsworth NM (2004) Mek1 kinase activity functions downstream of *RED1* in the regulation of meiotic double strand break repair in budding yeast. Mol Biol Cell 15: 11-23.

25. Niu H, Wan L, Baumgartner B, Schaefer D, Loidl J, et al. (2005) Partner choice during meiosis is regulated by Hop1-promoted dimerization of Mek1. Mol Biol Cell 16: 5804-18.

26. Niu H, Li X, Job E, Park C, Moazed D, et al. (2007) Mek1 kinase is regulated to suppress double-strand break repair between sister chromatids during budding yeast meiosis. Mol Cell Biol 27: 5456-67.

27. Niu H, Wan L, Busygina V, Kwon Y, Allen JA, et al. (2009) Regulation of meiotic recombination via Mek1-mediated Rad54 phosphorylation. Mol Cell 36: 393-404.

28. Arbel A, Zenvirth D, Simchen G (1999) Sister chromatid-based DNA repair is mediated by *RAD54*, not by *DMC1* or *TID1*. Embo J 18: 2648-58.

29. Shinohara M, Shita-Yamaguchi E, Buerstedde JM, Shinagawa H, Ogawa H, et al. (1997) Characterization of the roles of the *Saccharomyces cerevisiae RAD54* gene and a homologue of *RAD54*, *RDH54/TID1*, in mitosis and meiosis. Genetics 147: 1545-56.

30. Chen SY, Tsubouchi T, Rockmill B, Sandler JS, Richards DR, et al. (2008) Global analysis of the meiotic crossover landscape. Dev Cell 15: 401-15.

31. Mancera E, Bourgon R, Brozzi A, Huber W, Steinmetz LM (2008) High-resolution mapping of meiotic crossovers and non-crossovers in yeast. Nature 454: 479-85.

32. de los Santos T, Hunter N, Lee C, Larkin B, Loidl J, et al. (2003) The Mus81/Mms4 endonuclease acts independently of double-Holliday junction resolution to promote a distinct subset of crossovers during meiosis in budding yeast. Genetics 164: 81-94.

33. Argueso JL, Wanat J, Gemici Z, Alani E (2004) Competing crossover pathways act during meiosis in *Saccharomyces cerevisiae*. Genetics 168: 1805-16.

34. Berchowitz LE, Copenhaver GP (2010) Genetic Interference: Don't Stand So Close to Me. Current Genomics 11: 91-102.

35. Dresser ME, Ewing DJ, Conrad MN, Dominguez AM, Barstead R, et al. (1997) *DMC1* functions in a *Saccharomyces cerevisiae* meiotic pathway that is largely independent of the *RAD51* pathway. Genetics 147: 533-44.

36. Klein HL (1997) *RDH54*, a *RAD54* homologue in *Saccharomyces cerevisiae*, is required for mitotic diploid-specific recombination and repair and for meiosis. Genetics 147: 1533-43.

37. Hollingsworth NM (2010) Phosphorylation and the creation of interhomolog bias during meiosis in yeast. Cell Cycle 9: 436-7.

38. Hunter N, Kleckner N (2001) The single-end invasion: an asymmetric intermediate at the double-strand break to double-holliday junction transition of meiotic recombination. Cell 106: 59-70.

39. Jessop L, Lichten M (2008) Mus81/Mms4 endonuclease and Sgs1 helicase collaborate to ensure proper recombination intermediate metabolism during meiosis. Mol Cell 31: 313-23.

40. Schwacha A, Kleckner N (1995) Identification of double Holliday junctions as intermediates in meiotic recombination. Cell 83: 783-91.

41. Borner GV, Kleckner N, Hunter N (2004) Crossover/noncrossover differentiation, synaptonemal complex formation, and regulatory surveillance at the leptotene/zygotene transition of meiosis. Cell 117: 29-45.

42. Allers T, Lichten M (2001) Differential timing and control of noncrossover and crossover recombination during meiosis. Cell 106: 47-57.

43. de los Santos T, Loidl J, Larkin B, Hollingsworth NM (2001) A role for *MMS4* in the processing of recombination intermediates during meiosis in *Saccharomyces cerevisiae*. Genetics 159: 1511-25.

44. Cromie GA, Hyppa RW, Taylor AF, Zakharyevich K, Hunter N, et al. (2006) Single Holliday junctions are intermediates of meiotic recombination. Cell 127: 1167-78.

45. Baudat F, de Massy B (2007) Regulating double-stranded DNA break repair towards crossover or non-crossover during mammalian meiosis. Chromosome Res 15:565-77.

46. Cromie GA, Smith GR (2007) Branching out: meiotic recombination and its regulation. Trends Cell Biol 17: 448-55.

47. Tsai CJ, Mets DG, Albrecht MR, Nix P, Chan A, et al. (2008) Meiotic crossover number and distribution are regulated by a dosage compensation protein that resembles a condensin subunit. Genes Dev 22: 194-211.

48. McMahill MS, Sham CW, Bishop DK (2007) Synthesis-dependent strand annealing in meiosis. PLoS Biol 5: e299.

49. Lynn A, Soucek R, Borner GV (2007) ZMM proteins during meiosis: crossover artists at work. Chromosome Res 15: 591-605.

50. Hollingsworth NM, Byers B (1989) *HOP1*: a yeast meiotic pairing gene. Genetics 121: 445-62.

51. Hollingsworth NM, Goetsch L, Byers B (1990) The *HOP1* gene encodes a meiosis-specific component of yeast chromosomes. Cell 61: 73-84.

52. Rockmill B, Roeder GS (1988) *RED1*: a yeast gene required for the segregation of chromosomes during the reductional division of meiosis. Proc Natl Acad Sci U S A 85: 6057-61.

53. Rockmill B, Roeder GS (1990) Meiosis in asynaptic yeast. Genetics 126: 563-74.

54. Sym M, Engebrecht JA, Roeder GS (1993) *ZIP1* is a synaptonemal complex protein required for meiotic chromosome synapsis. Cell 72: 365-78.

55. Sym M, Roeder GS (1994) Crossover interference is abolished in the absence of a synaptonemal complex protein. Cell 79: 283-92.

56. Sym M, Roeder GS (1995) Zip1-induced changes in synaptonemal complex structure and polycomplex assembly. J Cell Biol 128: 455-66.

57. Scherthan H, Wang H, Adelfalk C, White EJ, Cowan C, et al. (2007) Chromosome mobility during meiotic prophase in *Saccharomyces cerevisiae*. Proc Natl Acad Sci U S A 104: 16934-9.

58. Koszul R, Kim KP, Prentiss M, Kleckner N, Kameoka S (2008) Meiotic chromosomes move by linkage to dynamic actin cables with transduction of force through the nuclear envelope. Cell 133: 1188-201.

59. Kosaka H, Shinohara M, Shinohara A (2008) Csm4-dependent telomere movement on nuclear envelope promotes meiotic recombination. PLoS Genet 4:e1000196.

60. Wanat JJ, Kim KP, Koszul R, Zanders S, Weiner B, et al. (2008) Csm4, in collaboration with Ndj1, mediates telomere-led chromosome dynamics and recombination during yeast meiosis. PLoS Genet 4: e1000188.

61. Conrad MN, Lee CY, Chao G, Shinohara M, Kosaka H, et al. (2008) Rapid telomere movement in meiotic prophase is promoted by *NDJ1*, *MPS3*, and *CSM4* and is modulated by recombination. Cell 133: 1175-87.

62. Trelles-Sticken E, Dresser ME, Scherthan H (2000) Meiotic telomere protein Ndj1p is required for meiosis-specific telomere distribution, bouquet formation and efficient homologue pairing. J Cell Biol 151: 95-106.

63. Mao-Draayer Y, Galbraith AM, Pittman DL, Cool M, Malone RE (1996) Analysis of meiotic recombination pathways in the yeast *Saccharomyces cerevisiae*. Genetics 144: 71-86.

64. Xu L, Weiner BM, Kleckner N (1997) Meiotic cells monitor the status of the interhomolog recombination complex. Genes Dev 11: 106-18.

65. Hochwagen A, Amon A (2006) Checking your breaks: surveillance mechanisms of meiotic recombination. Curr Biol 16: R217-28.

66. Bishop DK, Park D, Xu L, Kleckner N (1992) *DMC1*: a meiosis-specific yeast homolog of E. coli *recA* required for recombination, synaptonemal complex formation, and cell cycle progression. Cell 69: 439-56.

67. Lydall D, Nikolsky Y, Bishop DK, Weinert T (1996) A meiotic recombination checkpoint controlled by mitotic checkpoint genes. Nature 383: 840-3.

68. Wu HY, Burgess SM (2006) Ndj1, a telomere-associated protein, promotes meiotic recombination in budding yeast. Mol Cell Biol 26: 3683-94.

69. Borner GV, Barot A, Kleckner N (2008) Yeast Pch2 promotes domainal axis organization, timely recombination progression, and arrest of defective recombinosomes during meiosis. Proc Natl Acad Sci U S A 105: 3327-32.

70. San-Segundo PA, Roeder GS (1999) Pch2 links chromatin silencing to meiotic checkpoint control. Cell 97: 313-24.

71. Mitra N, Roeder GS (2007) A novel nonnull *ZIP1* allele triggers meiotic arrest with synapsed chromosomes in *Saccharomyces cerevisiae*. Genetics 176: 773-87.

72. Zierhut C, Berlinger M, Rupp C, Shinohara A, Klein F (2004) Mnd1 is required for meiotic interhomolog repair. Curr Biol 14: 752-62.

73. Hochwagen A, Tham WH, Brar GA, Amon A (2005) The FK506 binding protein Fpr3 counteracts protein phosphatase 1 to maintain meiotic recombination checkpoint activity. Cell 122: 861-73.

74. Wu HY, Burgess SM (2006) Two distinct surveillance mechanisms monitor meiotic chromosome metabolism in budding yeast. Curr Biol 16: 2473-9.

75. Bhalla N, Dernburg AF (2005) A conserved checkpoint monitors meiotic chromosome synapsis in Caenorhabditis elegans. Science 310: 1683-6.

76. MacQueen AJ, Phillips CM, Bhalla N, Weiser P, Villeneuve AM, et al. (2005) Chromosome sites play dual roles to establish homologous synapsis during meiosis in *C. elegans*. Cell 123: 1037-50.

77. Malone RE, Haring SJ, Foreman KE, Pansegrau ML, Smith SM, et al. (2004) The signal from the initiation of meiotic recombination to the first division of meiosis. Eukaryot Cell 3: 598-609.

78. Joyce EF, McKim KS (2009) Drosophila *PCH2* is required for a pachytene checkpoint that monitors double-strand-break-independent events leading to meiotic crossover formation. Genetics 181: 39-51.

79. San-Segundo PA, Roeder GS (2000) Role for the silencing protein Dot1 in meiotic checkpoint control. Mol Biol Cell 11: 3601-15.

80. Joshi N, Barot A, Jamison C, Borner GV (2009) Pch2 links chromosome axis remodeling at future crossover sites and crossover distribution during yeast meiosis. PLoS Genet 5: e1000557.

81. Wojtasz L, Daniel K, Roig I, Bolcun-Filas E, Xu H, et al. (2009) Mouse *HORMAD1*and *HORMAD2*, two conserved meiotic chromosomal proteins, are depleted from synapsed chromosome axes with the help of *TRIP13* AAA-ATPase. PLoS Genet 5: e1000702.

82. Klapholz S, Esposito RE (1980) Isolation of *SPO12-1* and *SPO13-1* from a natural variant of yeast that undergoes a single meiotic division. Genetics 96: 567-88.

83. Hugerat Y, Simchen G (1993) Mixed segregation and recombination of chromosomes and YACs during single-division meiosis in *spo13* strains of *Saccharomyces cerevisiae*. Genetics 135: 297-308.

84. Malone RE, Esposito RE (1981) Recombinationless meiosis in *Saccharomyces cerevisiae*. Mol Cell Biol 1: 891-901.

85. Alani E, Padmore R, Kleckner N (1990) Analysis of wild-type and *rad50* mutants of yeast suggests an intimate relationship between meiotic chromosome synapsis and recombination. Cell 61: 419-36.

86. Conrad MN, Dominguez AM, Dresser ME (1997) Ndj1p, a meiotic telomere protein required for normal chromosome synapsis and segregation in yeast. Science 276: 1252-5.

87. Chua PR, Roeder GS (1997) Tam1, a telomere-associated meiotic protein, functions in chromosome synapsis and crossover interference. Genes Dev 11: 1786-800.

88. Getz TJ, Banse SA, Young LS, Banse AV, Swanson J, et al. (2008) Reduced mismatch repair of heteroduplexes reveals "non"-interfering crossing over in wild-type *Saccharomyces cerevisiae*. Genetics 178: 1251-69.

89. Bennett CB, Lewis AL, Baldwin KK, Resnick MA (1993) Lethality induced by a single site-specific double-strand break in a dispensable yeast plasmid. Proc Natl Acad Sci U S A 90: 5613-7.

90. Heck, JA, Gresham D, Botstein D, Alani E (2006) Accumulation of recessive lethal mutations in *Saccharomyces cerevisiae mlh1* mismatch repair mutants is not associated with gross chromosomal rearrangements. Genetics 174: 519-23.

CHAPTER 2

The *pch2Δ* mutation in baker's yeast alters meiotic crossover levels and confers a defect in crossover interference[1].

[1]This chapter is published as Zanders S, Alani A (2009) PLoS Genet 5: e1000571 and also appears as reference 19 of Chapter 4.

ABSTRACT

Pch2 is a widely conserved protein that is required in baker's yeast for the organization of meiotic chromosome axes into specific domains. We provide four lines of evidence suggesting that it regulates the formation and distribution of crossover events required to promote chromosome segregation at Meiosis I. First, *pch2*Δ mutants display wild-type crossover levels on a small (III) chromosome, but increased levels on larger (VII, VIII, XV) chromosomes. Second, *pch2*Δ mutants show defects in crossover interference. Third, crossovers observed in *pch2*Δ require both Msh4-Msh5 and Mms4-Mus81 functions. Lastly, the *pch2*Δ mutation decreases spore viability and disrupts crossover interference in *spo11* hypomorph strains that have reduced levels of meiosis-induced double-strand breaks. Based on these and previous observations, we propose a model in which Pch2 functions at an early step in crossover control to ensure that every homolog pair receives an obligate crossover.

AUTHOR SUMMARY

During meiosis, cells that ultimately become gametes (such as eggs or sperm) undergo a single round of DNA replication followed by two consecutive divisions. In most organisms, the segregation of chromosomes at the first meiotic division is dependent upon genetic exchange, or crossing over, at homologous sites along chromosomes. Crossing over must therefore be regulated to ensure that every pair of matched chromosomes receives at least one crossover. Matched chromosomes that do not receive a crossover frequently undergo missegregation at the first meiotic division, yielding gametes that do not contain the normal chromosome number. Such missegregation events have been linked to human infertility syndromes. We used a

genetic approach to study meiotic crossover control in baker's yeast. Our work suggests that Pch2 is required in crossover control during meiosis; mutants lacking Pch2 display altered crossover levels and distribution. Furthermore, *pch2* mutations cause enhanced gamete inviability in strains that are mildly defective in initiating recombination. Based on these observations, we hypothesize that Pch2 acts early in crossover control, in steps that occur prior to those proposed for previously characterized crossover-promoting factors.

INTRODUCTION

Meiosis generates haploid gametes from diploid progenitor cells. The reduction in ploidy results from the segregation of homologous chromosome pairs in the first meiotic division (MI, [1]). Prior to MI, each chromosome is joined to its homolog at chiasmata, which serve to tether homologs to each other. This interaction promotes the tension between homologs needed to form a bipolar spindle that facilitates homolog segregation. Homologous chromosome pairs lacking chiasmata connections often fail to segregate properly at MI. Chromosome nondisjunction can also result if chiasmata are present, but not properly placed on chromosomes, or if sister chromatid cohesion is disrupted [2-5]. Regardless of the cause, chromosome missegregation produces aneuploid gametes that lead to infertility or conditions like Down syndrome in humans [6].

Chiasmata form at sites where programmed Spo11-catalyzed DNA double-stranded breaks (DSBs), induced early in meiotic prophase, are repaired to form crossovers [1]. In baker's yeast, crossovers (COs) are formed via two main pathways. The first pathway, by which the majority of COs are made, involves Msh4-Msh5 and Mlh1-Mlh3 [7-15]. In this pathway, DSBs are processed and acted upon by strand

exchange enzymes to form single-end invasion intermediates (SEIs) that are converted into double Holliday junctions (dHJs). The latter are resolved into crossovers which display interference; the COs are more uniformly spaced than if placed at random (see below; [16-22]). The COs formed via the second major pathway, which require Mms4-Mus81, are not subject to CO interference [10, 11, 23]. Little is known about the intermediates that form in this latter pathway.

The recombination steps that lead to CO formation occur in meiotic prophase. In leptotene, when meiotic DSB formation initiates recombination, an axial element containing Hop1 and Red1 proteins assembles along each pair of sister chromatids. In zygotene, when SEIs are detected, mature tripartite synaptonemal complex (SC) starts to form when the Zip1-containing central element connects the axial elements, which are now termed "lateral elements." Mature SC initiation begins at centromeres and later at CO-designated sites. These SC initiation events then spread outward until synapsis is completed in pachytene [24, 25]. Hop1/Red1 and Zip1 are enriched in separate domains on the mature SC. This organization is Pch2-dependent because in *pch2*Δ mutants, Zip1 and Hop1 appear to be more uniformly distributed along the chromosome axes [26, 27]. At the end of pachytene, recombination intermediates are resolved (reviewed in [28]).

In yeast, ~40% of the ~140-170 meiotic DSBs are repaired to generate noncrossover (NCO) products [29, 30]. These NCO products are thought to form by a synthesis-dependent strand annealing mechanism (SDSA, [31]), separate from the interfering CO mechanism, and do not result in MI disjunction-promoting chiasmata. Martini *et al.* [32] found that when meiotic programmed DSBs are decreased in *spo11* hypomorphic strains, COs are favored at the expense of NCOs [24]. This CO homeostasis phenomenon may be an additional manifestation of CO interference [32, 33]. The above studies indicate that DSBs are subject to a CO vs. NCO decision step,

which is regulated by interference. Interference regulates this decision by ensuring that CO designation for a given DSB inhibits nearby DSBs from receiving this designation, thereby relegating them to a NCO fate. It is not clear whether non-interfering COs are formed through such a decision process; these COs are thought to form through a parallel pathway [10, 23]. For this paper, the CO vs. NCO decision refers solely to COs that are subject to interference.

The interference-regulated CO vs. NCO decision likely occurs very early in recombination, roughly at the time of SEI formation (late leptotene-early zygotene) and does not appear to be controlled by domains or sequences contained within the chromosome [17, 18, 20, 21, 34, 35]. CO interference is strongest near a CO event and weakens with distance along the chromosome, although interference can act over large distances, up to ~150 kb in yeast and ~60 Mb in mice [30, 33, 36, 37]. In addition, interference between COs appears stronger on longer chromosomes compared to shorter chromosomes [35, 38-40], but see [41]. However, smaller chromosomes have relatively high DSB density and may also have a higher density of non-interfering COs [39, 41, 42].

The mechanisms underlying interference regulation of the CO vs. NCO decision are unknown, despite the fact that numerous mutants showing defects in CO interference have been identified in baker's yeast. For at least a subset of these mutants, the defects in CO interference likely reflect problems in CO formation and not in the early CO vs. NCO decision (reviewed in [28]). For example, mutants defective in either the SC central element protein Zip1 or the CO-promoting factor Msh4 have reduced CO levels and the remaining COs show reduced or no interference [7, 33, 43-45]. However, Zip2 foci, which mark the early CO designated sites, still display interference in *zip1* and *msh4* mutants [35]. This result, combined with the fact that NCOs form in *zip1*Δ and *msh4*Δ, suggests that interference regulation of the

CO vs. NCO decision requires neither these factors nor the mature SC [20, 22, 35, 46]. Rather, Zip1 and Msh4 are needed downstream of the decision to ensure CO formation [22, 35]. It is likely that these results are applicable to other members of the ZMM (Zip, Msh, Mer) class of proteins.

We examined the *PCH2* gene for a role in interference regulation of the CO vs. NCO decision. *PCH2* is a putative AAA-ATPase widely conserved in organisms that construct a synaptonemal complex in meiosis [26, 47]. *PCH2* was first identified in *S. cerevisiae* as a meiotic checkpoint factor due to the ability of *pch2*Δ to suppress the meiotic arrest of *zip1*Δ mutants [26]. This observation was extended by Wu and Burgess [47]; they proposed that Pch2 and Rad17 comprise separate branches of a checkpoint that ensures proper timing of the MI division, with the Pch2-dependent branch monitoring synaptonemal complex formation and the Rad17-dependent branch monitoring recombination events. Other checkpoint roles for Pch2 were reported in *C. elegans*, where it is required for apoptosis in response to unsynapsed pairing centers and in *Drosophila*, where it is required to delay meiotic progression in certain CO formation mutants [48, 49].

Recent studies indicate that *PCH2* is not solely a checkpoint factor; it is essential for proper meiotic axis organization and timely meiotic progression in baker's yeast, and complete DSB repair and fertility in mice [27, 47, 50]. Here we report that *pch2* mutants display increased meiotic CO levels on larger chromosomes and are defective in CO interference. We also show that mutation of *PCH2* reduces spore viability in *spo11* hypomorphic strains. These data support an early role for Pch2 in DSB repair and a model in which Pch2-promoted meiotic axis organization controls CO levels and their distribution.

RESULTS

Genetic analysis of recombination.

A new phenotype for pch2Δ mutants: increased crossing over on large chromosomes. We analyzed the *pch2*Δ phenotype in two different strain backgrounds at 30°C. In the EAY1108/1112 (EAY) SK1 congenic strain background, one large chromosome (XV, 1095 kb) is marked, whereas large (VII, 1040 kb), medium (VIII, 582 kb), and small (III, 333 kb) chromosomes are marked in the SK1 isogenic NHY942/943 (NHY) strain background ([10, 11]; Figures 2-1A, 2-2A; Table 2-1). Similar to previous studies, *pch2*Δ mutants show wild-type spore viability (~95%; [26, 47, 51]; Figures 2-3, 2-4).

In the EAY strain background, the total map distance across four intervals on chromosome XV was 152 cM in *pch2*Δ compared to 101 cM in wild-type (Figure 2-1; Table 2-2). Increased crossing over in *pch2*Δ was statistically significant in all four intervals (G-test where $p<0.017$ is considered significant due to Dunn-Sidak correction for multiple tests; see Table 2-2 for p values). Similar results were observed on the large (VII) and medium (VIII) chromosomes in the NHY background (Figure 2-2B; Table 2-2). Significantly more crossing over was observed in each of three intervals on chromosome VII, raising the map distance of the marked region from 69 cM in wild-type to 115 cM in *pch2*Δ (G-test where $p<0.017$ is considered significant due to Dunn-Sidak correction for multiple tests; see Table 2-2 for p values). For chromosome VIII, statistically significant increases in crossing over were observed in both genetic intervals, raising the map distance from 46 cM in wild-type to 72 cM in *pch2*Δ. The increases in crossing over observed in *pch2*Δ on chromosomes XV, VII, and VIII resulted from an increase in both tetratype and non-

Figure 2-1. *pch2*Δ has increased levels of meiotic COs on the large chromosome XV.

Recombination levels in four genetic intervals were analyzed on chromosome XV in the EAY1108/EAY1112 strain background (A). CO frequencies were calculated in cM from tetrads (B) and as recombination frequencies in spores (C). See Tables 2-1 and 2-2 for raw data and statistical analyses.

A

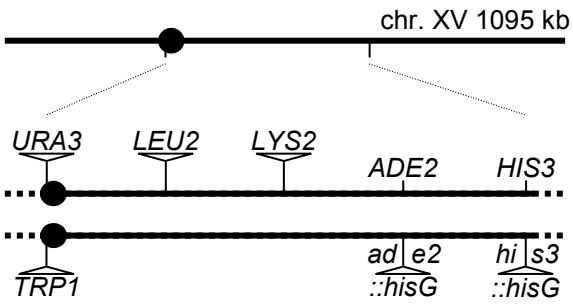
chr. XV 1095 kb
URA3
LEU2
LYS2
ADE2
HIS3
TRP1
ad e2
::hisG
hi s3
::hisG

B

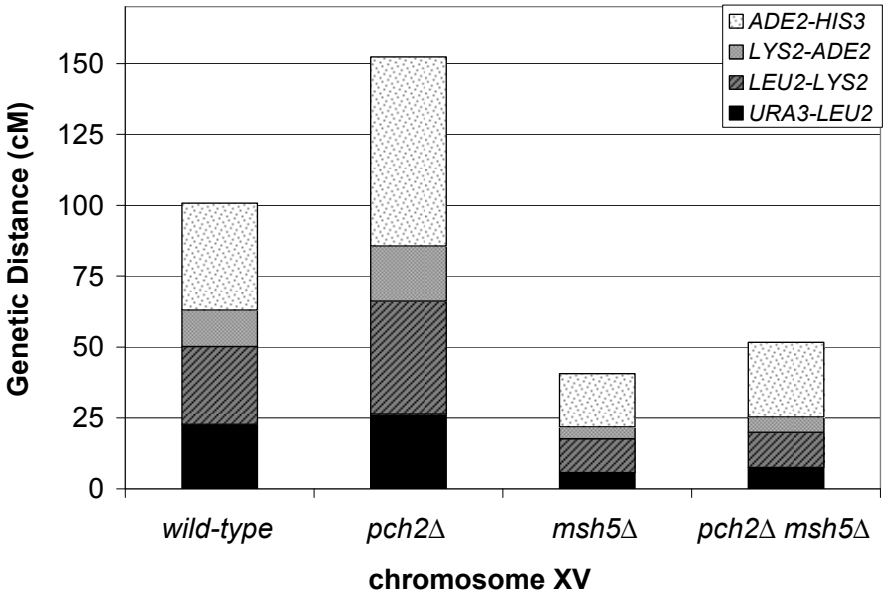
ADE2-HIS3
LYS2-ADE2
LEU2-LYS2
URA3-LEU2
Genetic Distance (cM)
150
125
100
75
50
25
0
wild-type
pch2Δ
msh5Δ
pch2Δ msh5Δ
chromosome XV

C

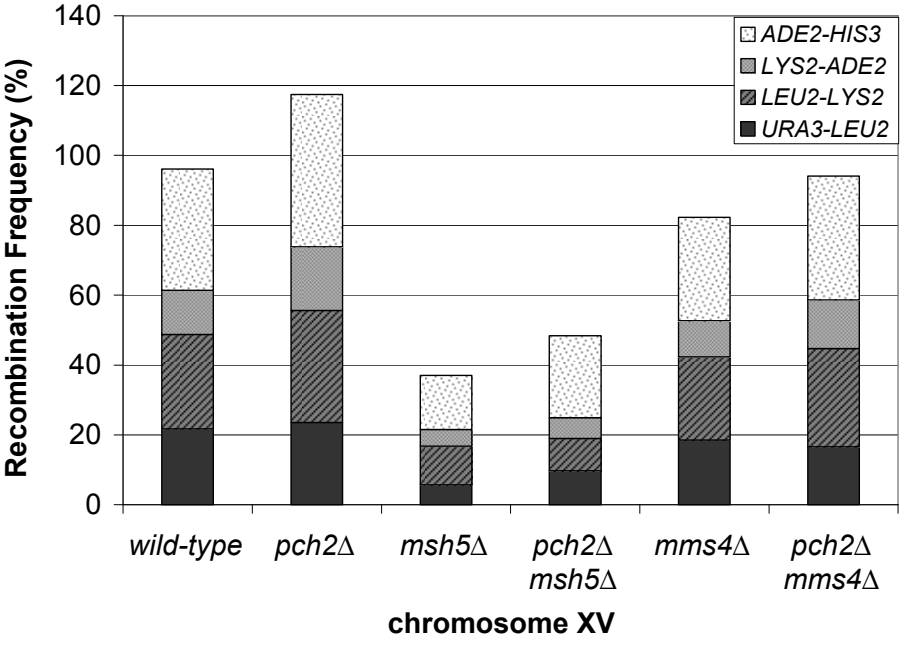
ADE2-HIS3
LYS2-ADE2
LEU2-LYS2
URA3-LEU2
Recombination Frequency (%)
140
120
100
80
60
40
20
0
wild-type
pch2Δ
msh5Δ
pch2Δ msh5Δ
mms4Δ
pch2Δ mms4Δ
chromosome XV

A

B

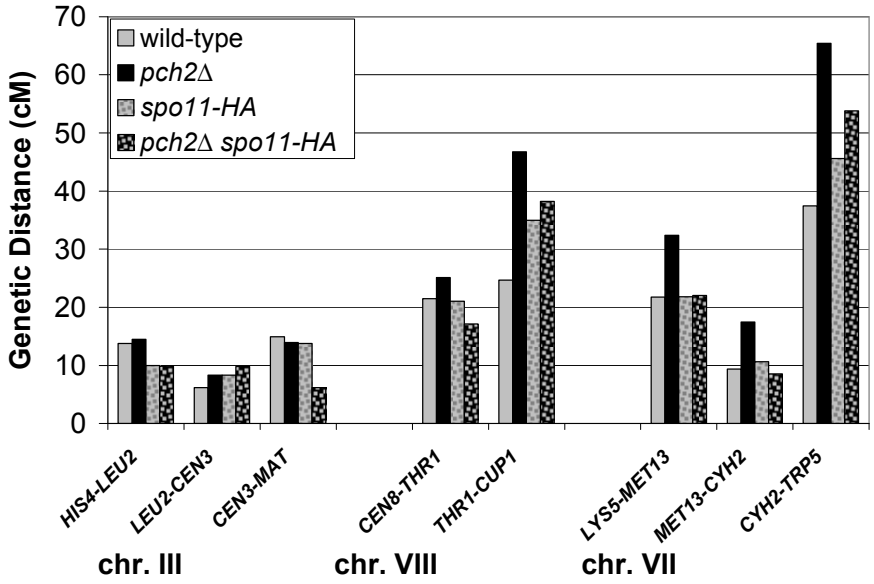

Figure 2-2. *pch2*Δ has increased meiotic CO levels on chromosomes VII and VIII, but not the small chromosome III.

A) The organization of genetic markers assayed on a small (III), medium (VIII), and large (VII) chromosome in the NHY942/NHY943 strain background is shown. B) CO frequencies in cM were calculated from four-spore viable tetrads in wild-type, *pch2*Δ/*pch2*Δ, *spo11-HA/spo11-HA* and *pch2*Δ *spo11-HA/spo11-HA* strains. See Table 2-2 for raw data and statistical analyses.

Table 2-1. Yeast Strains

The strains used are listed with their genotypes and the papers in which the strains were originally used. EAY1108 and EAY1112 and their derivatives are SK1 congenic strains. NHY942 and NHY943 and their derivatives are SK1 isogenic strains.

Strain name	Genotype	Source
EAY1108	*MATa, ho::hisG, lys2, ura3, leu2::hisG, trp1::hisG, URA3-CEN15, iLEU2-chXV, iLYS2-chXV*	Argueso *et al.* [11]
EAY1975	as EAY1108 except *pch2Δ::NATMX4*	this work
EAY1281	as EAY1108 except *msh5Δ::NATMX4*	Argueso *et al.* [11]
EAY1167	as EAY1108 except *mms4Δ::KANMX4*	Argueso *et al.* [11]
EAY2332	as EAY1281except *pch2Δ::KANMX4*	this work
EAY2343	as EAY1167 except *pch2Δ::NATMX4*	this work
EAY1112	*MATα, ho::hisG, lys2, ura3, leu2::hisG, trp1::hisG, ade2::hisG, his3::hisG, TRP1-CEN15*	Argueso *et al.* [11]
EAY1976	as EAY1112 except *pch2Δ::NATMX4*	this work
EAY1280	as EAY1112 except *msh5Δ::NATMX4*	Argueso *et al.* [11]
EAY1168	as EAY1112 except *mms4Δ::KANMX4*	Argueso *et al.* [11]
EAY2333	as EAY1280 except *pch2Δ::KANMX4*	this work
EAY2341	as EAY1168 except *pch2Δ::NATMX4*	this work
NH942	*MATα, ho::hisG, ade2Δ, can1, ura3(ΔSma-Pst), met13-B, trp5-S, CEN8::URA3, thr1-A, cup1^{s}*	de los Santos *et al.* [10]
EAY2209	as NH942 except *pch2Δ::NATMX4*	this work
EAY2256	as NH942 except *dmc1Δ::KANMX4*	this work
EAY2260	as EAY2209 except *dmc1Δ::KANMX4*	this work
SKY633	as NH942 except *MATa, spo11-HA3His6::KANMX4*	Martini *et al.* [32]
SKY1062	as NH942 except *MATa, spo11(D290A)-HA3His6::KANMX4*	Martini *et al.* [32]
EAY2267	as SKY633 except *pch2Δ::NATMX4*	this work
EAY2269	as SKY1062 except *pch2Δ::NATMX4*	this work
EAY2545	as EAY2267 except *dmc1Δ::HPHMX4*	this work
EAY2546	as SKY633 except *dmc1Δ::HPHMX4*	this work
EAY2562	as NH942 except *MATa*, *dmc1Δ::KANMX4*, *spo11-HA3His6::KANMX4*	this work
EAY2563	as NH942 except *dmc1Δ::KANMX4, spo11-HA3His6::KANMX4*	this work
EAY2564	as NH942 except *MATa*, *dmc1Δ::KANMX4*, *spo11-HA3His6::KANMX4, pch2Δ::NATMX4*	this work
EAY2565	as NH942 except *dmc1Δ::KANMX4, spo11-HA3His6::KANMX4, pch2Δ::NATMX4*	this work
NH943	*MATa, ho::hisG, ade2Δ, ura3(ΔSma-Pst), leu2::hisG, CEN3::ADE2, lys5-P, cyh2^{r}, his4-B*	de los Santos *et al.* [10]

Table 2-1 (Continued)

Strain name	Genotype	Source
EAY2210	as NH943 except *pch2Δ::NATMX4*	this work
EAY2257	as NH943 except *dmc1Δ::KANMX4*	this work
EAY2261	as EAY2210 except *dmc1Δ::KANMX4*	this work
SKY635	as NH943 except *MATα, spo11-HA3His6::KANMX4*	Martini *et al.* [32]
SKY638	as NH943 except *MATα, spo11(D290A)-HA3His6::KANMX4*	Martini *et al.* [32]
SKY665	as NH943 except *MATα, spo11(Y135F)-HA3His6::KANMX4*	Martini *et al.* [32]
EAY2264	as SKY635 except *pch2Δ::NATMX4*	this work
EAY2265	as SKY665 except *pch2Δ::NATMX4*	this work
EAY2271	as SKY638 except *pch2Δ::NATMX4*	this work
EAY2535	as SKY635 except *dmc1Δ::HPHMX4*	this work
EAY2540	as EAY2264 except *dmc1Δ::HPHMX4*	this work

Figure 2-3. Pch2 promotes spore viability in *spo11* hypomorphs.

A) Spore viability distributions of wild-type and mutant strains in the NHY942/NHY943 strain background are displayed. The X-axes represent the number of viable spores per tetrad and the Y-axes represent the percent of tetrads comprising each class. The total number of tetrads dissected (n) and the overall percent spore viability (% SV) are shown. B) Bar graph showing spore viability in wild-type (gray) and *pch2*Δ (black) mutants containing the indicated *spo11* mutations. The *SPO11/SPO11*, *spo11-HA/spo11-HA*, *spo11-HA/spo11yf-HA*, and *spo11da-HA/spo11da-HA* alleles confer 100, 80, 30 and 20% total DSB levels, respectively, in the *PCH2* background [32].

A

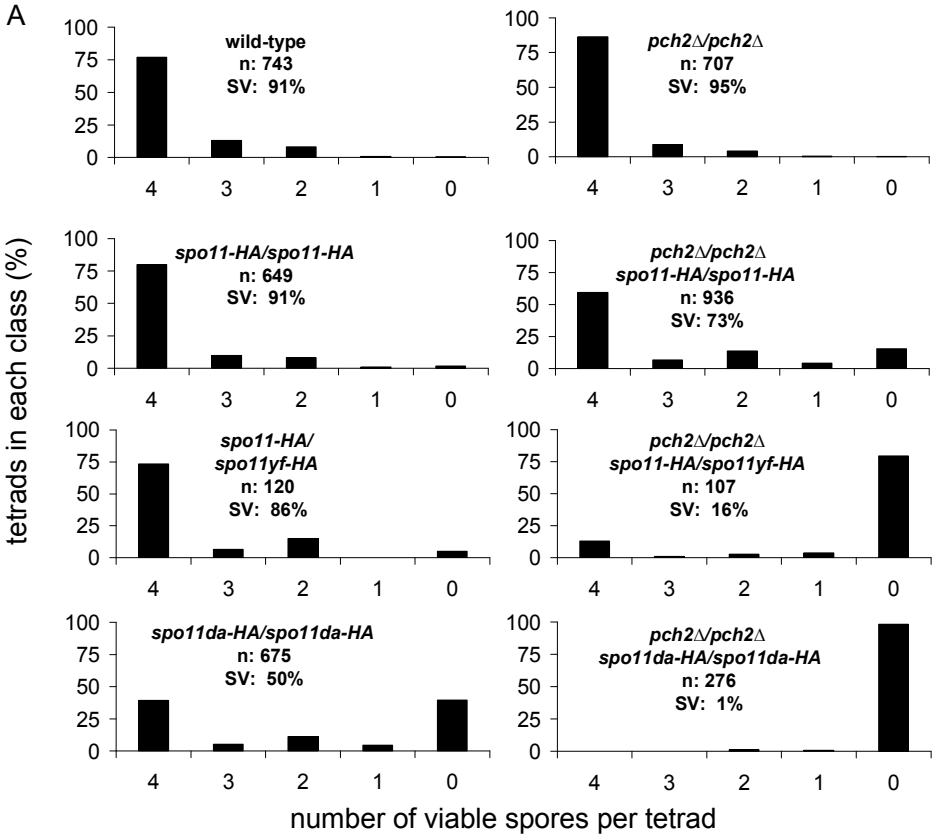
wild-type
n: 743
SV: 91%
pch2Δ/pch2Δ
n: 707
SV: 95%
spo11-HA/spo11-HA
n: 649
SV: 91%
pch2Δ/pch2Δ
spo11-HA/spo11-HA
n: 936
SV: 73%
spo11-HA/
spo11yf-HA
n: 120
SV: 86%
pch2Δ/pch2Δ
spo11-HA/spo11yf-HA
n: 107
SV: 16%
spo11da-HA/spo11da-HA
n: 675
SV: 50%
pch2Δ/pch2Δ
spo11da-HA/spo11da-HA
n: 276
SV: 1%
tetrads in each class (%)
number of viable spores per tetrad

B

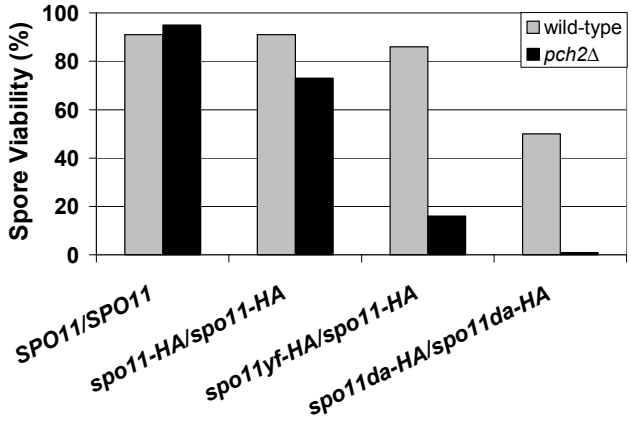
Spore Viability (%)
wild-type
pch2Δ
SPO11/SPO11
spo11-HA/spo11-HA
spo11yf-HA/spo11-HA
spo11da-HA/spo11da-HA

Figure 2-4. *pch2*Δ mutants display a synthetic decrease in spore viability when combined with *msh5*Δ or *mms4*Δ mutations.

Spore viability distributions of wild-type and mutant strains in the EAY1108/EAY1112 strain background are displayed. The X-axes represent the number of viable spores per tetrad and the Y-axes represent the percent of tetrads comprising each class. The total number of tetrads dissected (n) and the overall percent spore viability (% SV) are shown.

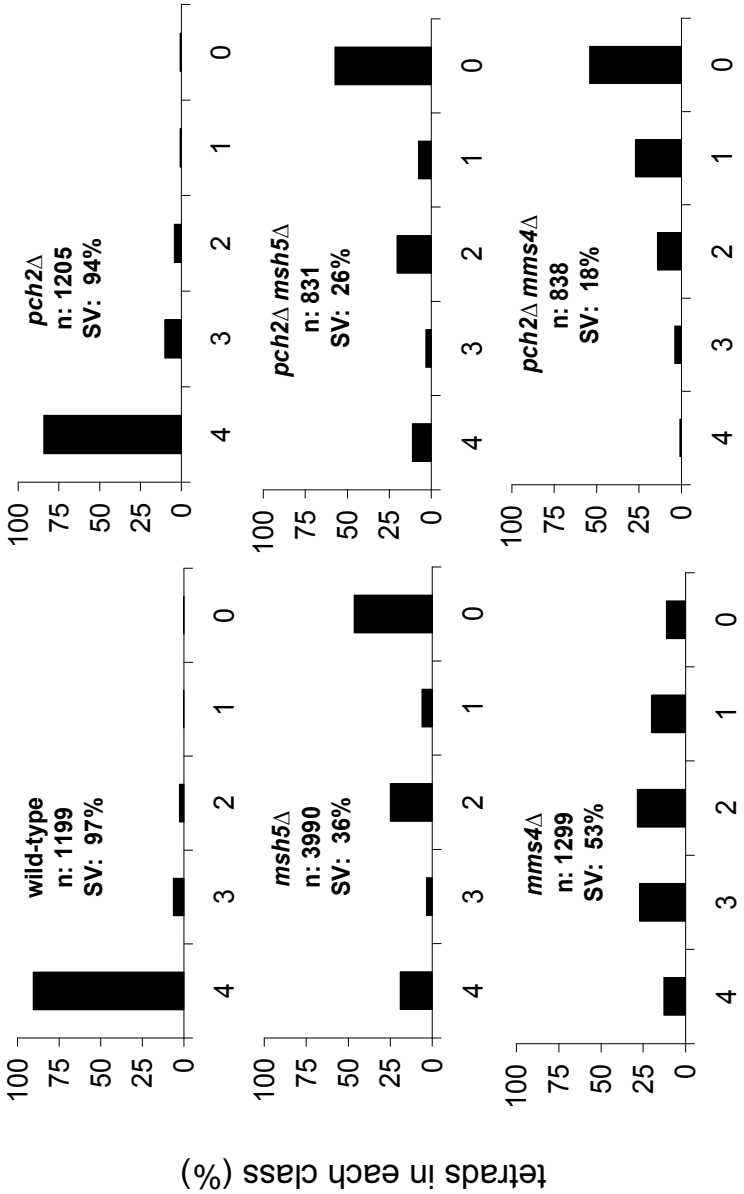
wild-type
n: 1199
SV: 97%
msh5Δ
n: 3990
SV: 36%
mms4Δ
n: 1299
SV: 53%
pch2Δ
n: 1205
SV: 94%
pch2Δ msh5Δ
n: 831
SV: 26%
pch2Δ mms4Δ
n: 838
SV: 18%
tetrads in each class (%)
number of viable spores per tetrad

Table 2-2. Genetic map distances calculated from four-spore viable tetrads.

The map distances in cM between the indicated markers and the number of each tetrad type observed (as calculated by RANA software; Argueso et al. [11]) are shown. Chromosome XV data were obtained from EAY background strains; chromosome III, VII and VIII data were obtained from NHY background strains. The Stahl lab online tools (http://www.molbio.uoregon.edu/~fstahl/) were used to calculate the genetic distances and standard errors (SE). p values for G-tests comparing the tetrad type distributions for all mutant combinations were calculated using the spreadsheet available from The Online Handbook of Biological Statistics (http://udel.edu/~mcdonald/statintro.html).

	4-spore viable tetrads	PD	TT	NPD	cM	SE	p values to wild-type	p values to *pch2*Δ	p values to *msh5*Δ
Chromosome XV									
URA3-LEU2									
wild-type	1087	607	456	5	22.8	1.0			
*pch2*Δ	1015	563	423	18	26.4	1.4	<0.0001		
*msh5*Δ	757	643	76	1	5.7	0.7	<0.0001	<0.0001	
*pch2*Δ *msh5*Δ	94	79	14	0	7.5	1.9	<0.0001	<0.0001	0.3620
LEU2-LYS2									
wild-type	1087	496	569	3	27.5	0.9			
*pch2*Δ	1015	395	561	39	40.0	1.8	<0.0001		
*msh5*Δ	757	562	155	3	12.0	1.0	<0.0001	<0.0001	
*pch2*Δ *msh5*Δ	94	74	17	1	12.5	3.7	<0.0001	<0.0001	0.5576
LYS2-ADE2									
wild-type	1087	803	263	2	12.9	0.8			
*pch2*Δ	1015	649	344	7	19.3	1.1	<0.0001		
*msh5*Δ	757	659	61	0	4.2	0.5	<0.0001	<0.0001	
*pch2*Δ *msh5*Δ	94	82	10	0	5.4	1.6	<0.0001	<0.0001	0.7296
ADE2-HIS3									
wild-type	1087	343	709	16	37.7	1.2			
*pch2*Δ	1015	243	638	115	66.7	2.3	<0.0001		
*msh5*Δ	757	496	215	9	18.7	1.5	<0.0001	<0.0001	
*pch2*Δ *msh5*Δ	94	54	37	2	26.3	4.9	<0.0001	<0.0001	0.0845
Chromosome III									
HIS4-LEU2									
wild-type	572	414	142	2	13.8	1.2			
*pch2*Δ	611	427	150	3	14.5	1.3	0.8093	0.0001	
spo11-HA	518	411	96	1	10.0	1.0	0.0016		
*pch2*Δ *spo11-HA*	556	438	100	1	9.8	1.0	0.0005	0.9772	0.0001

Table 2-2 (Continued)

	4-spore viable tetrads	PD	TT	NPD	cM	SE	p values to wild-type	p values to *pch2*Δ	p values to *msh5*Δ
LEU2-CEN3									
wild-type	572	499	70	0	6.2	0.7			
*pch2*Δ	611	503	100	0	8.3	0.8	0.0092	0.9995	
spo11-HA	518	429	85	0	8.3	0.8	0.0200		
*pch2*Δ *spo11-HA*	556	453	96	2	9.8	1.1	0.0004	0.1311	0.0939
CEN3-MAT									
wild-type	572	405	164	1	14.9	1.1			
*pch2*Δ	611	440	162	1	13.9	1.0	0.5796	0.0007	
spo11-HA	518	398	112	5	13.8	1.5	<0.0001		
*pch2*Δ *spo11-HA*	556	487	68	0	6.1	0.7	<0.0001	<0.0001	<0.0001
Chromosome VII									
TRP5-CYH2									
wild-type	572	202	352	12	37.5	1.9			
*pch2*Δ	611	153	371	67	65.4	3.6	<0.0001	<0.0001	
spo11-HA	518	155	336	22	45.6	2.6	0.0008		
*pch2*Δ *spo11-HA*	556	173	335	43	53.8	3.2	<0.0001	0.0006	0.0014
CYH2-MET13									
wild-type	572	452	104	0	9.4	0.8			
*pch2*Δ	611	372	156	5	17.5	1.5	<0.0001	<0.0001	
spo11-HA	518	378	102	0	10.6	0.9	0.3720		
*pch2*Δ *spo11-HA*	556	433	82	1	8.5	1.0	0.0730	0.0036	<0.0001
MET13-LYS5									
wild-type	572	335	209	5	21.8	1.5			
*pch2*Δ	611	273	243	17	32.4	2.4	<0.0001	<0.0001	
spo11-HA	518	277	204	1	21.8	1.3	0.0295		
*pch2*Δ *spo11-HA*	556	343	161	11	22.0	2.1	0.0005	<0.0001	<0.0001

Table 2-2 (Continued)

	4-spore viable tetrads	PD	TT	NPD	cM	SE	p values to wild-type	p values to *pch2*Δ	p values to *msh5*Δ
CEN8-THR1									
wild-type	572	319	221	2	21.5	1.3			
*pch2*Δ	611	302	228	7	25.1	1.7	0.0133	0.0227	
spo11-HA	518	309	195	3	21.0	1.4	0.4436		
*pch2*Δ *spo11-HA*	556	375	161	4	17.1	1.4	<0.0001	0.0001	<0.0001
THR1-CUP1									
wild-type	572	278	260	1	24.7	1.2			
*pch2*Δ	611	189	305	31	46.8	3.0	<0.0001	<0.0001	
spo11-HA	518	186	312	7	35.1	1.8	<0.0001		
*pch2*Δ *spo11-HA*	556	227	292	20	38.2	2.5	<0.0001	<0.0001	0.0027

parental ditype tetrads (Table 2-2). These data argue against the increase being due to multiple COs resulting from a single initiating DSB [52].

The effect of *pch2*Δ on crossing over on the small chromosome III was similar to that reported by San Segundo and Roeder [26], who saw no effect of the *pch2*Δ mutation on crossing over. We observed a significant increase in crossing over in *pch2*Δ in only one (*LEU2-CEN3*) of three genetic intervals (Figure 2-2B; Table 2-2). However, the overall map distance for the marked region in *pch2*Δ was 37 cM, which was not significantly different from wild-type (35 cM).

Gene conversion is elevated in pch2*Δ *mutants. The *pch2*Δ mutation conferred an increase in gene conversion for 15 of the 17 markers that were examined (Table 2-3). Two markers with the most dramatic increases in gene conversion were *met13* (2.4% in wild-type, 11.0% in *pch2*Δ) and *thr1* (5.1% in wild-type, 11.9% in *pch2*Δ), both in the NHY strain background. Tetrads in which high levels of gene conversion were observed (*THR1*, chromosome VIII, *MET13*, chromosome VII) were analyzed for exchange of flanking markers (Table 2-4; see [32]). For example, tetrads containing *MET13* gene conversions were scored in the CO class if *LYS5* and *CYH2* markers were non-parental ditype or tetratype, but were in the NCO class if those markers were parental ditype. A ratio of CO:NCO was then computed from these classes. At *MET13*, the CO:NCO ratio was 1.8 in wild-type and 2.6 in *pch2*Δ, but this difference was not statistically significant (G-test where $p<0.05$ is significant). At *THR1* the ratio was 1.9 in wild-type and 9.4 in *pch2*Δ ($p<0.0001$; Table 2-4). Assuming no change in DSB formation in *pch2*Δ (see below), these data suggest that at least for the *THR1* locus, the increase in crossing over observed in *pch2*Δ was accompanied by a relative decrease in noncrossover events. However, more extensive genetic analyses at multiple loci, using markers that can eliminate incidental COs, will be required to solidify this observation (see Discussion).

Table 2-3. *pch2*Δ increases the frequency of aberrant marker segregation.

The percent of non 2:2 marker segregations were calculated for the indicated loci. Chromosome XV data were obtained from EAY background strains; chromosomes III, VII, and VIII data were obtained from NHY background strains. Most events were 3:1 or 1:3 gene conversions although one 4:0 event in the EAY background and two 4:0 events in the NHY background were observed in pch2Δ mutants. In addition, one post-meiotic segregation event (5:3) was observed in the *pch2*Δ *spo11-HA* mutant.

Chromosome XV

	Tetrads	*TRP1*	*URA3*	*LEU2*	*LYS2*	*ADE2*	*HIS3*	Total
wild-type	1087	0.0	0.0	0.2	0.6	0.1	0.8	1.7
*pch2*Δ	1015	0.3	0.2	1.1	0.4	0.4	1.5	3.9
*msh5*Δ	757	0.1	0.1	1.6	1.2	0.8	1.2	5.0
*pch2*Δ *msh5*Δ	94	0.0	0.0	1.1	1.1	1.1	0.0	3.3

Chromosome III

	Tetrads	*HIS4*	*LEU2*	*ADE2*	*MATa*	Total
wild-type	572	2.1	0.3	0.2	0.2	2.8
*pch2*Δ	611	3.8	1.3	0.0	1.3	6.4
spo11-HA	518	1.2	0.8	0.0	0.6	2.6
*pch2*Δ *spo11-HA*	556	2.2	0.9	0.0	0.2	3.3

Chromosome VII

	Tetrads	*LYS5*	*MET13*	*CYH2*	*TRP5*	Total
wild-type	572	1.6	2.4	0.3	0.7	5.0
*pch2*Δ	611	1.8	11.0	1.8	1.5	16.1
spo11-HA	518	0.2	6.8	0.6	0.4	8.0
*pch2*Δ *spo11-HA*	556	0.4	7.0	0.2	0.7	8.3

Chromosome VIII

	Tetrads	*URA3*	*THR1*	*CUP1*	Total
wild-type	572	0.2	5.1	0.7	6.0
*pch2*Δ	611	0.2	11.9	2.1	14.2
spo11-HA	518	0.0	2.1	0.4	2.5
*pch2*Δ *spo11-HA*	556	0.0	2.9	0.2	3.1

Table 2-4. CO:NCO ratio of markers flanking gene conversion events on chromosomes VII and VIII.

Tetrads containing a gene conversion at the *MET13* or *THR1* loci were analyzed in wild-type and p*ch2*Δ mutants in the NHY background. The markers flanking the gene conversion event were scored as CO (TT or NPD) or NCO (PD) and the CO:NCO ratio was calculated at each site. The wild-type and *pch2*Δ CO and NCO numbers were compared using a G-test and the p values are shown.

	4-spore viable tetrads	***MET13* conversions**	**CO (*LYS5-CYH2*)**	**NCO (*LYS5-CYH2*)**	**CO:NCO ratio**	**p value**
wild-type	572	14	9	5	1.8	
*pch2*Δ	611	65	47	18	2.6	0.169
	4-spore viable tetrads	***THR1* conversions**	**CO (*CEN8-CUP1*)**	**NCO (*CEN8-CUP1*)**	**CO:NCO ratio**	**p value**
wild-type	572	29	19	10	1.9	
*pch2*Δ	611	73	66	7	9.4	<0.0001

Genetic analysis of meiotic CO control.

Pch2 is required for wild-type levels of CO interference. The crossover phenotype of *pch2*Δ mutants, increased crossing over on large chromosomes, encouraged us to test a role for Pch2 in CO interference. As shown below, our data, and work by Joshi *et al*. [53], indicate that *pch2*Δ mutants are defective in CO interference. We employed three methods to measure CO interference. First, we measured the NPD ratio for those loci in which a significant number of NPD events were expected (>10; chromosome III data are thus excluded) using Stahl's "Better Way" calculator. This method compares the observed number of each tetrad class (NPD, PD and TT), to the numbers expected if CO distribution was random [54-56]. In the absence of CO interference, the NPD ratio is expected to be one. Values significantly less than one reflect the presence of CO interference with smaller numbers indicating stronger interference. We found *pch2*Δ mutants had a larger NPD ratio than wild-type in all genetic intervals in both strain backgrounds (Table 2-5). In the EAY strain, statistically significant levels of interference were seen in all genetic intervals in wild-type and in two of three intervals in *pch2*Δ (where $p<0.05$ is considered significant; see Table 2-5). In the NHY strain interference was seen in all four intervals in wild-type, but in only one interval in *pch2*Δ (Table 2-5). These results are similar to those reported for a previously identified interference mutant *tid1*. Shinohara and colleagues found that *tid1* mutants showed larger NPD ratios than wild-type in all six genetic intervals assayed and a decrease in the number of intervals where interference was statistically significant, from five in wild-type to three in *tid1* [34, 57].

Second, we measured the coefficient of coincidence (COC). This method compares the observed number of times that a CO occurs in each of two adjacent genetic intervals to the number of such double COs expected due to chance. In the

Table 2-5. Interference calculations using NPD ratios.

The number of NPDs was compared to the expected number using the Stahl Online Laboratory "Better Way" calculator (http//www.molbio.uoregon.edu/~fstahl/). Chromosome XV data were obtained from EAY background strains; chromosomes III, VII, and VIII data were obtained from NHY background strains. The total number of 4-spore viable tetrads used for analysis is shown. The number of PD, NPD and TT tetrads can be found in Table 1. p values were calculated from the chi-square values provided by the "Better Way" program using Vasserstats (http://faculty.vassar.edu/lowry/VassarStats.html) chi-square to p calculator with one degree of freedom. "I" indicates if interference was statistically detectable.

	4-spore viable tetrads	NPD obs.	NPD exp.	obs./exp.	p	I
Chromosome XV						
URA3-LEU2						
wild-type	1087	5	27.7	0.18	<0.0001	YES
*pch2*Δ	1015	18	28.7	0.63	0.0212	YES
LEU2-LYS2						
wild-type	1087	3	43.2	0.07	<0.0001	YES
*pch2*Δ	1015	39	58.8	0.66	0.0011	YES
ADE2-HIS3						
wild-type	1087	16	74.8	0.21	<0.0001	YES
*pch2*Δ	1015	115	117.0	0.98	0.7522	NO
Chromosome VII						
TRP5-CYH2						
wild-type	572	12	36.0	0.33	<0.0001	YES
*pch2*Δ	611	67	66.4	1.00	0.9191	NO
spo11-HA	518	22	41.6	0.53	<0.0001	YES
*pch2*Δ *spo11-HA*	556	43	47.9	0.90	0.3362	NO
MET13-LYS5						
wild-type	572	5	11.8	0.42	0.0256	YES
*pch2*Δ	611	17	20.0	0.85	0.4298	NO
spo11-HA	518	1	12.0	0.08	0.0003	YES
*pch2*Δ *spo11-HA*	556	11	8.7	1.26	0.3834	NO
Chromosome VIII						
CEN8-THR1						
wild-type	572	2	12.6	0.16	0.0007	YES
*pch2*Δ	611	7	14.9	0.47	0.0185	YES
spo11-HA	518	3	10.7	0.28	0.0077	YES
*pch2*Δ *spo11-HA*	556	4	7.0	0.57	0.2138	NO

Table 2-5 (Continued)

THR1-CUP1						
wild-type	572	1	17.5	0.06	<0.0001	YES
pch2Δ	611	31	37.4	0.83	0.1725	NO
spo11-HA	518	7	30.2	0.23	<0.0001	YES
pch2Δ spo11-HA	556	20	29.1	0.69	0.0359	YES

absence of interference, the COC value is expected to equal one. Values significantly less than one indicate interference, with smaller numbers indicating stronger interference. All intervals in the two strain backgrounds displayed COC values that were higher in *pch2*Δ than in wild-type (Table 2-6). For three intervals, interference could not be detected in either wild-type or *pch2*Δ. In one interval, interference was seen in wild-type, but not *pch2*Δ. For the remaining four intervals, interference was seen in both wild-type and *pch2*Δ, but was weaker in *pch2*Δ.

Lastly, we employed the method of Malkova *et al.* [37] to analyze CO interference. This method compares the map distance calculated for a given interval when a CO has occurred in the adjacent interval to the map distance calculated for the same given interval when a CO has not occurred in the adjacent interval. In the absence of interference, these map distances are expected to be the same and a ratio of the map distances is equal to one. However, in the presence of interference, a CO in one interval would make a nearby CO less likely. This would cause the map distance ratio to be less than one, with smaller ratios resulting from stronger interference [37]. In both strain backgrounds the map distance ratios were larger in *pch2*Δ than wild-type for all adjacent interval pairs, indicating that, as seen with the NPD ratio and COC tests, *pch2*Δ disrupted CO interference (Figure 2-5; Table 2-7). In the EAY strain background, G-tests indicated that interference was statistically detectable in wild-type between all three interval pairs, but was detectable between only two interval pairs in *pch2*Δ (Figure 2-5A; Table 2-7). In the NHY strain background, interference was statistically detectable in *pch2*Δ for two out of five interval pairs, although it was weaker than in wild-type. For one interval pair, interference was not detected in *pch2*Δ, whereas it was present in wild-type. For the remaining two intervals, interference was not detected in wild-type or *pch2*Δ (Figure 2-5B; Table 2-7). We saw no evidence of chromatid interference in any strain analyzed in this study.

Table 2-6. Interference calculations using coefficients of coincidence.

Chromosome XV data were obtained from EAY background strains; chromosomes III, VII and VIII data were obtained from NHY background strains. The number of double crossovers observed was compared to the expected number (as calculated by RANA software; [11]) for the EAY (A) and NHY (B) strain backgrounds. Two-tailed p values were calculated using the Vasserstats binomial properties calculator using a normal distribution. "I" indicates if interference was statistically detectable.

	4-spore viable tetrads	DCO obs.	DCO exp.	COC	p	I
Chromosome XV						
URA3-LEU2-LYS2						
wild-type	1087	177	246.9	0.72	<0.0001	YES
*pch2*Δ	1015	232	265.9	0.87	0.017	YES
LEU2-LYS2-ADE2						
wild-type	1087	65	141.9	0.46	<0.0001	YES
*pch2*Δ	1015	181	210.6	0.86	0.024	YES
LYS2-ADE2-HIS3						
wild-type	1087	158	179.9	0.88	0.080	NO
*pch2*Δ	1015	258	265.4	0.97	0.624	NO
Chromosome III						
HIS3-LEU2-CEN3						
wild-type	572	5	17.7	0.28	0.003	YES
*pch2*Δ	611	14	25.4	0.55	0.027	YES
spo11-HA	518	8	16.0	0.50	0.057	NO
*pch2*Δ *spo11-HA*	556	11	18.0	0.61	0.119	NO
LEU2-CEN3-MAT						
wild-type	572	17	20.3	0.84	0.529	NO
*pch2*Δ	611	31	27.0	1.15	0.490	NO
spo11-HA	518	16	19.3	0.83	0.516	NO
*pch2*Δ *spo11-HA*	556	17	12.0	1.42	0.190	NO
Chromosome VII						
TRP5-CYH2-MET13						
wild-type	572	59	68.1	0.87	0.267	NO
*pch2*Δ	611	122	132.3	0.92	0.337	NO
spo11-HA	518	63	76.1	0.83	0.119	NO
*pch2*Δ *spo11-HA*	556	55	60.8	0.91	0.472	NO
CYH2-MET13-LYS5						
wild-type	572	20	40.5	0.49	0.001	YES
*pch2*Δ	611	69	78.5	0.88	0.276	NO
spo11-HA	518	17	43.4	0.39	<0.0001	YES
*pch2*Δ *spo11-HA*	556	25	27.7	0.91	0.667	NO
Chromosome VIII						
CEN8-THR1-CUP1						
wild-type	572	67	108.0	0.62	<0.0001	YES
*pch2*Δ	611	125	150.4	0.83	0.019	YES
spo11-HA	518	85	125.1	0.68	<0.0001	YES
*pch2*Δ *spo11-HA*	556	76	95.5	0.80	0.032	YES

Figure 2-5. CO interference is reduced in absence of Pch2.

Interference was measured using the method of Malkova *et al.* [32, 37] for strains in the EAY (A) and NHY (B) strain backgrounds. For each interval, the map distance was separately calculated for tetrads in which the adjacent interval had (+) or did not have (-) a CO event. If the two map distances are significantly different (G-test), then CO interference is present between the two intervals. The ratio of the CO+ to CO- map distances gives the strength of the interference, with values nearer to zero indicating stronger interference. The average interference ratio between adjacent genetic intervals is shown above the intervals. Solid lines indicate interference was statistically significant when either interval was used as the reference. The broken lines indicate interference was not statistically significant when one or both intervals were used as the reference. See Table 2-7 for raw data and statistical analyses.

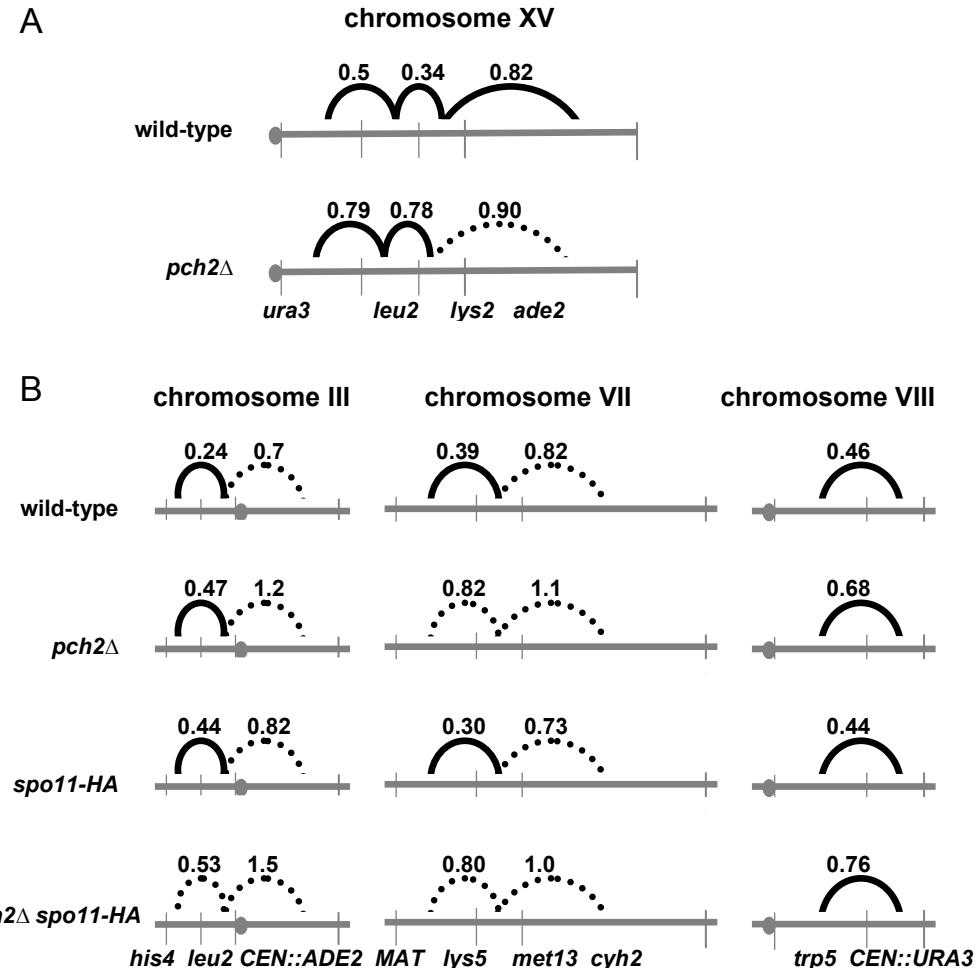
A
chromosome XV
0.5
0.34
0.82
wild-type
0.79
0.78
0.90
pch2Δ
ura3
leu2
lys2
ade2
B
chromosome III
chromosome VII
chromosome VIII
0.24
0.7
0.39
0.82
0.46
wild-type
0.47
1.2
0.82
1.1
0.68
pch2Δ
0.44
0.82
0.30
0.73
0.44
spo11-HA
0.53
1.5
0.80
1.0
0.76
pch2Δ spo11-HA
his4
leu2
CEN::ADE2
MAT
lys5
met13
cyh2
trp5
CEN::URA3

Table 2-7. Interference calculations using the method of Malkova et al. [37].

Chromosome XV data were obtained from EAY background strains; chromosomes III, VII, and VIII data were obtained from NHY background strains. All pair-wise comparisons between adjacent intervals are shown. The top genetic interval listed in each box is the reference interval. All tetrads were divided into two classes: those with (CO +; i.e. NPD or TT) and those without (CO-; i.e. PD) an observable CO event within the reference interval using Mactetrad 6.9. The genetic size and standard error (SE) of the adjacent genetic interval (the lower listing at the top of the box) was then calculated for each class (CO+ and CO-) using the Stahl Laboratory Online Tools (http://molbio.uoregon.edu/~fstahl/). A ratio of the CO+/CO- class cM values was computed. Interference was considered significant if the CO+ and CO- classes were found to be significantly different via G-tests calculated using the spreadsheet available from The Online Handbook of Biological Statistics (http://udel.edu/~mcdonald/statintro.html).

Chromosome XV

Reference		*URA3-LEU2* *LEU2-LYS2*							*URA3-LEU2* *LYS2-ADE2*						
	CO	PD	TT	NPD	cM	SE	ratio	p value	PD	TT	NPD	cM	SE	ratio	p value
wild-type	+	284	177	0	19.2 ±	1.1			346	115	0	12.5 ±	1.0		
	-	212	392	3	33.8 ±	1.2	0.568	<0.0001	457	148	2	13.2 ±	1.1	0.947	0.212
*pch2*Δ	+	203	214	18	37.0 ±	2.9			288	143	4	19.2 ±	1.7		
	-	190	347	21	42.4 ±	2.4	0.873	<0.0001	353	199	3	19.6 ±	1.3	0.980	0.284
Reference		*URA3-LEU2* *ADE2-HIS3*							*LEU2-LYS2* *URA3-LEU2*						
	CO	PD	TT	NPD	cM	SE	ratio	p value	PD	TT	NPD	cM	SE	ratio	p value
wild-type	+	163	294	4	34.5 ±	1.8			395	176	1	15.9 ±	1.1		
	-	180	415	12	40.1 ±	1.6	0.860	0.007	212	280	4	30.6 ±	1.6	0.520	<0.0001
*pch2*Δ	+	114	270	50	65.7 ±	4.2			368	224	8	22.7 ±	1.6		
	-	129	359	64	67.3 ±	3.7	0.976	0.360	190	193	10	32.2 ±	2.5	0.705	<0.0001
Reference		*LEU2-LYS2* *LYS2-ADE2*							*LEU2-LYS2* *ADE2-HIS3*						
	CO	PD	TT	NPD	cM	SE	ratio	p value	PD	TT	NPD	cM	SE	ratio	p value
wild-type	+	507	65	0	5.7 ±	0.7			186	378	8	37.2 ±	1.6		
	-	296	198	2	21.2 ±	1.4	0.269	<0.0001	157	331	8	38.2 ±	1.8	0.974	0.843
*pch2*Δ	+	418	176	5	17.2 ±	1.4			148	385	60	62.8 ±	3.4		
	-	225	166	2	22.7 ±	1.6	0.758	<0.0001	93	240	52	71.7 ±	4.7	0.876	0.043

Table 2-7 (Continued)

Reference			*LYS2-ADE2* *URA3-LEU2*								*LYS2-ADE2* *LEU2-LYS2*						
	CO	PD	TT	NPD	cM		SE	ratio	p value	PD	TT	NPD	cM		SE	ratio	p value
wild-type	+	150	115	0	21.7	±	1.5			200	64	1	13.2	±	2.0		
	-	457	351	5	23.1	±	1.2	0.939	0.195	396	505	2	32.2	±	1.0	0.410	<0.0001
*pch2*Δ	+	202	142	5	24.6	±	2.2			168	169	12	34.5	±	3.0		
	-	353	275	13	27.5	±	1.8	0.895	0.454	225	391	27	43.0	±	2.3	0.802	<0.0001
Reference			*LYS2-ADE2* *ADE2-HIS3*								*ADE2-HIS3* *URA3-LEU2*						
	CO	PD	TT	NPD	cM		SE	ratio	p value	PD	TT	NPD	cM		SE	ratio	p value
wild-type	+	107	153	5	34.5	±	2.7			427	294	4	21.9	±	1.2		
	-	236	556	11	38.7	±	1.4	0.891	0.0004	180	160	1	24.5	±	1.6	0.894	0.002
*pch2*Δ	+	87	219	39	65.7	±	4.7			423	310	10	24.9	±	1.5		
	-	154	413	74	66.9	±	3.4	0.982	0.875	129	106	8	31.7	±	3.4	0.785	0.001
Reference			*ADE2-HIS3* *LEU2-LYS2*								*ADE2-HIS3* *LYS2-ADE2*						
	CO	PD	TT	NPD	cM		SE	ratio	p value	PD	TT	NPD	cM		SE	ratio	p value
wild-type	+	339	384	2	27.3	±	1.0			567	156	2	11.6	±	0.9		
	-	157	185	1	27.8	±	2.0	0.982	0.867	236	102	0	15.6	±	1.3	0.744	<0.0001
*pch2*Δ	+	292	418	27	39.4	±	2.1			487	255	3	18.3	±	1.1		
	-	93	137	11	42.1	±	4.0	0.936	0.447	154	83	4	22.2	±	2.8	0.824	0.005

Table 2-7 (Continued)

Chromosome III

Reference		*HIS4-LEU2* *LEU2-CEN3*								*HIS4-LEU2* *CEN3-MAT*							
	CO	PD	TT	NPD	cM		SE	ratio	p value	PD	TT	NPD	cM		SE	ratio	p value
wild-type	+	140	5	0	1.7	±	0.8			111	32	1	13.2	±	2.6		
	-	349	63	0	7.7	±	0.9	0.221	<0.0001	284	128	0	15.5	±	1.1	0.852	<0.0001
*pch2*Δ	+	139	14	0	4.6	±	1.2			107	44	0	14.6	±	1.9		
	-	345	81	0	9.5	±	1.0	0.484	0.003	310	109	1	13.7	±	1.3	1.07	0.480
spo11-HA	+	89	8	0	4.1	±	1.4			77	18	1	12.5	±	3.6		
	-	335	76	0	9.3	±	1.0	0.441	0.017	310	95	4	14.6	±	1.8	0.856	0.567
*pch2*Δ *spo11-HA*	+	90	11	0	5.5	±	1.6			93	8	0	4.0	±	1.3		
	-	353	82	2	10.8	±	1.3	0.509	0.058	378	58	0	6.7	±	0.8	0.597	0.234
Reference		*LEU2-CEN3* *HIS4-LEU2*								*LEU2-CEN3* *CEN3-MAT*							
	CO	PD	TT	NPD	cM		SE	ratio	p value	PD	TT	NPD	cM		SE	ratio	p value
wild-type	+	63	5	0	3.7	±	1.6			53	17	0	12.1	±	2.6		
	-	349	139	1	14.8	±	1.2	0.25	<0.0001	350	147	1	15.4	±	1.2	0.786	0.533
*pch2*Δ	+	81	14	0	7.4	±	1.8			68	31	0	15.7	±	2.3		
	-	345	136	3	15.9	±	1.4	0.465	0.004	366	128	1	13.5	±	1.1	1.16	0.398
spo11-HA	+	76	8	0	4.8	±	1.6			69	15	1	12.4	±	4.0		
	-	335	88	1	11.1	±	1.2	0.432	0.017	324	98	4	14.3	±	1.7	0.867	0.475

Table 2-7 (Continued)

Reference		*LEU2-CEN3* *HIS4-LEU2*								*LEU2-CEN3* *CEN3-MAT*							
	CO	PD	TT	NPD	cM		SE	ratio	p value	PD	TT	NPD	cM		SE	ratio	p value
pch2Δ spo11-HA	+	84	11	0	5.8	±	1.6			81	17	0	8.7	±	1.9		
	-	353	89	1	10.7	±	1.2	0.542	0.069	401	50	0	5.5	±	0.7	1.58	0.183

Reference		*CEN3-MAT* *HIS4-LEU2*								*CEN3-MAT* *LEU2-CEN3*							
	CO	PD	TT	NPD	cM		SE	ratio	p value	PD	TT	NPD	cM		SE	ratio	p value
wild-type	+	128	33	0	10.3	±	1.6			148	17	0	5.2	±	1.2		
	-	284	110	1	14.7+	±	1.3	0.701	0.064	350	53	0	6.6	±	0.8	0.787	0.534
pch2Δ	+	110	43	1	15.9	±	2.6			129	31	0	9.7	±	1.6		
	-	310	105	2	14.0	±	1.4	1.14	0.703	366	68	0	7.8	±	0.9	1.24	0.456
spo11-HA	+	99	19	0	8.1	±	1.7			102	16	0	6.8	±	1.6		
	-	310	76	1	10.6	±	1.3	0.764	0.445	324	69	0	8.8	±	1.0	0.773	0.499
pch2Δ spo11-HA	+	58	8	0	6.1	±	2.0			50	17	0	12.7	±	2.7		
	-	378	92	1	10.4	±	1.1	0.587	0.235	401	79	2	9.4	±	1.2	1.35	0.136

Chromosome VIII

Reference		*CEN8-THR1* *THR1-CUP1*								*THR1-CUP1* *CEN8-THR1*							
	CO	PD	TT	NPD	cM		SE	ratio	p value	PD	TT	NPD	cM		SE	ratio	p value
wild-type	+	154	67	0	15.2	±	1.6			194	67	0	12.8	±	1.4		
	-	123	193	1	31.4	±	1.6	0.484	<0.0001	123	152	2	29.6	±	2.0	0.432	<0.0001

Table 2-7 (Continued)

Reference		*CEN8-THR1* *THR1-CUP1*							*THR1-CUP1* *CEN8-THR1*						
	CO	PD	TT	NPD	cM	SE	ratio	p value	PD	TT	NPD	cM	SE	ratio	p value
pch2Δ	+	108	113	12	39.7 ±	4.3			212	122	3	20.8 ±	1.9		
	-	80	193	19	52.6 ±	4.0	0.755	<0.0001	80	104	4	34.0 ±	3.4	0.612	<0.0001
spo11-HA	+	112	85	0	21.6 ±	1.8			234	85	0	13.3 ±	1.2		
	-	74	227	7	43.7 ±	2.5	0.494	<0.0001	74	109	3	34.1 ±	3.1	0.39	<0.0001
pch2Δ spo11-HA	+	88	67	9	36.9 ±	5.3			236	75	1	13.0 ±	1.5		
	-	139	225	11	38.8 ±	2.7	0.951	<0.0001	139	85	3	22.7 ±	2.7	0.573	<0.0001

Chromosome VII

Reference		*TRP5-CYH2* *CYH2-MET13*							*TRP5-CYH2* *MET13-LYS5*						
	CO	PD	TT	NPD	cM	SE	ratio	p value	PD	TT	NPD	cM	SE	ratio	p value
wild-type	+	295	59	0	8.3 ±	1.0			225	118	3	19.7 ±	1.9		
	-	154	44	0	11.1 ±	1.5	0.748	0.034	109	87	1	23.6 ±	2.3	0.835	0.001
pch2Δ	+	275	116	5	18.4 ±	2.0			193	183	12	32.9 ±	2.7		
	-	93	38	0	14.5 ±	2.0	1.27	0.187	71	53	5	32.2 ±	5.2	1.02	0.049
spo11-HA	+	265	63	0	9.6 ±	1.1			187	140	0	21.4 ±	1.4		
	-	110	39	0	13.1 ±	1.8	0.733	0.012	85	63	1	23.2 ±	2.8	0.922	0.110
pch2Δ spo11-HA	+	297	54	1	8.5 ±	1.3			235	109	6	20.7 ±	2.3		
	-	133	28	0	8.7 ±	1.5	0.977	0.497	105	51	5	25.2 ±	4.3	0.821	0.242

Table 2-7 (Continued)

Reference		*CYH2-MET13* *TRP5-CYH2*								*CYH2-MET13* *MET13-LYS5*						
	CO	PD	TT	NPD	cM		SE	ratio	p value	PD	TT	NPD	cM		SE	ratio	p value
wild-type	+	44	57	2	33.5	±	4.4			82	20	0	9.8	±	2.0		
	-	154	286	9	37.9	±	2.1	0.884	0.206	253	187	5	24.4	±	1.8	0.402	<0.0001
pch2Δ	+	38	108	13	58.5	±	6.0			89	65	3	26.4	±	3.6		
	-	93	227	48	70.0	±	4.8	0.836	0.109	180	174	14	35.1	±	3.0	0.752	0.088
spo11-HA	+	39	61	2	35.8	±	4.4			85	17	0	8.3	±	1.9		
	-	110	245	20	48.7	±	3.3	0.735	0.053	189	186	1	25.5	±	1.5	0.325	<0.0001
pch2Δ spo11-HA	+	28	47	8	57.2	±	9.1			58	24	1	18.1	±	4.2		
	-	133	266	31	52.6	±	3.5	1.09	0.550	285	136	10	22.7	±	2.3	0.797	0.637
Reference		*MET13-LYS5* *TRP5-CYH2*								*MET13-LYS5* *CYH2-MET13*						
	CO	PD	TT	NPD	cM		SE	ratio	p value	PD	TT	NPD	cM		SE	ratio	p value
wild-type	+	88	120	1	30.1	±	2.1			192	20	0	4.7	±	1.0		
	-	109	218	7	38.9	±	2.5	0.774	0.004	253	82	0	12.2	±	1.2	0.385	<0.0001
pch2Δ	+	58	167	28	66.2	±	5.3			188	65	3	16.2	±	2.4		
	-	71	162	31	65.9	±	5.4	1.00	0.282	180	87	2	18.4	±	2.1	0.88	0.044
spo11-HA	+	64	128	12	49.0	±	4.7			187	17	0	4.2	±	1.0		
	-	85	177	10	43.6	±	3.3	1.12	0.293	189	85	0	15.5	±	1.4	0.271	<0.0001
pch2Δ spo11-HA	+	56	103	12	51.2	±	5.5			146	25	0	7.3	±	1.4		
	-	105	208	27	54.4	±	4.1	0.941	0.817	285	57	1	9.2	±	1.3	0.793	0.465

We also found no evidence for negative interference between genetic intervals on different chromosomes or between widely spaced intervals on the same chromosome in *pch2*Δ*,* suggesting that the decreases in positive interference we observed did not result from variability in recombination between meioses (data not shown; [58, 59]).

Pch2 is required for maintaining spore viability in spo11 hypomorphs. Previously, Martini *et al.* [32] observed that CO levels were maintained at the expense of NCOs when meiotic DSBs became limiting in *spo11* hypomorphs showing reduced DSB levels (20-80%; [24, 32, 33, 60]). This homeostasis mechanism is thought to ensure obligate CO formation between all homologous chromosome pairs and thereby promote spore viability. If interference and homeostasis result from a common mechanism, a mutation disrupting CO interference (e.g. *pch2*Δ) would severely compromise the spore viability of *spo11* hypomorph strains [33].

We tested the effect of the *pch2*Δ mutation on the spore viability of *spo11* hypomorph strains (NHY background). As shown in Figure 2-3, spore viability was similar in wild-type (91%) and the *spo11-HA/spo11-HA* hypomorph (91%), which displays 80% of the wild-type level of DSBs. These results confirm work by Martini *et al.* [32]. Interestingly, the *pch2*Δ*/pch2*Δ *spo11-HA/spo11-HA* mutant displayed significantly lower spore viability, 73%, despite having CO levels (165 cM total) that were similar to *spo11-HA/spo11-HA* (166 cM) and above wild-type levels (150 cM; Figures 2-2 and 2-3). Spore viability in *pch2*Δ strains was compromised even further, relative to *PCH2*, in strains bearing more defective *spo11* alleles (Figure 2-3; 86% spore viability in *spo11-HA/spo11yf-HA* vs. 16% in *pch2*Δ*/pch2*Δ *spo11-HA/spo11yf-HA*; 50% in *spo11da-HA/spo11da-HA* vs. 1% in *pch2*Δ*/pch2*Δ *spo11da-HA/spo11da-HA*). We also observed that the *pch2-G319A* mutation, which maps to the Walker A motif and is predicted to disrupt Pch2 ATP binding/hydrolysis activities [26, 47], is

unable to complement the *pch2*Δ mutation (S. Zanders, J. Olszewski, M. Dowicki, E. Alani, unpublished data).

The excess of tetrads with 4, 2, and 0 viable spores per tetrad observed in the *pch2*Δ *spo11*-hypomorph double mutants suggests that the spore death results from MI chromosome nondisjunction, although we are unable to rule out additional causes (see Discussion). In support of this, we observed that 68% (n=130) of two-spore viable tetrads were sisters in the *pch2*Δ*/pch2*Δ *spo11-HA/spo11-HA* double mutant, as determined by the centromere-linked markers *URA3* and *ADE2*. This was higher than what we observed in *spo11-HA/spo11-HA* and *pch2*Δ*/pch2*Δ where only 35% (n=52) and 48% (n=29), respectively, of the two-spore viable tetrads were sisters (G-test where $p<0.025$ is significant due to correction for multiple comparisons). We also observed significantly more (9/936) tetrads in which chromosome III had undergone MI nondisjunction, as determined by the *ADE2* centromere-linked marker and an inability to mate, in the *pch2*Δ*/pch2*Δ *spo11-HA/spo11-HA* double mutant as compared to *spo11-HA/spo11-HA* (0/649) and *pch2*Δ*/pch2*Δ (1/707). Together these observations are consistent with Pch2 regulating the distribution of CO events required to promote MI disjunction.

The interference defect in pch2*Δ *is not dependent upon extra COs. Previous studies suggested that the CO interference mechanism is intact in *ndj1* and *csm4* mutants but appears to be disrupted due to excess non-interfering COs [7, 8, 10, 15, 23, 45]. We entertained such a mechanism to explain the interference defect in *pch2*Δ by examining interference in *pch2*Δ *spo11* hypomorphs and *pch2*Δ mutants defective in the non-interfering (Mms4-Mus81) and interfering (Msh4-Msh5) CO pathways. As described below, our data do not support the excess non-interfering CO hypothesis.

First, *pch2*Δ*/pch2*Δ *spo11-HA/spo11-HA* mutants showed interference defects similar to *pch2*Δ */pch2*Δ (Figures 2-2, 2-5B; Tables 2-5, 2-6, 2-7). This defect was

seen even though the total number of COs decreased from 224 cM in *pch2*Δ/*pch2*Δ to 165 cM in *pch2*Δ/*pch2*Δ *spo11-HA/spo11-HA*.

Second, we tested if the decreased interference in *pch2*Δ was due to additional COs formed through the Mms4-Mus81 non-interfering CO pathway. This was done by analyzing *pch2*Δ *mms4*Δ and *pch2*Δ *msh5*Δ tetrads in the EAY strain background. The *pch2*Δ *mms4*Δ mutant had considerably lower spore viability (18%) than the *mms4*Δ mutant (53%; Figure 2-4). Overall, the recombination frequency of *pch2*Δ *mms4*Δ spores was about 14% higher than *mms4*Δ spores, but still lower than *pch2*Δ (Figure 2-1C; Table 2-8). In three out of four genetic intervals, the recombination frequencies were significantly higher in *pch2*Δ *mms4*Δ than in *mms4*Δ spores (G-test where $p<0.025$ is considered significant due to Dunn-Sidak correction for multiple comparisons; Table 2-8). These data suggest that the elevated crossing over seen in *pch2*Δ was not solely due to Mms4-Mus81-specific crossing over.

The spore viability of the *pch2*Δ *msh5*Δ mutant was 26%, compared to 36% for the *msh5*Δ single mutant (Figure 2-4). Like the *mms4*Δ mutant, overall CO frequencies (in tetrads and spores) were higher in the *pch2*Δ *msh5*Δ double mutant than in *msh5*Δ (~30%; Figures 2-1B, 2-1C; Tables 2-2, 2-8), but were much lower than in *pch2*Δ. When only data from complete tetrads were compared, there were no statistically significant difference between *msh5*Δ and *pch2*Δ *msh5*Δ (G-test where $p<0.025$ is considered significant due to Dunn-Sidak correction for multiple tests). However, when data from all surviving spores were analyzed, *pch2*Δ *msh5*Δ had significantly higher recombination frequencies than *msh5*Δ in two out of the four genetic intervals (G-test where $p<0.025$ is considered significant due to Dunn-Sidak correction for multiple tests). A caveat to these analyses is that the low spore viabilities observed in both the *pch2*Δ *mms4*Δ and *pch2*Δ *msh5*Δ mutants constrained analysis to a selected minority of meiotic products. Together, these data are consistent

Table 2-8. Genetic recombination frequencies in spores.

The recombination frequencies between the indicated markers and the number of parental and recombinant spores (as calculated by RANA software; Argueso et al. [11]) in the EAY strain background are shown. p values for G-tests comparing the recombinant and parental spore numbers for all mutant combinations were calculated using the spreadsheet available from The Online Handbook of Biological Statistics (http://udel.edu/~mcdonald/statintro.html).

Chromosome XV

	Total Spores	Recombinant	Parental	% Recombinant	p values to wild-type	to *pch2*Δ	to *msh5*Δ	to *pch2*Δ *msh5*Δ	to *mms4*Δ
URA3-LEU2									
wild-type	4644	1009	3635	21.7					
*pch2*Δ	4538	1067	3471	23.5	0.0039				
*msh5*Δ	5674	322	5352	5.7	<0.0001	<0.0001			
*pch2*Δ *msh5*Δ	859	83	776	9.7	<0.0001	<0.0001	<0.0001		
*mms4*Δ	2732	505	2227	18.5	<0.0001	<0.0001	<0.0001	<0.0001	
*mms4*Δ *pch2*Δ	591	98	49	16.6	0.0017	<0.0001	<0.0001	<0.0001	0.23
LEU2-LYS2									
wild-type	4644	1256	3388	27.0					
*pch2*Δ	4538	1458	3080	32.1	<0.0001				
*msh5*Δ	5674	627	5047	11.1	<0.0001	<0.0001			
*pch2*Δ *msh5*Δ	859	80	779	9.3	<0.0001	<0.0001	0.096		
*mms4*Δ	2732	651	2081	23.8	0.0001	<0.0001	<0.0001	<0.0001	
*mms4*Δ *pch2*Δ	591	166	425	28.1	0.570	0.033	<0.0001	<0.0001	0.017
LYS2-ADE2									
wild-type	4644	592	4052	12.7					
*pch2*Δ	4538	828	3710	18.2	<0.0001				
*msh5*Δ	5674	265	5409	4.7	<0.0001	<0.0001			
*pch2*Δ *msh5*Δ	859	51	808	5.9	<0.0001	<0.0001	0.091		
*mms4*Δ	2732	285	2447	10.4	0.0002	<0.0001	<0.0001	<0.0001	
*mms4*Δ *pch2*Δ	591	82	509	13.9	0.42	0.0044	<0.0001	<0.0001	0.0088
ADE2-HIS3									
wild-type	4644	1611	3033	34.7					
*pch2*Δ	4538	1978	2560	43.6	<0.0001				
*msh5*Δ	5674	877	4797	15.5	<0.0001	<0.0001			
*pch2*Δ *msh5*Δ	859	202	657	23.5	<0.0001	<0.0001	<0.0001		
*mms4*Δ	2732	809	1923	29.6	<0.0001	<0.0001	<0.0001	<0.0001	
*mms4*Δ *pch2*Δ	591	210	381	35.5	0.67	<0.0001	<0.0001	<0.0001	0.0019

with COs in *pch2*Δ requiring both Mms4-Mus81 and Msh4-Msh5 pathways and argue against the idea that *pch2*Δ mutants show decreased CO interference due to additional COs formed through a non-interfering CO pathway.

***pch2*Δ does not increase DSB formation at two sites.** Previous work indicated that *pch2*Δ mutants show delays in meiotic DSB repair; thus, a time course comparison of DSB levels in meiotic prophase between *pch2*Δ and wild-type could be misleading [27, 47, 61]. Wu and Burgess [47] assayed DSB formation at the well-characterized *HIS4LEU2* hotspot in wild-type and *pch2*Δ in a *sae2*Δ strain background where DSBs are formed but not resected or repaired. They reported that wild-type and *pch2*Δ strains displayed similar DSB levels. More recently, the Hochwagen group, using microarray analysis, observed increases in DSB formation in *pch2*Δ surrounding the rDNA on chromosome XII, but nowhere else in the genome (A. Hochwagen personal communication).

We assayed DSB formation in *pch2*Δ mutants at the *YCR048W* hotspot on chromosome III and near the centromere on chromosome XV [42, 62, 63]. These experiments were performed in a *dmc1*Δ background where DSBs are formed at wild-type levels and resected (eventually hyperresected), but not repaired [29, 42, 64]. This approach allowed us to assay total DSB at loci other than *HIS4LEU2*, where DSBs are thought to occur at saturating levels, and avoid the use of the *sae2*Δ background where maximal DSB levels may not be reached [29, 32, 42, 65]. One concern with performing this analysis in the *dmc1*Δ background is that two reports [26, 66] indicated that the checkpoint arrest seen in *dmc1* mutants is bypassed in *pch2 dmc1* strains; however, a more recent report [61] indicated that it is not. Our *pch2*Δ *dmc1*Δ mutants displayed a meiotic arrest as measured by a failure to form spores (< 0.6% spore formation for *pch2*Δ *dmc1*Δ vs. ~90% for wild-type at T=24 hrs). However as

shown below, we observed a significant bypass of the *dmc1* arrest in *pch2*Δ *spo11-HA* *dmc1*Δ strains.

Quantification of DSB levels in the *dmc1*Δ background is difficult due to the extensive resection of the breaks. We therefore analyzed five independent cultures of *dmc1*Δ and *pch2*Δ *dmc1*Δ strains. Similar to previous work ([47]; A. Hochwagen personal communication), we saw no difference in DSB levels (% of total DNA) between *dmc1*Δ and *pch2*Δ *dmc1*Δ strains at the *YCR048W* (5 and 6 kb DSB bands; 19 $\pm$ 6% for *dmc1*Δ, 18 $\pm$ 5% for *pch2*Δ *dmc1*Δ) and *CEN15* (8 kb DSB band; 4.7 $\pm$ 1.2% for *dmc1*Δ, 4.5 $\pm$ 1.0% for *pch2*Δ *dmc1*Δ) hotspots (Figures 2-6A, 2-6B; T=7 hrs in meiosis). It is important to note that Hochwagen *et al.* [61] reported that *pch2*Δ *dmc1*Δ mutants do not resect DSB ends as rapidly as *dmc1*Δ; however, such a difference in resection rate could only result in an overestimation of the level of DSBs in *pch2*Δ *dmc1*Δ. These data, together with previous work, suggest that the *pch2* mutation does not disrupt DSB levels in a *SPO11* background.

As shown above, the *pch2*Δ mutation severely compromised the spore viability of *spo11* hypomorph strains. Because some *spo11* mutations confer semi-dominant and conditional phenotypes, as well as alter DSB patterns [60], we assayed DSB levels at *YCR048W* in *spo11-HA dmc1*Δ strains in the presence or absence of the *pch2*Δ mutation (Figure 2-6C). At T=3.5 hrs in meiosis, similar DSB levels were observed in *pch2*Δ *spo11-HA dmc1*Δ (16%) and *spo11-HA dmc1*Δ (15%) strains. However, at T=7 hrs, lower levels were observed in *pch2*Δ *spo11-HA dmc1*Δ (13 $\pm$ 6 %; seven independent cultures) compared to *spo11-HA dmc1*Δ (18 $\pm$ 6%; seven independent cultures). In time courses performed side by side, *pch2*Δ *spo11-HA dmc1*Δ strains displayed 30 to 90% of the *spo11-HA dmc1*Δ levels at T=7 hrs. Such variability was not observed in side-by-side experiments involving *pch2*Δ *dmc1*Δ and *dmc1*Δ strains. As shown below and analyzed in the Discussion, we attribute the variability in DSB

Figure 2-6. *pch2*Δ does not appear to have increased levels of meiotic DSBs.

Southern blots were performed to measure meiotic DSBs in *dmc1*Δ, *pch2*Δ *dmc1*Δ, *spo11-HA dmc1*Δ, and *pch2*Δ *spo11-HA dmc1*Δ strains. For the *YCR048w* hotspot on chromosome III (A) DNA was digested with *Bgl*II and probed with a chromosome III fragment (SGD coordinates 215,422-216,703, [63]). For the *CEN15* hotspot (B), DNA was digested with *Sph*I and *Nhe*I and probed with a chromosome XV fragment (SGD coordinates 331,713-332,402, [42]). The parental bands are marked with asterisks and arrows show bands that form due to DSB formation. Approximate sizes for all bands are shown [42, 63]. The lanes on the *CEN15* blot have been reordered for easy comparison of the two strains. C) Analysis of DSBs at the *YCR048W* hotspot at T=3.5 and 7 hrs in *spo11-HA dmc1*Δ (EAY2562/EAY2563) and *pch2*Δ *spo11-HA dmc1*Δ (EAY2564/EAY2565) strains. A representative blot is shown. In side-by-side experiments the DSB levels at T=7 hrs in *pch2*Δ *spo11-HA dmc1*Δ ranged from 30-90% (30, 61, 72, 76, 80, 89, and 90%) of the levels observed in *spo11-HA dmc1*Δ.

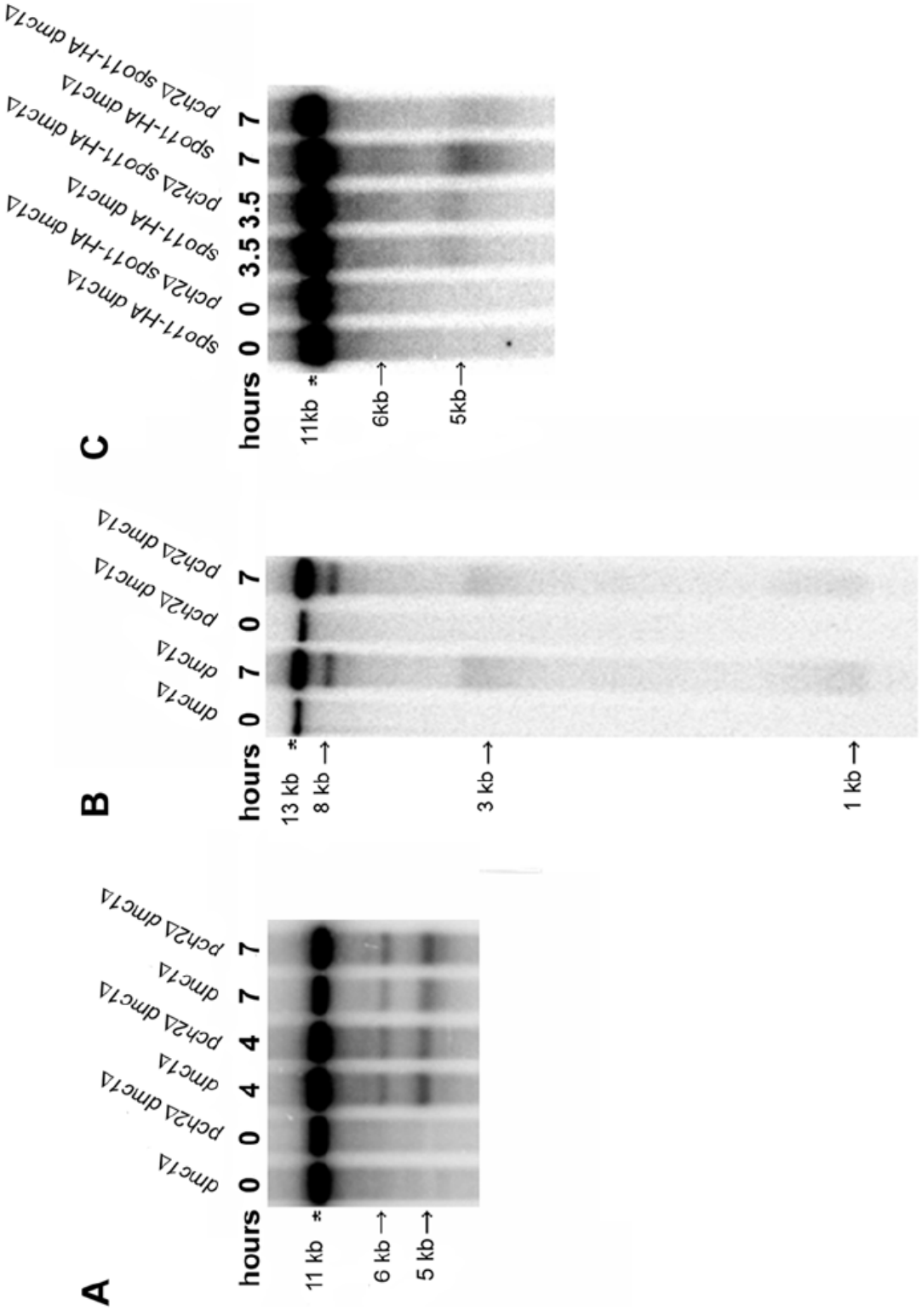
A
hours 0 0 4 4 7 7
dmc1Δ
pch2Δ dmc1Δ
dmc1Δ
pch2Δ dmc1Δ
dmc1Δ
pch2Δ dmc1Δ
11 kb *
6 kb →
5 kb →
B
hours 0 7 0 7
dmc1Δ
dmc1Δ
pch2Δ dmc1Δ
pch2Δ dmc1Δ
13 kb *
8 kb →
3 kb →
1 kb →
C
hours 0 0 3.5 3.5 7 7
spo11-HA dmc1Δ
pch2Δ spo11-HA dmc1Δ
spo11-HA dmc1Δ
pch2Δ spo11-HA dmc1Δ
spo11-HA dmc1Δ
pch2Δ spo11-HA dmc1Δ
11kb *
6kb →
5kb →

levels to the bypass of the *dmc1*Δ arrest in *pch2*Δ *spo11-HA dmc1*Δ. This was determined by measuring the completion of the MI division in *spo11-HA dmc1*Δ and *pch2*Δ *spo11-HA dmc1*Δ strains. At T=28 hrs in meiosis, only 1-2% of *spo11-HA dmc1*Δ strains completed MI; this indicates that the *dmc1*Δ arrest is maintained in these strains. For *pch2*Δ *spo11-HA dmc1*Δ, at T=4.5 hrs, no cells (n>200) had completed the MI division. However, at T=6.5 hrs, 8 to 30% of the cells completed MI, and these values increased to 54 to 60% (with similar spore formation levels) at T=28 hrs. As predicted for a *dmc1*Δ mutant, the spores produced by *pch2*Δ *spo11-HA dmc1*Δ were inviable.

***The spo11-HA hypomorph suppresses the MI delay of pch2*Δ.** Wu and Burgess [47] showed that the *pch2*Δ MI delay is suppressed by a null mutation in the mitotic and meiotic checkpoint gene *RAD17*. The delay is also suppressed by the *spo11*Δ mutation [47, 67]. One interpretation of these and our data is that the greater than wild-type number of COs in *pch2*Δ*,* rather than a recombination-associated DNA aberration inherent to the mutant, triggers the Rad17-dependent checkpoint. If the additional time required to complete the additional COs causes the delay in *pch2*Δ, then reducing the number of recombination events by lowering the number of DSBs should suppress the delay. We assayed MI division timing in *pch2*Δ/*pch2*Δ *spo11-HA/spo11-HA* mutants displaying total CO levels (165 cM) that are somewhat similar to wild-type (150 cM) but significantly lower than *pch2*Δ/*pch2*Δ (224 cM; Figures 2B; [24, 32]). *pch2*Δ/*pch2*Δ *spo11-HA/spo11-HA* strains progressed through meiosis with timing indistinguishable from *spo11-HA/spo11-HA* and wild-type (Figure 2-7). These data suggest there are no inherent recombination defects recognized by a Rad17-dependent checkpoint in *pch2*Δ mutants, unless the defect appears only when DSBs are at wild-type levels [32, but see 27]. We favor the idea that the MI delay in *pch2*Δ is caused by the prolonged recombination period needed to generate the additional

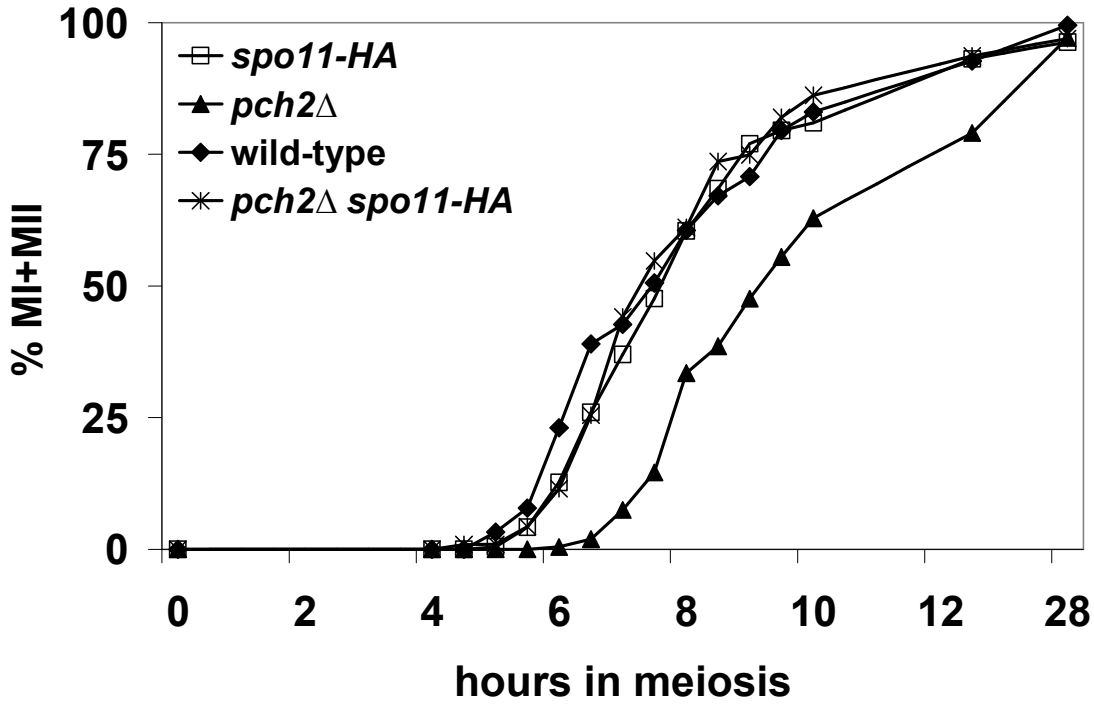

Figure 2-7. The *pch2*Δ MI delay is suppressed by the *spo11-HA* hypomorph.

Synchronous cultures were induced to undergo meiosis and progression past MI (MI ± MII) was assayed in the NHY background for wild-type (diamonds), *spo11-HA* (open squares), *pch2*Δ (triangles), and *pch2*Δ *spo11-HA* (stars; Materials and Methods). A representative time course is shown.

COs observed in *pch2*Δ. Alternatively, the extra COs observed in *pch2*Δ could result from, rather than cause, the MI delay [68]. In this case, it is unclear what could be eliciting the delay in *pch2*Δ. Importantly, the fact that the *pch2*Δ *spo11-HA* double mutant has wild-type MI timing *and* disrupted CO interference (Figures 2-5, 2-7; Tables 2-5, 2-6, 2-7) demonstrates that the interference defects observed in *pch2*Δ are not simply the result of a prolonged CO designation period [68].

DISCUSSION

In this study we show that *pch2* mutants display elevated crossing over on medium and large chromosomes and are defective in CO interference. Based on this work, our initial studies suggesting an increased CO:NCO ratio in *pch2*Δ mutants (Table 2-4), and previous work [27, 32, 47], we hypothesize that the increase in COs in *pch2*Δ on the medium and large chromosomes results from a greater than normal proportion of DSBs being repaired as COs at the expense of non COs, due to the loss of CO interference, rather than an increase in initiating DSBs (Figure 2-6; Table 2-4). In other words, we propose Pch2-mediated CO control acts not only to uniformly space COs within the genome, but also to limit the overall number of COs. The same defect in *pch2*Δ that disrupts interference could lead to longer heteroduplex tracts, causing the increases in gene conversion frequencies observed in *pch2*Δ.

We favor a model in which Pch2 promotes wild-type levels of CO interference at the CO vs. NCO decision, which is though to occur in late leptotene, perhaps by acting in meiotic axis organization/assembly (Figure 2-8; [17, 18, 20]). In this model, CO designation at one site inhibits nearby DSBs from receiving CO designation; such a decision could then influence the Pch2-dependent domainal organization of Hop1 and Zip1 observed in pachytene [27; see below]. Two recent studies support the idea

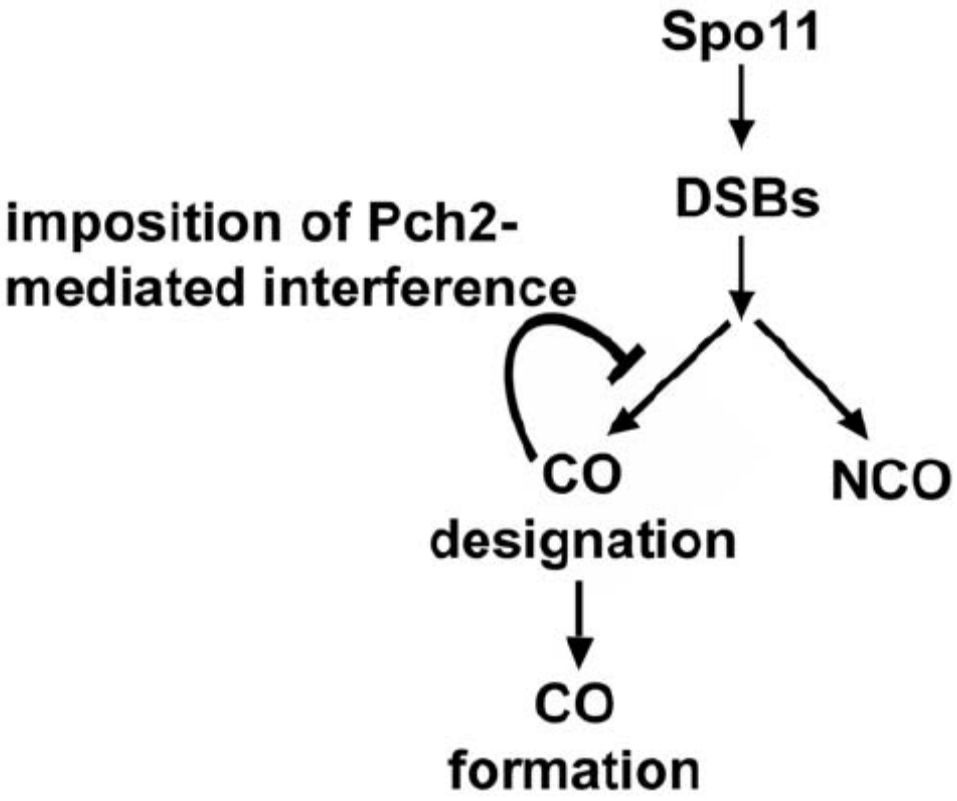

Figure 2-8. Model for interference-regulation of the CO vs. NCO decision.

We propose that Pch2 acts to inhibit CO designation in a chromosomal region in response to a prior crossover-designated recombination event in that region. See text for details.

that Pch2 acts in early prophase. 1. Hochwagen *et al.* observed changes in DSB processing in *pch2* mutants [61]. 2. Shinohara and colleagues (personal communication) found that meiotic depletion of *CDC53* causes a defect in meiotic axis construction in leptotene, resulting in aberrant SC formation. A *pch2* mutation fully suppresses the SC construction defect of *CDC53* meiotic depletion, suggesting that Pch2 is a negative regulator of meiotic axis assembly.

Our proposal that Pch2 acts at the CO vs. NCO decision differs from interpretations presented by Börner *et al.* [27]. They examined NCO and CO formation at the *HIS4LEU2* hotspot on chromosome III in *pch2*Δ mutants using Southern blot analysis and found that CO levels were decreased and NCO levels were increased at this site [27, 69]. They also monitored progression through recombination at *HIS4LEU2* and found that *pch2*Δ mutants were delayed after SEI formation and accumulate SEIs and dHJs. Given these results and the finding that CO and NCO formation were coordinately delayed, Börner *et al.* [27] proposed that the meiotic delay in *pch2*Δ is caused by a defect downstream of the CO vs. NCO decision. We did not observe an effect of the *pch2*Δ mutation on crossing over on chromosome III. One explanation for this difference is that the Börner *et al.* [27] performed their analysis at *HIS4LEU2*, which was shown previously to lack CO homeostasis [32]. Additionally, the delay that they saw in processing recombination intermediates in *pch2*Δ may be due to an upstream defect at the CO vs. NCO decision. Specifically, the additional load of SEIs and dHJs that the recombination machinery must process in a *pch2*Δ mutant could delay their turnover genome-wide. It is important to note that we do not have a clear explanation for why CO levels on chromosome III are not elevated in *pch2*Δ. However, smaller chromosomes in yeast, such as chromosome III, have higher map distances per kb compared to larger chromosomes, and CO interference appears weaker on smaller chromosomes compared to larger ones [38,

39]. Thus, because interference is stronger on larger chromosomes, eliminating interference should have a more pronounced effect on CO levels on larger chromosomes, as was seen in our study.

Meiotic axis organization appears to be conserved in *S. cerevisiae* and *C. elegans*. Martinez-Perez [70] recently reported a link between meiotic axis protein organization and CO interference in *C. elegans*. They analyzed the distribution patterns of the central element protein SYP-1 and the axial element proteins HTP-1 and HTP-2, which, like Hop1, are HORMA domain proteins. Analogous to observations made for Hop1 and Zip1 in yeast, Martinez-Perez *et al.* [70] found that the HTP axial element and the SYP-1 central element proteins sort into reciprocal domains on late pachytene chromosome axes. Based on the above, the finding that HTP1/2 is depleted at COs, the fact that Spo11 and Msh5 are required for domain formation, and the correlation seen between HTP1/2 depletion sites and chiasmata, Martinez-Perez *et al.* [70] suggest that HTP/SYP-1 domain boundaries mark CO sites. This information suggests that Hop1/Zip1 boundaries indicate where the CO/NCO decision marks subsequent CO sites. Such a model takes into account the finding that *C. elegans* displays only one domain of each type whereas *S. cerevisiae* contains a large number of alternating Zip1/Hop1 domains. This pattern is consistent with the fact that each chromosome pair in *C. elegans* typically enjoys a single CO whereas chromosome pairs in *S. cerevisiae* enjoy multiple COs (~80-90 total COs in *S. cerevisiae* [30, 35] vs. six in *C. elegans* [21, 70]).

Based on observations presented in Martinez-Perez *et al*. [70] we suggest that the altered pattern of Hop1 and Zip1 localization on the chromosome axis seen in *pch2*Δ mutants results from, but is not the cause of, the increase in COs. In this interpretation, the defect in CO control in *pch2*Δ mutants leads to additional COs, reflected by a greater number of domains, thus making the axis distribution of Hop1

and Zip1 appear more uniform. This model fits with respect to the known timing of the CO vs. NCO decision [17, 18, 20, 21, 34, 35], and the finding that early Hop1 organization appears normal in *pch2*Δ mutants [27]. Testing such a model will require an examination of Hop1 and Zip1 localization patterns in strains (e.g. *pch2*Δ*spo11* hypomorphs) containing decreased levels of DSBs; our model predicts that the Hop1 and Zip1 domains would become more distinct due to fewer COs, although not completely like wild-type due to defects in CO interference.

Why do *pch2* mutants show wild-type spore viability? The wild-type spore viability seen in *pch2*Δ mutants suggests that Pch2-mediated CO control is not required to maintain the viability of yeast grown in lab conditions. We offer two explanations for this finding: 1) COs are present in excess (~80-90 per cell) of the number needed for all homologs to receive an obligate CO (16 per cell). 2) The reduction in interference in *pch2*Δ is accompanied by, and likely causes, an increase in the overall number of COs. This increase in crossing over could compensate for distribution failures that jeopardized obligate CO formation ([30, 33]; Figures 2-3, 2-4; Tables 2-5, 2-6, 2-7). Our results and those of Martini *et al.* [32] demonstrate a buffered system in baker's yeast in which excess DSBs and COs lessen the need for interference to ensure obligate CO formation. Because of this buffer, obligate CO formation can be maintained if interference or DSBs are reduced, but not both (Figure 2-3; [32]). Such buffering may exist because the consequences of having too many COs are less severe than too few. For example, *pch2*Δ mutants have dramatic increases in CO levels, but show wild-type spore viability, whereas mutants that significantly decrease CO levels like *mlh3*Δ, have reduced spore viabilities due to MI nondisjunction [9, 11]. Future searches for mutants that disrupt the CO vs. NCO decision must be broadened to include genes with high spore viability or synthetic phenotypes with *spo11* hypomorphs.

Although the role of Pch2 in limiting CO levels, after the requisite number required for ensuring obligate CO formation is reached, is not required, it is likely to be advantageous. Too many COs, especially closely spaced ones, have been suggested to disrupt the sister chromatid cohesion required to create tension on the MI spindles and ensure proper homolog disjunction at MI [71, 72]. In addition, our data suggests that the CO limiting role of Pch2 also promotes timely meiotic progression, which could also be advantageous to cells (Figure 2-7).

What causes the loss in spore viability seen in *pch2*Δ *spo11* hypomorphs? *pch2*Δ/*pch2*Δ *spo11-HA/spo11-HA* strains displayed an excess of tetrads with 4, 2, and 0 viable spores, a high percentage of two-spore viable tetrads containing sisters, and an increased frequency of chromosome III nondisjunction. Our data are consistent with MI chromosome nondisjunction being a major component of the spore death phenotype, perhaps due to a failure to ensure obligate CO formation on all chromosomes. In such a model, when DSBs become limiting, the proper distribution of COs becomes even more critical to ensure obligate CO formation. Similar DSB levels were seen at *YCRO48W* at 3.5 hours in meiosis in *spo11-HA dmc1*Δ and *pch2*Δ *spo11-HA dmc1*Δ; however, by 7 hrs, fewer breaks were observed in the triple mutant (Figure 2-6C and D). Our DSB level measurements are not definitive due to the checkpoint bypass observed in the triple mutant. We provide two explanations for the triple mutant phenotype. In one scenario, early forming DSBs appear at wild-type levels while later-forming DSBs form at lower levels that are insufficient for sustained recombination checkpoint activation. In a second scenario, DSBs form normally, but undergo some level of Dmc1-independent, possibly intersister, repair that permits a bypass of the checkpoint. Such repair would not lead to MI disjunction-promoting chiasmata. Both of these scenarios are sufficient to explain the spore inviability seen in *pch2*Δ *spo11* hypomorphs (Figure 2-3). Future experiments to distinguish these

hypotheses should include an analysis of meiotic Rad51foci in *spo11-HA dmc1*Δ and *pch2*Δ *spo11-HA dmc1*Δ strains [73].

We cannot rule out that other cellular defects contribute to the MI non-disjunction phenotype seen in *pch2*Δ *spo11* mutants. For example, both *pch2*Δ and *spo11* hypomorphs have SC defects, which could lead to CO control-independent synthetic phenotypes in the double mutants [24, 27]. It is also possible that Pch2 promotes MI disjunction by regulating sister chromatid cohesion establishment and/or removal, or by preventing/resolving chromosome entanglements [2-4, 68], or that some spore death in *pch2*Δ *spo11* hypomorphs is independent of MI non-disjunction.

Additional factors are likely to act early in meiosis to establish CO interference. Interference mutants have been proposed to act downstream of the CO vs. NCO decision (e.g. *zip1, msh4*; Introduction; [22, 35]), or display an apparent defect in interference due to an increase in non-interfering COs (*ndj1, csm4*; [15, 35]). The only other yeast interference mutants that appear similar to *pch2*Δ are *tid1*Δ and *dmc1*Δ-*2μRad54* [34; but see 58]. We will focus on *tid1*Δ, because its CO phenotype is better characterized. Tid1/Rdh54 is a member of the Swi2/Snf2 family, and thus may act in meiotic chromatin axis remodeling, though this has yet to be tested [74]. *tid1*Δ mutants display moderate levels of spore viability (58% 4-spore viable tetrads), and Tid1 has been shown to be involved in the strand exchange step of recombination [57]. Similar to *pch2*Δ, *tid1*Δ mutants display a defect in interference and increased gene conversion. Also, like *pch2*Δ, CO levels in *tid1*Δ appear similar to wild-type on a small chromosome (III). On a medium-sized chromosome (V), *tid1*Δ mutants displayed wild-type CO levels in two intervals, but a significant (2.4-fold) increase in a third [34]. These data suggest that *tid1*Δ and *pch2*Δ have similar CO patterns. We are eager to test this hypothesis in the strain sets used in this study. Furthermore, we are intrigued by the idea that strand exchange and meiotic chromatin axis components

are both required/involved in interference-regulation of the CO vs. NCO decision.

MATERIALS AND METHODS

Media and yeast strains. Yeast strains are listed in Table 2-1. All strains were grown at 30°C on standard YPD (yeast peptone dextrose; [75]). The sporulation media was described previously [11, 68]. For tetrad genotyping, synthetic minimal selective media, synthetic complete media with 5 μM Cu, and YPD supplemented with complete amino acid mix and 3 mg/L cycloheximide were used [75]. When required, Geneticin (Invitrogen), nourseothricin (Hans-Knoll Institute fur Naturstoff-Forschung), and hygromycin B (Calbiochem) were added to YPD media as described [76, 77].

The EAY1108/EAY1112 SK1 congenic strain set is described in Argueso *et al.* [11], and the NHY942/NHY943 SK1 isogenic strain set is described in de los Santos *et al*. [10]. The *spo11* hypomorphic mutants were described by Diaz *et al*. [60] and Henderson and Keeney [24] although the NHY942/NHY943 strains containing these alleles, which are used in this work, are described in Martini *et al.* [32]. As in Martini *et al.* [32], we refer to *spo11-HA3His6* as *spo11-HA*, *spo11(D290A)-HA3His6* as *spo11da-HA*, and *spo11(Y135F)-HA3His6* as *spo11yf-HA*. Strains EAY2562-2565 are derivatives of a cross between EAY2260 and SKY633. The *msh5*Δ, *mms4*Δ, and *dmc1*Δ alleles used in this work were all complete open reading frame (ORF) deletions. The *pch2*Δ allele contains a deletion of amino acids 17-587 (in the 603 amino acid ORF). All deleted regions were replaced with *HPHMX4*, *KANMX4,* or *NATMX4* as shown in Table S1 [76, 77]. The deletion cassettes were made via PCR and integrated into the genome using standard techniques [78]. Details on strain construction and primer sequences are available on request.

Tetrad analysis. Diploids for tetrad analysis were all made using the zero growth mating protocol [79]. The haploid parental strains were patched together on YPD for 4 hours and then spread on sporulation plates. The plates were incubated at 30°C for 2 days, after which tetrads were dissected. Tetrads from the EAY1108/EAY1112 strain background were dissected on synthetic complete media, whereas tetrads from the NHY942/NHY943 strain background were dissected on YPD media supplemented with complete amino acids. All tetrads were incubated 3-4 days at 30°C and then replica-plated to various selective media. The replica plates were scored after one day of incubation at 30°C. In the EAY strain background, the data for wild-type, *mms4*Δ, and *msh5*Δ were originally published in Argueso *et al.* [11]. In the NHY strain background, a subset of the wild-type data was originally published in Wanat *et al.* [68]. The distributions of each tetrad type were calculated using RANA software [11].

Genetic map distances +/- the standard error were calculated using the Stahl Laboratory Online Tools (http://www.molbio.uoregon.edu/~fstahl/) which utilizes the formula of Perkins [54]. The G-test spreadsheet, available from The Online Handbook of Biological Statistics (http://udel.edu/~mcdonald/statintro.html), was used to compare tetrad distribution patterns between strains. The Dunn-Sidak correction (p value of 0.05/ number of comparisons) was applied when multiple comparisons per data set were performed [80]. Recombination frequencies from spore data were calculated as described previously (RANA software; [11]), with p-values determined as above (http://udel.edu/~mcdonald/statintro.html).

Three different analyses were performed to measure interference. The NPD ratio (Table 2-5) was determined using the "Better Way" calculator (http://www.molbio.uoregon.edu/~fstahl/). This method compares the number of each tetrad type observed to the numbers expected if CO distribution was random and

calculates a chi square value, which was converted to a p value using VassarStats (http://faculty.vassar.edu/lowry/VassarStats.html). Coefficients of coincidence (Table 2-6) were determined as described previously [11, 68]. Tetrads were sorted using Mactetrad 6.9 software to calculate interference via the Malkova *et al*. method ([37], Figure 2-5; Table 2-7).

Meiotic time courses and DSB Southern blotting. For all time courses, a saturated YPD overnight culture from each strain to be analyzed was diluted in 200 ml YPA (2% potassium acetate) and grown for 17 hours. The YPA culture was then spun down, washed once in 1% potassium acetate and resuspended in 100 ml 1% potassium acetate (similar to [81]). All strains were grown in the same batches of media and treated identically. DAPI staining to analyze progression past MI (MI + MII) was performed as described [81]. Cells were visualized using an Olympus BX60 microscope and at least 200 cells were counted for each time point. DNA was isolated from meiotic cultures as described [29]. Southern blotting was performed using standard techniques [82]. The percent of DSB formation for four to six independent time courses (% of hybridizing bands +/- standard deviation, SD) was calculated using Image Quant software.

ACKNOWLEDGEMENTS

We thank Valentin Börner, Andreas Hochwagen, and Akira Shinohara for sharing unpublished data, Scott Keeney for providing strains, Demelza Kohn for DSB Southern blot advice, and Ken Kemphues and Tom Fox for sharing equipment. We are also grateful to Sean Burgess, Neil Hunter, Nancy Kleckner, Frank Stahl, and all Alani lab members for helpful discussions, and the anonymous reviewers for their comments. We thank Megan Sonntag for constructing the *msh5*Δ *pch2*Δ strain.

REFERENCES

1. Roeder GS (1997) Meiotic chromosomes: it takes two to tango. Genes Dev 11: 2600-2621.

2. Buonomo SB, Clyne RK, Fuchs J, Loidl J, Uhlmann F, Nasmyth K (2000) Disjunction of homologous chromosomes in meiosis I depends on proteolytic cleavage of the meiotic cohesin Rec8 by separin. Cell 103: 387-398.

3. Bickel SE, Orr-Weaver TL, Balicky EM (2002) The sister-chromatid cohesion protein ORD is required for chiasma maintenance in *Drosophila* oocytes. Curr Biol 12: 925-929.

4. Hodges CA, Revenkova E, Jessberger R, Hassold TJ, Hunt PA (2005) SMC1beta-deficient female mice provide evidence that cohesins are a missing link in age-related nondisjunction. Nat Genet 37: 1351-1355.

5. Rockmill B, Voelkel-Meiman K, Roeder GS (2006) Centromere-proximal crossovers are associated with precocious separation of sister chromatids during meiosis in *Saccharomyces cerevisiae*. Genetics 174: 1745-1754.

6. Hassold T, Hall H, Hunt P (2007) The origin of human aneuploidy: where we have been, where we are going. Hum Mol Genet 16: R203-208.

7. Ross-Macdonald P, Roeder GS (1994) Mutation of a meiosis-specific MutS homolog decreases crossing over but not mismatch correction. Cell 79: 1069-1080.

8. Hollingsworth NM, Ponte L, Halsey C (1995) *MSH5*, a novel MutS homolog, facilitates meiotic reciprocal recombination between homologs in *Saccharomyces cerevisiae* but not mismatch repair. Genes Dev 9: 1728-1739.

9. Wang TF, Kleckner N, Hunter N (1999) Functional specificity of MutL homologs in yeast: evidence for three Mlh1-based heterocomplexes with distinct roles during meiosis in recombination and mismatch correction. Proc Natl Acad Sci U S A 96: 13914-13919.

10. de los Santos T, Hunter N, Lee C, Larkin B, Loidl J, Hollingsworth NM (2003) The Mus81/Mms4 endonuclease acts independently of double-Holliday junction resolution to promote a distinct subset of crossovers during meiosis in budding yeast. Genetics 164: 81-94.

11. Argueso JL, Wanat J, Gemici Z, Alani E (2004) Competing crossover pathways act during meiosis in *Saccharomyces cerevisiae*. Genetics 168: 1805-1816.

12. Franklin FC, Higgins JD, Sanchez-Moran E, Armstrong SJ, Osman KE*, et al.* (2006) Control of meiotic recombination in *Arabidopsis*: role of the MutL and MutS homologues. Biochem Soc Trans 34: 542-544.

13. de Boer E, Stam P, Dietrich AJ, Pastink A, Heyting C (2006) Two levels of interference in mouse meiotic recombination. Proc Natl Acad Sci USA 103: 9607-9612.

14. Nishant KT, Plys AJ, Alani E (2008) A mutation in the putative MLH3 endonuclease domain confers a defect in both mismatch repair and meiosis in *Saccharomyces cerevisiae*. Genetics 179: 747-755.

15. Getz TJ, Banse SA, Young LS, Banse AV, Swanson J, Wang GM, Browne BL, Foss HM, Stahl FW (2008) Reduced mismatch repair of heteroduplexes reveals "non"-interfering crossing over in wild-type *Saccharomyces cerevisiae*. Genetics 178: 1251-1269.

16. Muller HJ (1916) The mechanism of crossing-over. Am Nat 50: 193–221.

17. Hunter N, Kleckner N (2001) The single-end invasion: an asymmetric intermediate at the
double-strand break to double-holliday junction transition of meiotic recombination. Cell 106: 59-70.

18. Allers T, Lichten, M (2001) Differential timing and control of noncrossover and crossover recombination during meiosis. Cell 106: 47-57.

19. Schwacha A, Kleckner N (1995) Identification of double Holliday junctions as intermediates in meiotic recombination. Cell 83: 783-791.

20. Börner GV, Kleckner N, Hunter N (2004) Crossover/noncrossover differentiation, synaptonemal complex formation, and regulatory surveillance at the leptotene/zygotene transition of meiosis. Cell 117: 29-45.

21. Hillers KJ, Villeneuve AM (2003) Chromosome-wide control of meiotic crossing over in C. elegans. Curr Biol 13: 1641-1647.

22. Bishop, DK, Zickler D (2004) Early decision: meiotic crossover interference prior to stable strand exchange and synapsis. Cell 117: 9-15.

23. de los Santos T, Loidl J, Larkin B, Hollingsworth NM (2001) A role for *MMS4* in the processing of recombination intermediates during meiosis in *Saccharomyces cerevisiae*. Genetics 159: 1511-1525.

24. Henderson KA, Keeney S (2004) Tying synaptonemal complex initiation to the formation and programmed repair of DNA double-strand breaks. Proc Natl Acad Sci USA 101: 4519-4524.

25. Tsubouchi T, Macqueen AJ, Roeder GS (2008) Initiation of meiotic chromosome synapsis at centromeres in budding yeast. Genes Dev 22: 3217-3226.

26. San-Segundo PA Roeder GS (1999) Pch2 links chromatin silencing to meiotic checkpoint control. Cell 97: 313-324.

27. Börner GV, Barot A, Kleckner N (2008) Yeast Pch2 promotes domainal axis organization, timely recombination progression, and arrest of defective recombinosomes during meiosis. Proc Natl Acad Sci U S A 105: 3327-3332.

28. Lynn A, Soucek R, Börner GV (2007) ZMM proteins during meiosis: crossover artists at work. Chromosome Res 15: 591-605.

29. Buhler CV Borde V, Lichten M (2007) Mapping meiotic single-strand DNA reveals a new landscape of DNA double-strand breaks in *Saccharomyces cerevisiae*. PLoS Biol 5: e324.

30. Mancera E, Bourgon R, Brozzi A, Huber W, Steinmetz LM (2008) High-resolution mapping of meiotic crossovers and non-crossovers in yeast. Nature 454: 479-485.

31. McMahill MS, Sham CW, Bishop DK (2007) Synthesis-dependent strand annealing in meiosis. PLoS Biol 5: e299.

32. Martini E, Diaz RL, Hunter N, Keeney S (2006) Crossover homeostasis in yeast meiosis. Cell 126: 285-295.

33. Chen SY, Tsubouchi T, Rockmill B, Sandler JS, Richards DR, Vader G, Hochwagen A, Roeder GS, Fung JC (2008) Global Analysis of the Meiotic Crossover Landscape. Dev Cell 15: 401-415.

34. Shinohara M, Sakai K, Shinohara A, Bishop DK (2003) Crossover interference in *Saccharomyces cerevisiae* requires a *TID1/RDH54*- and *DMC1*-dependent pathway. Genetics 163: 1273-1286.

35. Fung JC, Rockmill B, Odell M, Roeder GS (2004) Imposition of crossover interference through the nonrandom distribution of synapsis initiation complexes. Cell 116: 795-802.

36. Lawrie NM, Tease C, Hulton MA (1995) Chiasma frequency, distribution and interference maps of mouse autosomes. Chromosoma 104: 308-314.

37. Malkova A, Swanson J, German M, McCusker JH, Housworth EA, *et al.* (2004) Gene conversion and crossing over along the 405-kb left arm of *Saccharomyces cerevisiae* chromosome VII. Genetics 168: 49-63.

38. Kaback DB, Guacci V, Barber D, Mahon JW (1992) Chromosome size-dependent control of meiotic recombination. Science 256: 228-232.

39. Kaback DB, Barber D, Mahon J, Lamb J, You J (1999) Chromosome size-dependent control of meiotic reciprocal recombination in *Saccharomyces cerevisiae*: the role of crossover interference. Genetics 152: 1475-1486.

40. Stahl FW, Foss HM, Young LS, Borts RH, Abdullah MF, Copenhaver GP (2004) Does crossover interference count in *Saccharomyces cerevisiae*? Genetics 168: 35-48.

41. Turney D, de Los Santos T, Hollingsworth NM (2004) Does chromosome size affect map distance and genetic interference in budding yeast? Genetics168: 2421-2424.

42. Blitzblau HG, Bell GW, Rodriguez J, Bell SP, Hochwagen A (2007) Mapping of meiotic single-stranded DNA reveals double-stranded-break hotspots near centromeres and telomeres. Curr Biol 17: 2003-2012.

43. Sym M, Roeder GS (1994) Crossover interference is abolished in the absence of a synaptonemal complex protein. Cell 79: 283-292.

44. Novak JE, Ross-Macdonald PB, Roeder GS (2001) The budding yeast Msh4 protein functions in chromosome synapsis and the regulation of crossover distribution. Genetics 58: 1013-1025.

45. Shinohara M, Oh SD, Hunter N, Shinohara A (2008) Crossover assurance and crossover interference are distinctly regulated by the ZMM proteins during yeast meiosis. Nat Genet 40: 299-309.

46. Kosaka H, Shinohara M, Shinohara A (2008) Csm4-dependent telomere movement on nuclear envelope promotes meiotic recombination. PLoS Genetics 4: e1000196

47. Wu HY, Burgess SM (2006) Two distinct surveillance mechanisms monitor meiotic chromosome metabolism in budding yeast. Curr Biol 16: 2473-2479.

48. Bhalla N, Dernberg AF (2005) A conserved checkpoint monitors meiotic chromosome synapsis in Caenorhabditis elegans. Science 310: 1683-1686.

49. Joyce EF, McKim KS (2009) Drosophila PCH2 is required for a pachytene checkpoint that monitors double-strand-break-independent events leading to meiotic crossover formation. Genetics 181: 39-51.

50. Li XC, Schimenti JC (2007) Mouse pachytene checkpoint 2 (trip13) is required for completing meiotic recombination but not synapsis. PLoS Genet 3: e130.

51. Mitra N, Roeder GS (2007) A novel nonnull *ZIP1* allele triggers meiotic arrest with synapsed chromosomes in *Saccharomyces cerevisiae*. Genetics 176: 773-787.

52. Oh SD, Lao JP, Hwang PY, Taylor AF, Smith, GR, *et al.* (2007) BLM ortholog, Sgs1, prevents aberrant crossing over by suppressing formation of multichromatid joint molecules. Cell 130: 259-272.

53. Joshi N, Barot A, Jamison C, and Börner GV (2009) Pch2 links chromosome axis remodeling at future crossover sites and crossover distribution during yeast meiosis. PLoS Genet 5(7): e1000557. doi:10.1371/journal.pgen.1000557

54. Perkins DD (1949) Biochemical mutants in the smut fungus *Ustilago maydis*. Genetics 34: 607-626.

55. Papazian HP (1952) The analysis of tetrad data. Genetics 37: 175-188.

56. Stahl, FW (2008) On the "NPD ratio" as a test for crossover interference. Genetics 179: 701-704.

57. Shinohara M, Shita-Yamaguchi E, Buerstedde JM, Shinagawa H, Ogawa H, Shinohara A (1997) Characterization of the roles of the *Saccharomyces cerevisiae RAD54* gene and a homologue of *RAD54*, *RDH54/TID1*, in mitosis and meiosis. Genetics 147: 1545-1556.

58. Stahl FW (2008) The phage mating theory, with lessons for yeast geneticists. Genetics 180: 1-6.

59. Sall T, Bengtsson BO (1989) Apparent negative interference due to variation in recombination frequencies. Genetics 122: 935–942.

60. Diaz RL, Alcid AD, Berger JM, Keeney S (2002) Identification of residues in yeast Spo11p critical for meiotic DNA double-strand break formation. Mol. Cell Biol. 22: 1106-1115.

61. Hochwagen A, Tham WH, Brar GA, Amon A (2005) The FK506 binding protein Fpr3 counteracts protein phosphatase 1 to maintain meiotic recombination checkpoint activity. Cell 122: 861-873.

62. Liu J, Wu TC, Lichten M (1995) The location and structure of double-strand DNA breaks induced during yeast meiosis: evidence for a covalently linked DNA-protein intermediate. EMBO J 14: 4599-4608.

63. Yamashita K, Shinohara M, Shinohara A (2004) Rad6-Bre1-mediated histone H2B ubiquitylation modulates the formation of double-strand breaks during meiosis. Proc Natl Acad Sci USA 101: 11380-11385.

64. Bishop DK, Park D, Xu L, Kleckner N (1992) *DMC1*: a meiosis-specific yeast homolog of *E. coli* recA required for recombination, synaptonemal complex formation, and cell cycle progression. Cell 69: 439-456.

65. Alani E, Padmore R, Kleckner N (1990) Analysis of wild-type and *rad50* mutants of yeast suggests an intimate relationship between meiotic chromosome synapsis and recombination. Cell 61: 419-436.

66. Zierhut C, Berlinger M, Rupp C, Shinohara A, and Klein F (2004) Mnd1 is required for meiotic interhomolog repair. Curr Biol 14: 752–762.

67. Hochwagen A, Amon A (2006) Checking your breaks: surveillance mechanisms of meiotic recombination. Curr Biol 16: R217-28.

68. Wanat JJ, Kim KP, Koszul R, Zanders S, Weiner B, Kleckner N, Alani E (2008). Csm4, in collaboration with Ndj1, mediates telomere-led chromosome dynamics and recombination during yeast meiosis. PLoS Genet 4: e1000188.

69. Cao L, Alani E., and Kleckner N (1990) A pathway for generation and processing of double-strand breaks during meiotic recombination in *S. cerevisiae*. Cell 61: 1089-1101.

70. Martinez-Perez E, Schvarzstein M, Barroso C, Lightfoot J, Dernburg AF, Villeneuve AM (2008) Crossovers trigger a remodeling of meiotic chromosome axis composition that is linked to two-step loss of sister chromatid cohesion. Genes Dev 22: 2886-2901.

71. Nilsson NO, Sall T (1995) A model of chiasma reduction of closely formed crossovers. J Theor Biol 173: 93-98.

72. van Veen JE Hawley RS (2003) Meiosis: when even two is a crowd. Curr Biol 13: R831- 833.

73. Lydall D, Nikolsky Y, Bishop DK, Weinert T (1996) A meiotic recombination checkpoint controlled by mitotic checkpoint genes. Nature 383: 840-843.

74. Petukhova G, Sung P and Klein H (2000) Promotion of Rad51-dependent D-loop formation by yeast recombination factor Rdh54/Tid1. Genes Dev 14: 2206-2215.

75. Rose MD, Winston F, Hieter P (1990) Methods in yeast genetics: A laboratory course manual. Cold Spring Harbor, NY: Cold Spring Harbor Laboratory Press.

76. Wach A, Brachat A, Pohlmann R, Philippsen P (1994) New heterologous modules for classical or PCR-based gene disruptions in *Saccharomyces cerevisiae.* Yeast 10: 1793-1808.

77. Goldstein AL, McCusker JH (1999) Three new dominant drug resistance cassettes for gene disruption in *Saccharomyces cerevisiae*. Yeast 15: 1541-1553.

78. Gietz RD, Schiestl, RH, Willems AR, Woods RA (1995) Studies on the transformation of intact yeast cells by the LiAc/SS-DNA/PEG procedure. Yeast 11: 355-360.

79. Argueso JL, Kijas AW, Sarin S, Heck J, Waase M, Alani E (2003) Systematic mutagenesis of the *Saccharomyces cerevisiae MLH1* gene reveals distinct roles for Mlh1p in meiotic crossing over and in vegetative and meiotic mismatch repair. Mol Cell Biol 23: 873-886.

80. Hoffmann ER, Shcherbakova PV, Kunkel TA, Borts RH (2003) *MLH1* mutations differentially affect meiotic functions in *Saccharomyces cerevisiae*. Genetics 163: 515–526.

81. Galbraith AM, Bullard SA, Jiao K, Nau JJ, Malone RE (1997) Recombination and the progression of meiosis in *Saccharomyces cerevisiae*. Genetics 146: 481-489.

82. Lyndaker AM. Goldfarb T, Alani E (2008) Mutants defective in Rad1-Rad10-Slx4 exhibit a unique pattern of viability during mating-type switching in *Saccharomyces cerevisiae*. Genetics 179: 1807-1821.

CHAPTER 3

Pch2 regulates interhomolog and intersister double-strand break repair in budding yeast meiosis[1].

[1]A version of this chapter has been submitted for publication by Zanders S and Alani E. Chapter 2 is reference [19] of this chapter.

ABSTRACT

PCH2 is a widely conserved gene reported to be a meiotic checkpoint factor in *S. cerevisiae*, *C. elegans* and *D. melanogaster*. However, several non-checkpoint roles in meiotic chromosome axis organization and the regulation of interhomolog double-strand break (DSB) repair have been described for *PCH2* and its mouse ortholog, *Trip13*. Here we find that Pch2's role in DSB repair can explain many of the protein's checkpoint phenotypes in budding yeast. Specifically, we found that the recombination checkpoint requires a threshold level of unrepaired DSBs to halt meiotic progression and that *pch2*Δ lowers the level of checkpoint-eliciting lesions in recombination mutants by allowing some DSB repair. Genetic experiments are consistent with an increase in the Rad54-dependent intersister DSB repair in *pch2*Δ mutants, but physical analyses of DSB levels suggests aberrant DSB repair may still occur in *pch2*Δ *dmc1*Δ *rad54*Δ mutants. We propose a model in which a Pch2-dependent meiotic chromosome structure suppresses intersister DSB repair and regulates interhomolog repair decisions.

AUTHOR'S SUMMARY

During the cell cycle, chromosomes are replicated and held together as sister chromatids until just before cell division. If one chromatid is broken, it is preferentially repaired using information from its sister, rather than from the other parental chromosome. During meiosis, the cell division pathway that makes gametes, chromosome breaks are induced and preferentially repaired using information from the other parental chromosome. This shift in repair preferences, from using the sister chromatid to using the other parental chromosome in meiosis is known as

"interhomolog bias." This bias promotes fertility because interhomolog break repair can generate crossovers between homologous chromosomes which help chromosomes segregate properly into gametes. We discovered that the yeast Pch2 protein acts to promote interhomolog bias. In its absence, a smaller proportion of meiotic chromosome breaks are repaired using the homologous chromosome. This observation may help explain why the mouse version of Pch2 is required for fertility.

INTRODUCTION

DNA double-strand breaks (DSBs) that occur during vegetative growth are preferentially repaired via homologous recombination (HR) between sister chromatids. Strand exchange during intersister HR is mediated by the Rad51 recombinase and its partner Rad54. This intersister repair occurs even in diploid cells where a homologous chromosome template is available, and is thought to help prevent chromosome rearrangements [1-4]. In meiosis, repair of programmed DSBs using the homologous chromosome is essential for the production of viable gametes [5]. Although Rad51 and Rad54 are still present, meiotic interhomolog strand exchange is accomplished by their respective homologs, Dmc1 and Rdh54 [2,3,6-8]. Interhomolog DSB repair can create crossovers (CO) between homologous chromosomes. In many organisms these crossovers are required for reductional chromosome segregation at the meiosis I (MI) division, which reduces cell ploidy by half, allowing for the generation of haploid gametes [5]. If any pair of homologous chromosomes fails to receive a crossover, MI nondisjunction can occur and produce aneuploid gametes, which in humans can cause conditions such as Down syndrome and infertility [9].

During meiotic prophase I in budding yeast, ~140-170 DNA double-strand breaks are introduced into the genome by a group of ten proteins, of which Spo11 is

the catalytic component [5, 10-12]. Although crossovers are the only repair products known to promote MI disjunction, only ~50% of DSBs seen in yeast meiosis are repaired to form interhomolog crossovers. Some DSBs are repaired using the homologous chromosome without producing a CO; this is known as a noncrossover (NCO) [10-13]. Obligate CO formation, crossover interference, and crossover homeostasis are thought to regulate the interhomolog DSB repair to ensure each pair of homologous chromosomes disjoins at MI [13-17]. The obligate CO refers to the observation that all homologous chromosome pairs receive at least one crossover. Crossover interference promotes the nonrandom, evenly spaced distribution of CO events and crossover homeostasis maintains CO levels as DSB frequencies are decreased (reviewed in [17-18]). Little is known about the mechanisms or relatedness of the different aspects of CO control, although one mutant, *pch2*Δ, has decreased crossover interference and may also be defective for crossover homeostasis [19, 20].

The ~10-33% of meiotic DSBs estimated to not be repaired using a homologous chromosome are repaired via HR using the sister chromatid as a template [21-26]. The shift in DSB repair template preference from the sister chromatid in the mitotic cell cycle, to the homologous chromosome in meiosis, is referred to as "interhomolog bias" [22, 24, 25-31]. Interhomolog bias is established shortly after DSB formation and requires components of the axial elements, which are linear structures that form along each pair of sister chromatids early in meiotic prophase [8]. An early step in instituting interhomolog bias is phosphorylation of Hop1 of the Hop1/Red1 axial element duo by the Mec1 and Tel1 kinases [32-35]. Red1 and phosphorylated Hop1 are required for the activation of the effector kinase Mek1 [29, 30, 35]. Mek1 phosphorylates Rad54, which inhibits the interaction between the sister-chromatid recombinase partners Rad51 and Rad54 [31]. Activated Mek1 has an additional role in promoting interhomolog bias, independent of Rad54

phosphorylation, that is yet to be elucidated [31]. The meiosis-specific protein Hed1 also contributes to interhomolog bias by preventing Rad51-Rad54 complex formation by competing with Rad54 for Rad51 binding [36, 37]. Interhomolog bias is maintained in haploid meiosis and inhibits DSB repair, suggesting that interhomolog interactions are not required [38, 39]. At hemizygous DSB sites in diploid meiosis, intersister repair is still constrained by a Mek1-dependent delay, although efficient intersister DSB repair does occur [26].

The mechanisms promoting interhomolog bias are often studied in *dmc1* null mutant backgrounds in which unrepaired DSBs trigger the meiotic recombination checkpoint to arrest cells at pachytene, the last stage of meiotic prophase before cells are committed to undergo the MI division [10, 11, 27, 29-31, 40-43]. There are two ways recombination checkpoint arrest can be overcome in a *dmc1* mutant background. The first is to eliminate any of the essential checkpoint genes such as *MEC1*, *RAD17*, or *RAD24*. In such cases, meiosis proceeds with unrepaired breaks to form inviable gametes [43]. The second is to eliminate (or reduce; see below) the checkpoint-eliciting DNA lesions by either preventing DSB formation or by allowing inappropriate Dmc1-independent DSB repair [24, 25, 42, 44-46]. The latter can be accomplished by several mechanisms. Overexpressing *RAD51* or *RAD54* and/or mutating *HED1* in a *dmc1* background allows for meiotic progression and the production of moderate to wild-type levels of interhomolog COs and thus viable spores [36, 37, 45, 47]. Alternatively, when *RED1*, *HOP1*, or *MEK1* are mutated, interhomolog bias is lost and DSBs are rapidly repaired via Rad51-Rad54-dependent strand exchange using the sister chromatid as a template and meiosis progresses to produce inviable spores [27, 29, 30, 45].

Pch2 (Pachytene checkpoint) is a putative AAA ATPase reported to cause checkpoint arrest/delay in the following recombination mutants: *zip1*, *rad17*, *mms4*,

and *sae2* [48-51]. The ability of the *pch2*Δ mutation to suppress the *dmc1*Δ arrest is disputed. Two groups found that mutation of *PCH2* also allows partial bypass of the recombination checkpoint in *dmc1* mutants [48, 52], but this finding was not seen by others [19, 49, 53]. It is likely these discrepancies are due to differences in strain background and experimental conditions, as meiosis in *pch2*Δ and *pch2*Δ *dmc1*Δ mutants is especially sensitive to slight changes in strain background, sporulation media, and temperature (SZ, unpublished data; [19, 20]).

Additional studies concluded that *PCH2* orthologs also function in a meiotic checkpoint capacity in *C. elegans*, and *D. melanogaster* [54, 55]. However, it is becoming clear that classifying *PCH2* and its orthologs as "checkpoint factors" is insufficient to explain all the phenotypes associated with *pch2* mutants. In budding yeast, Pch2 is required for wild-type kinetics of meiotic progression, crossover interference, and establishing proper organization of Hop1 and Zip1 on meiotic chromosomes [19, 20, 56, 57]. An additional study suggested that Pch2 may also regulate DSB processing steps [53]. Several of these non-checkpoint roles appear conserved in the *PCH2* ortholog in mouse, *Trip13*. *Trip13* is required for wild-type levels of DSB repair, crossover interference, wild-type crossover distribution, and proper organization of HORMADs (which share homology with Hop1) and the synaptonemal complex central element protein SYCP1 on meiotic axes [58-60].

Here we investigated the mechanisms by which the *pch2*Δ mutation suppresses the meiotic arrest/delay phenotypes of both *dmc1*Δ and *zip1*Δ mutations. We find Pch2 is not acting as a *bona fide* checkpoint factor to mediate the checkpoint arrests/delays [40]. Rather, we discovered 1) that the recombination checkpoint is sensitive to DSB levels and 2) that Pch2 prevents inappropriate intersister recombination, which lowers the levels of checkpoint-eliciting lesions below the level required for full checkpoint activation. These results, combined with earlier studies,

redefine Pch2's role in budding yeast meiosis as a regulator of interhomolog and intersister DSB repair.

RESULTS

We initiated this study in the budding yeast SK1 strain background to understand the involvement of Pch2 in ensuring meiotic arrest/delay in the absence of Dmc1 or Zip1 proteins. Recent work demonstrating Pch2 acts to regulate the interhomolog CO vs. NCO DSB repair decision suggested that the initial interpretations of Pch2's checkpoint activities needed to be re-examined [19, 20, 49, 53, 57]. We hypothesize that *pch2*Δ relieves the *dmc1*Δ (and *zip1*Δ) arrest by allowing elevated levels of DSB repair.

The recombination checkpoint is sensitive to DSB levels. Investigating suppression of the *dmc1*Δ arrest (0% sporulation) by the *pch2*Δ mutation was complicated by the fact that the suppression was incomplete; only ~5% of *pch2*Δ *dmc1*Δ cells completed meiosis to form spores (Table 3-1; [19, 48, 52, 53]). Because so few cells sporulated, we analyzed *dmc1*Δ arrest suppression in the *spo11-HA* background where the sporulation defect is less severe [19]. *spo11-HA* strains display ~80% of wild-type DSBs levels [16, 61]. Wild-type, *pch2*Δ, and *spo11-HA* strains all had roughly 80% sporulation efficiencies. Whereas 0% *dmc1*Δ cells and 0.4% of *spo11-HA dmc1*Δ cells formed spores, 39% of *pch2*Δ *spo11-HA dmc1*Δ sporulated (Table 3-1). The spores produced by *pch2*Δ *dmc1*Δ and *spo11-HA pch2*Δ *dmc1*Δ were mostly inviable (<3% spore viability for each), suggesting that interhomolog recombination was not restored in these mutants (Table 3-1; [19, 48]).

Table 3-1. Spore formation efficiency and viability in *pch2Δ* mutants

Sporulation efficiencies for the above strains were counted after five days on sporulation media at 30° C. Tetrads (for *SPO13* strains) or dyads (from *spo13* strains) were dissected on YPD and scored for spore viability after three days. NA indicates that % spore viability is not applicable for strains that do not sporulate. ND indicates that spore viability was not assayed.

Genotype	% sporulation	number analyzed	% spore viability	spores analyzed
wild-type	79.1	436	93.5	400
pch2Δ	80.9	429	95.3	400
spo11-HA	81.1	434	92.5	400
pch2Δ spo11-HA	74.9	453	56.8	400
dmc1Δ	0.0	406	NA	NA
pch2Δ dmc1Δ	4.6	431	2.9	148
spo11-HA dmc1Δ	0.4	239	NA	NA
pch2Δ spo11-HA dmc1Δ	39.0	439	1.3	160
spo11-HA/spo11yf-HA	79.6	421	ND	ND
pch2Δ/pch2Δ; spo11-HA/spo11yf-HA	67.7	440	ND	ND
spo11-HA/spo11yf-HA; dmc1Δ/dmc1Δ	4.6	415	ND	ND
pch2Δ/pch2Δ; spo1l-HA/spo11yf-HA; dmc1Δ/dmc1Δ	42.8	523	ND	ND
rad54Δ	58.3	439	59.5	400
pch2Δ rad54Δ	46.0	443	47.0	400
spo11-HA rad54Δ	63.5	425	62.8	400
pch2Δ spo11-HA rad54Δ	30.7	440	38.0	400
dmc1Δ rad54Δ	0.2	422	NA	NA
pch2Δ dmc1Δ rad54Δ	0.0	444	NA	NA
spo11-HA dmc1Δ rad54Δ	0.0	409	NA	NA
pch2Δ spo11-HA dmc1Δ rad54Δ	0.0	403	NA	NA
spo13	63.3	441	47.3	400
pch2Δ spo13	49.2	417	44.8	400
spo11-HA spo13	51.8	454	44.8	400
pch2Δ spo11-HA spo13	56.9	457	44.3	400
dmc1Δ spo13	9.6	428	7.3	400
pch2Δ dmc1Δ spo13	43.4	422	15.5	400
spo11-HA dmc1Δ spo13	16.6	441	16.0	400
pch2Δ spo11-HA dmc1Δ spo13	57.9	480	25.5	396
pch2Δ spo11-HA dmc1Δ rad54Δ spo13	14.0	222	0.0	120
zip1Δ	60.1	441	36.7	412
pch2Δ zip1Δ	61.8	437	17.5	400
zip1Δ spo13	60	408	25.0	400
pch2Δ zip1Δ spo13	55.8	430	25.0	400

The ability of the *spo11-HA* allele to allow a more efficient arrest bypass in *pch2*Δ *dmc1*Δ suggests that full activation of the recombination checkpoint requires a threshold level of DSBs. We tested this by analyzing the effect of further decreasing DSBs using strains heterozygous for the *spo11-HA* hypomorph and the *spo11yf-HA* allele, in which the catalytic tyrosine is changed to a phenylalanine [62]. *spo11-HA/spo11yf-HA* heterozygotes make ~30% of the wild-type level of DSBs; we observed 80% sporulation in these mutants [16]. We saw 5% sporulation in *dmc1*Δ/*dmc1*Δ *spo11-HA*/*spo11yf-HA* mutants compared to 0% in *dmc1*Δ/*dmc1*Δ, demonstrating that the recombination checkpoint is sensitive to DSB levels in budding yeast. The *pch2*Δ mutation increased sporulation in *dmc1*Δ/ *dmc1*Δ *spo11-HA/spo11yf-HA* mutants to 43% (Table 3-1). These results show that *spo11* hypomorphs and the *pch2*Δ mutation act synergistically to partially bypass the *dmc1*Δ arrest.

The pch2*Δ *dmc1*Δ *arrest bypass is not due to a decrease in DSB formation. As shown above, we found that complete meiotic arrest in *dmc1*Δ mutants requires a threshold level of DSBs. Thus it was possible that *pch2*Δ allows checkpoint bypass by decreasing DSB formation, rather than by permitting intersister DSB repair. Genetic and physical analyses, however, suggest *pch2*Δ mutants do not form fewer DSBs. *pch2*Δ mutants have increased COs on large chromosomes and increased gene conversion frequencies on chromosomes of all sizes; the opposite effect would be expected from a mutant with reduced DSB frequencies [19, but see 20]. The *pch2*Δ *spo11-HA* double mutant has near wild-type CO and gene conversion frequencies, which is not consistent with a large decrease in break formation in this mutant [19]. Additionally, several groups have assayed DSB formation in *pch2*Δ mutants and found no change in DSB formation, apart from an increase in breaks near the rDNA repeats,

suggesting the checkpoint bypass is not due to a reduction in DSBs in *pch2*Δ mutants ([19, 49]; A. Hochwagen personal communication).

Previously, we found that *dmc1*Δ*, pch2*Δ *dmc1*Δ, and *spo11-HA dmc1*Δ mutants form similar levels of DSBs at the *YCR048W* DSB hotspot on chromosome III, but fewer breaks were apparent in *pch2*Δ *spo11-HA dmc1*Δ mutants [19]. We repeated and expanded this analysis in the slightly different strains used in this study in which checkpoint bypass in *pch2*Δ *dmc1*Δ and *pch2*Δ *spo11-HA dmc1*Δ is more pronounced. In a representative experiment, the *dmc1*Δ mutant displayed 14.4% DSBs at *YCRO48W* 6 hours after meiotic induction. *pch2*Δ *dmc1*Δ and *spo11-HA dmc1*Δ mutants displayed fewer DSBs at this hotspot with 10.0 and 9.4% breaks, respectively. The *pch2*Δ *spo11-HA dmc1*Δ triple mutants showed even fewer DSBs at 3.6% (Figure 3-1). Similar differences in DSB formation were observed at the *HIS2* DSB hotspot where 3.5, 2.4, 1.8 and 0.4% DSBs were observed in *dmc1*Δ*, pch2*Δ *dmc1*Δ, *spo11-HA dmc1*Δ, and *pch2*Δ *spo11-HA dmc1*Δ mutants, respectively (Figure 3-2; [63]). The significance of the decreased break levels observed in *pch2*Δ *dmc1*Δ as compared to *dmc1*Δ is difficult to assess because they are small and were not observed in a slightly different strain background [19]. However, we contend that the decrease in break levels observed in *pch2*Δ *spo11-HA dmc1*Δ is significant because the decrease is pronounced and was previously observed in another strain [19]. The decrease in observable DSBs in the *pch2*Δ *spo11-HA dmc1*Δ (and perhaps *pch2*Δ *dmc1*Δ) mutant could result from an increase in Dmc1-independent intersister DSB repair [19]. However, it was still possible that fewer breaks occur in *pch2*Δ and/or *pch2*Δ *spo11-HA* mutants.

We employed the *rad50S* mutation to formally test if a decrease in DSB levels can explain why fewer DSBs are observable in the *pch2*Δ *spo11-HA dmc1*Δ mutant. *rad50S* mutants form DSBs, but the breaks are not resected or repaired [64]. In a

Figure 3-1. DSB levels observed in the *dmc1*Δ and *dmc1*Δ *rad54*Δ backgrounds at the *YCRO48W* hotspot.

Southern blots on DNA obtained from 0, 3, 4, 5 and 6 hrs post meiotic induction to measure DSBs at the *YCR048W* hotspot on chromosome III are shown. The DNA was digested with *BglII* and probed with a chromosome III fragment (SGD coordinates 215,422-216,703) (See Methods). A representative blot of *dmc1Δ* (n, number of replicates, =4), *pch2Δ dmc1Δ* (n=3)*, spo11-HA dmc1Δ* (n=2), *pch2Δ spo11-HA dmc1*Δ (n=5), *spo11-HA dmc1*Δ *rad54*Δ (n=4), *pch2*Δ *spo11-HA dmc1*Δ *rad54*Δ (n=4), *dmc1*Δ *rad54*Δ (n=3), and *pch2*Δ *dmc1*Δ *rad54*Δ (n=3) is shown in. The *dmc1*Δ *rad54*Δ and *pch2*Δ *dmc1*Δ *rad54*Δ lanes are from a different time course and blot from all other samples (which were from the same experiment). The asterisk denotes the parental band and the arrows designate the DSB bands quantified. The percent DSB signal present at 6 hours post meiotic induction for each strain is displayed at the bottom of the blots.

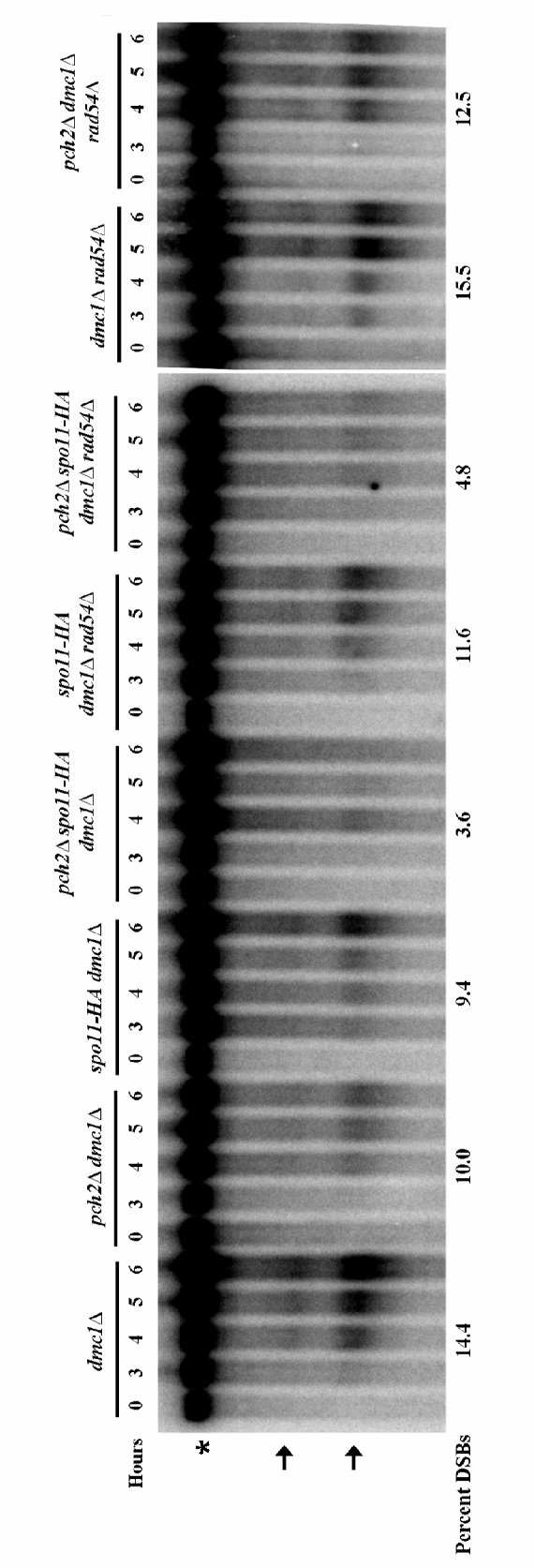
Hours
dmc1Δ
0 3 4 5 6
pch2Δ dmc1Δ
0 3 4 5 6
spo11-HA dmc1Δ
0 3 4 5 6
pch2Δ spo11-HA dmc1Δ
0 3 4 5 6
spo11-HA dmc1Δ rad54Δ
0 3 4 5 6
pch2Δ spo11-HA dmc1Δ rad54Δ
0 3 4 5 6
dmc1Δ rad54Δ
0 3 4 5 6
pch2Δ dmc1Δ rad54Δ
0 3 4 5 6
*
Percent DSBs
14.4
10.0
9.4
3.6
11.6
4.8
15.5
12.5

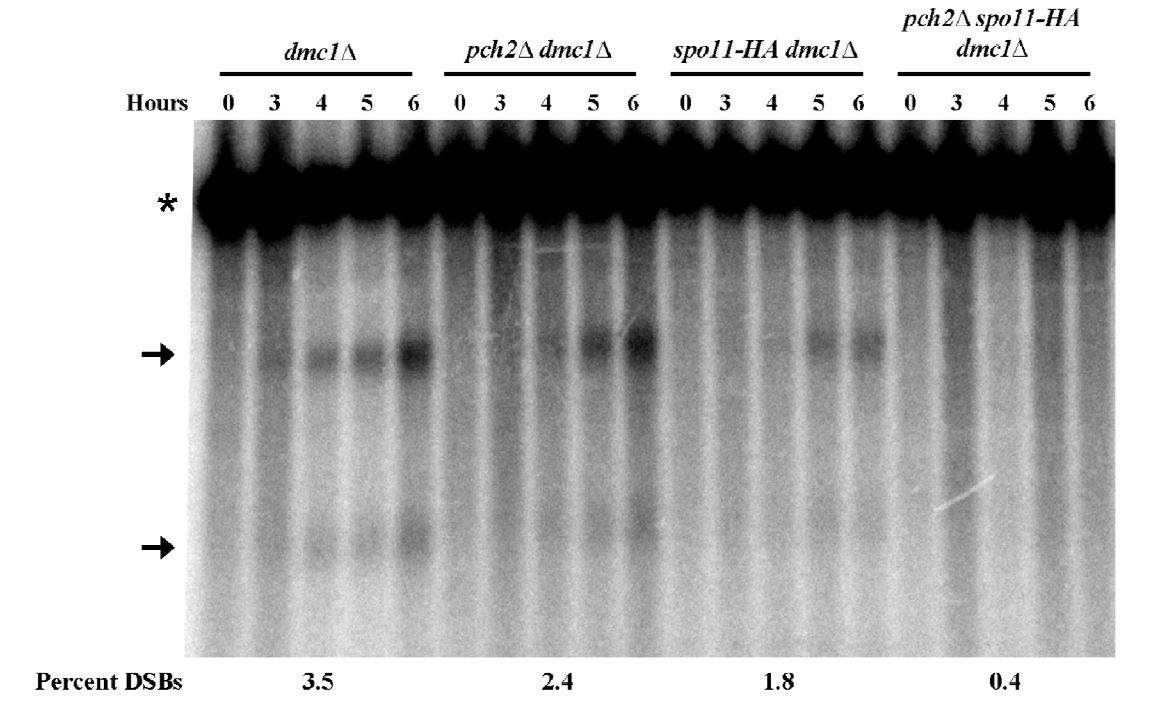

Figure 3-2. DSB levels observed in the *dmc1*Δ background at the *HIS2* hotspot.

Southern blots were performed on DNA obtained from 0, 3, 4, 5 and 6 hrs post meiotic induction to measure DSBs at the *HIS2* hotspot on chromosome VI [6]. The DNA was digested with *BglII* and probed as in [6]. A representative blot of *dmc1Δ* (n, number of replicates, =4), *pch2Δ dmc1Δ* (n=2), *spo11-HA dmc1Δ* (n=2), and *pch2Δ spo11-HA dmc1*Δ (n=4) is shown. The asterisk denotes the parental band and the arrows designate the DSB bands quantified. The percent DSB signal present at 6 hours post meiotic induction for each strain is displayed at the bottom of the blots.

representative Southern blot of the Y*CR048w* hotspot, *rad50S* and *pch2*Δ *rad50S* mutants showed similar DSB levels, 8.7 and 7.5%, respectively (Figure 3-3). The *spo11-HA rad50S* and *pch2*Δ *spo11-HA rad50S* also showed similar levels of DSBs, although the level was lower than *rad50S* alone (5.0 and 6.4%, respectively; Figure 3-3). These results demonstrate that the decrease in DSBs observed in *pch2*Δ *dmc1*Δ and *pch2*Δ *spo11-HA dmc1*Δ mutants was not due to a decrease in DSB formation, and are consistent with *pch2*Δ suppressing the *dmc1*Δ arrest by allowing Dmc1-independent DSB repair.

pch2*Δ *suppresses dmc1*Δ *arrest by allowing DSB repair. If *pch2*Δ suppresses the arrest of *dmc1*Δ mutants by allowing more DSB repair, then the spore inviability of *pch2*Δ *dmc1*Δ and *pch2*Δ *spo11-HA dmc1*Δ mutants should be suppressed by the *spo13* mutation [65]. Spo13 facilitates reductional chromosome segregation at Meiosis I by preventing the removal of centromeric sister chromatid cohesion and by promoting sister kinetochore coorientation by maintaining the monopolin complex at kinetochores [66-69]. In *spo13* mutants, meiosis consists of one chromosome division and produces two spores [65]. The meiotic division in *spo13* mutants is mixed: some chromosomes undergo an equational division (like wild-type MII) whereas others segregate reductionally (like wild-type MI) [70]. Because they can bypass the CO-dependent reductional division, *spo13* mutants can produce some viable meiotic progeny in the absence of meiotic DSBs; or if DSB repair does not yield COs, such as the case in intersister repair [29, 32, 43, 71, 72].

Similar to previous work in the SK1 strain background, we found that *spo13* *dmc1*Δ showed low levels of sporulation and spore viability, 10 and 7%, respectively, compared to *spo13* (63 and 47%, respectively; Table 3-1; [45]). Introducing the *spo11-HA* allele to *dmc1*Δ *spo13* increased sporulation to 17% and spore viability to 16% (Table 3-1). This is likely because fewer DSBs are produced in *spo11-HA* strains

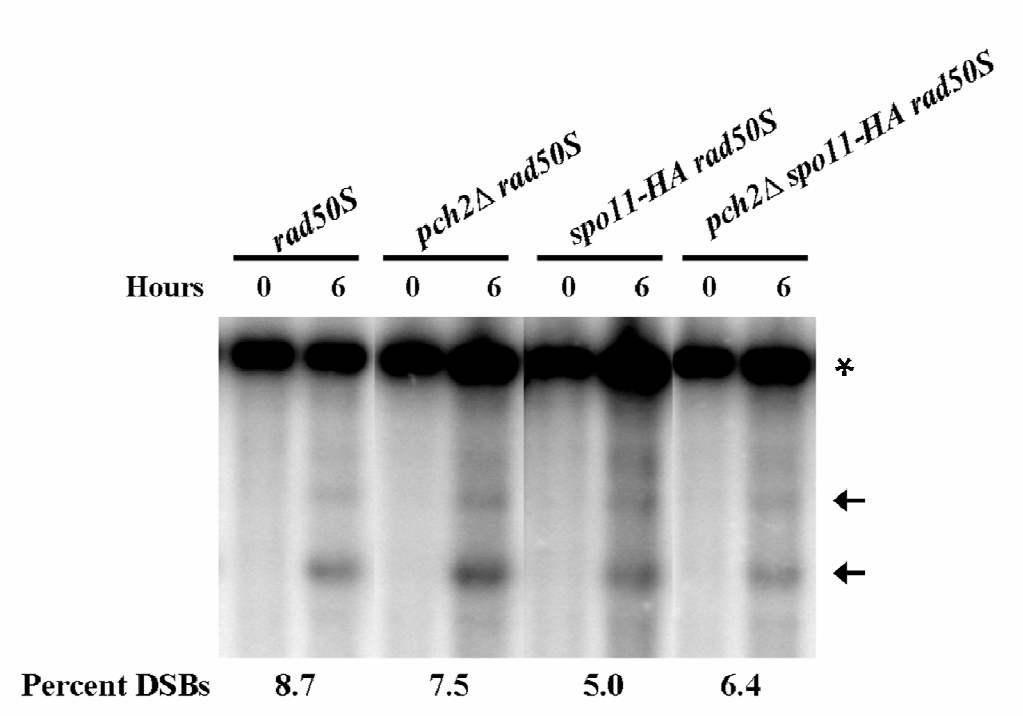

Figure 3-3. DSB levels observed in the *rad50S* background at the *YCRO48W* hotspot.

A representative blot of two showing DSB levels at the *YCRO48W* hotspot in *rad50S*, *pch2*Δ *rad50S*, *spo11*-HA *rad50S*, and *pch2*Δ *spo11-HA rad50S* is shown. The DNA was digested with *BglII* and probed with a chromosome III fragment (SGD coordinates 215,422-216,703) (See Methods). The lanes are all from the same blot, but have been rearranged for easy comparison. The asterisk denotes the parental band and the arrows designate the DSB bands quantified. The percent DSB signal present at 6 hours post meiotic induction for each strain is displayed at the bottom of the blots.

[16, 61]. Deleting *PCH2* in *dmc1*Δ *spo13* had a strong effect; sporulation increased from 10 to 43% and spore viability increased from 7 to 16% (Table 3-1). The s*po11-HA pch2*Δ *spo13 dmc1*Δ quadruple mutant showed even greater sporulation (58%) and spore viability (26%; Table 3-1). These results demonstrate that the spore inviability observed in *pch2*Δ *dmc1*Δ and *pch2*Δ *spo11-HA dmc1*Δ mutants is not caused by a complete lack of DSB repair: Dmc1-independent repair is occurring in these mutants [19, 48]. The increases in spore viability observed in *pch2*Δ *dmc1*Δ *spo13* and *pch2*Δ *spo11-HA dmc1*Δ *spo13* are smaller than the increases in sporulation efficiency. These spore viability phenotypes, combined with the physical analyses of DSBs (Figures 3-1, 3-2, 3-3), show that DSB repair is incomplete in *pch2*Δ *dmc1*Δ and *pch2*Δ *spo11-HA dmc1*Δ mutants. However, the increases in sporulation suggest that the remaining DSBs in these mutants are below the level required to trigger the recombination checkpoint in all cells.

Our main observations were: 1) complete meiotic arrest in *dmc1*Δ mutants requires a threshold level of unrepaired DSBs, 2) some *pch2*Δ *spo11-HA dmc1*Δ (and *pch2*Δ *dmc1*Δ) cells sporulate and 3) the *spo13* mutation partially suppressed the spore inviability observed in *pch2*Δ *spo11-HA dmc1*Δ and *pch2*Δ *dmc1*Δ. Together, these data are consistent with an increase in DSB repair occurring in the absence of Pch2, leading to suppression of the *dmc1*Δ arrest.

pch2*Δ *mutants have an increased dependence on Rad54 mediated repair. Intersister DSB repair is mediated by Rad51-Rad54 [2, 45]. If more intersister DSB repair occurs in *pch2*Δ mutants, then these mutants should show a greater dependence on Rad54 function. Although completion of meiosis is delayed, the *pch2*Δ single mutant has no defect in final sporulation efficiency or spore viability ([19, 48, 49]; Table 3-1). However, we observed a synthetic reduction in sporulation (46%) and spore viability (47%) in the *pch2*Δ *rad54*Δ double mutant compared to *pch2*Δ (81%

sporulation and 95% spore viability) and *rad54*Δ (58% sporulation and 60% spore viability) single mutants (Table 3-1). This synthetic phenotype is consistent with an increased requirement for Rad54-mediated intersister DSB repair in the absence of Pch2 [2].

If an increase in intersister DSB repair leads to checkpoint bypass in *pch2*Δ *dmc1*Δ and *pch2*Δ *spo11-HA dmc1*Δ mutants, then this checkpoint bypass phenotype should also be Rad54-dependent [2, 29, 45]. We found that all strains that all strains we analyzed that are *SPO13 dmc1*Δ *rad54*Δ failed to sporulate. *pch2*Δ *spo11-HA dmc1*Δ *rad54*Δ *spo13* mutants displayed a low level of sporulation (14%), with all spores being inviable (Table 3-1). These results are consistent with our hypothesis because the sporulation observed in *pch2*Δ *spo11-HA dmc1*Δ and *pch2*Δ *dmc1*Δ was Rad54-dependent, as was spore viability in *pch2*Δ *spo11-HA dmc1*Δ *spo13*.

Our genetic experiments suggest Rad54 is required for break repair that leads to checkpoint bypass in *pch2*Δ *dmc1*Δ and *pch2*Δ *spo11-HA dmc1*Δ mutants and spore viability in *pch2*Δ *spo11-HA dmc1*Δ *spo13* mutants. If so, Rad54 should be responsible for repairing a subset of DSBs in *pch2*Δ *dmc1*Δ and *pch2*Δ *spo11-HA dmc1*Δ mutants (10.0 and 3.6% DSBs in these mutants compared to 14.4% in *dmc1*Δ; Figure 3-1). We tested this hypothesis by analyzing DSBs in *rad54*Δ mutants at the *YCR048W* hotspot. Contrary to our predictions, *pch2*Δ *dmc1*Δ *rad54*Δ (12.5%) diplayed slightly fewer breaks than *dmc1*Δ *rad54*Δ (15.5%). Additionally, fewer breaks were apparent in the *pch2*Δ *spo11-HA dmc1*Δ *rad54*Δ (4.8%) mutant as compared to *spo11-HA dmc1*Δ *rad54*Δ (11.6%). These data are not consistent with Rad54-dependent repair alone causing the reduction in apparent DSBs in *pch2*Δ *spo11-HA dmc1*Δ mutants, unless additional repair pathways are allowed in *pch2*Δ *dmc1*Δ *rad54*Δ mutants. It is therefore unclear what factors contribute to the DSB repair observed in *pch2*Δ *spo11-HA dmc1*Δ mutants at this locus.

***pch2*Δ-mediated suppression of the *zip1*Δ meiotic delay phenotype is consistent with intersister DSB repair.** In the BR strain background, *zip1*Δ mutants arrest in pachytene [73]. In the SK1 strain background used in this study, *zip1*Δ mutants complete meiosis with delayed kinetics [74]. Deleting *PCH2* suppresses these delay/arrest phenotypes [48, 49, 50, 57]. Based on observations indicating relaxed recombination restraints in the absence of *PCH2* (above; [19, 20]) and the previous observation by Borner *et al.* [57] of increased intersister repair at the *HIS4-LEU2* hotspot in *pch2*Δ *zip1*Δ, we predicted that intersister recombination could also explain the bypass of *zip1*Δ arrest/delay in *pch2*Δ *zip1*Δ. We tested this hypothesis using spore viability analyses to obtain a genome-wide picture of DSB repair. We found that *zip1*Δ and *pch2*Δ *zip1*Δ mutants have very similar sporulation efficiencies (60 vs. 62%) on solid sporulation media (Table 3-1). Similar to the observations of Wu and Burgess [49], we found that the *pch2*Δ *zip1*Δ mutant displayed a synthetic spore viability defect, with only 18% spore viability compared to 95% in *pch2*Δ and 37% in *zip1*Δ (Table 3-1). The low spore viability observed in *zip1*Δ is thought to be caused by MI nondisjunction due to a failure to ensure CO formation between each pair of homologous chromosomes [74]. The synthetic decrease in spore viability observed in *pch2*Δ *zip1*Δ is consistent with an increase in DSB repair that does not promote MI disjunction, such as intersister repair. In support of this interpretation, the synthetic *pch2*Δ *zip1*Δ spore viability phenotype was completely suppressed by the *spo13* mutation because both *pch2*Δ *zip1*Δ *spo13* and *zip1*Δ *spo13* mutants displayed 25% spore viability (Table 3-1).

***pch2*Δ mutants display elevated rates of sister chromatid recombination**. Pch2 has been suggested to promote recombination progression in wild-type meiosis and inhibit aberrant recombination in mutant meiosis (i.e. *zip1*Δ and *dmc1*Δ; [57]). These observations suggest that intersister DSB repair observed in *pch2*Δ *dmc1*Δ and

*pch2*Δ *zip1*Δ may not occur in *pch2*Δ meiosis. This hypothesis is supported by the high level of spore viability seen in *pch2*Δ, as well as the increase in interhomolog CO frequencies observed on large chromosomes in *pch2*Δ mutants [19, 48, 49]. The synthetic spore viability defect observed in *pch2*Δ *rad54*Δ mutants (above), on the other hand, is consistent with excess interhomolog repair occurring in *pch2*Δ single mutants.

To distinguish between these hypotheses, we surveyed intersister recombination in wild-type and *pch2*Δ mutants using the sister chromatid exchange assay developed by Fasullo and Davis [75]. The sister-chromatid exchange assay utilizes a *HIS3* reporter gene rearranged such that the 3' end (*his3*-Δ*5'*) is placed before the 5' end (*his3*-Δ*3'*) and a central region of the gene (grey box) is included in both fragments (Figure 3-4A; [75]). In a *his3*Δ strain background, haploid cells containing the sister chromatid exchange reporter are His^-, but can become His^+ if a sister-chromatid recombination event (either a crossover or gene conversion) occurs between the *his3* truncations to produce full length *HIS3* (Figure 4B). To monitor sister chromatid exchange in meiosis, *his3*Δ diploid strains heterozygous for the reporter construct were constructed [29, 32, 46]. Meiotic sister chromatid recombination was quantified by dividing the number of His^+ colonies by the total number of colony forming units (on complete media) observed upon plating liquid sporulation cultures. The median frequencies of His^+ colonies was 1.1×10^{-6} (n=22) in wild-type and 2.1×10^{-6} in cells lacking Pch2 (n=24). *pch2*Δ values were significantly higher than wild-type (p=0.008, Mann-Whitney U test; Figure 4C).

The mitotic His^+ frequency observed was 100-fold lower and similar for wild-type and *pch2*Δ, indicating that the increase in His^+ colonies observed in *pch2*Δ was not a result of mitotic events (see Materials and Methods). Additionally, the observed increase is unlikely to be due to differences in DSB levels (Figures 3-1, 3-2, and 3-3)

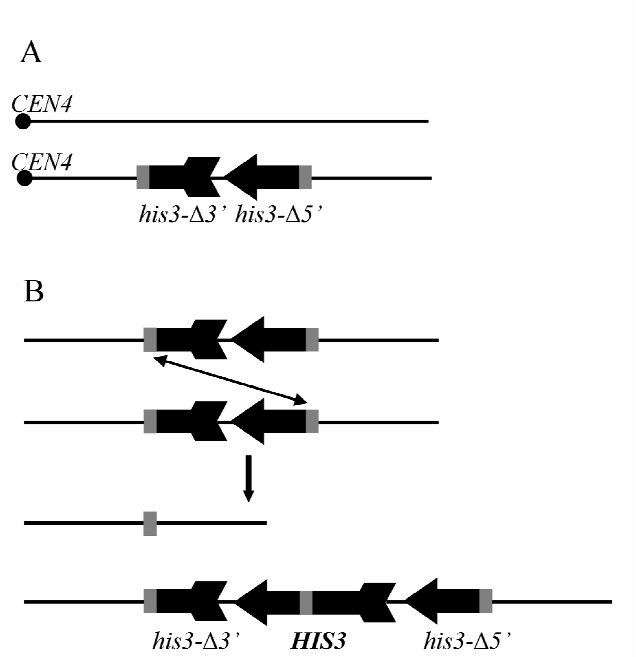

Figure 3-4. Intersister recombination is increased in *pch2*Δ.

(A) The intersister recombination assay of Fassullo and Davis [73] is shown. The *HIS3* gene is rearranged such that the 3' end (*his3*-Δ*5'*) comes before the 5' end (*his3*-Δ*3'*) and inserted into one copy of chromosome IV. Strains containing this construct are His^-, but can become His^+ if an intersister recombination event, either a crossover (represented by the double headed arrow), or gene conversion (not shown) creates a full-length *HIS3* gene (B). The frequency of post-meiotic His^+ colony forming units was assayed in wild-type and *pch2*Δ mutants. The average frequencies are shown in (C) and "n" represents the number of replicate of each genotype. The values observed in *pch2*Δ were significantly higher than wild-type (Mann-Whitney U test, p=0.008).

or meiotic completion as wild-type and *pch2*Δ have similar sporulation efficiencies and spore viabilities (Table 3-1; [19, 20, 48, 49]). These data suggest that a greater proportion of DSBs are repaired using the sister chromatid in *pch2*Δ mutants compared to wild-type.

DISCUSSION

The recombination checkpoint is sensitive to DSB levels. We find that both *pch2*Δ and *spo11* hypomorphic mutations can contribute to checkpoint bypass in *dmc1*Δ mutants. The checkpoint bypass facilitated by the *spo11* mutations is greater in a hypomorph which makes fewer DSBs, indicating that the suppression is most likely due to decreased DSB formation and not downstream DSB repair effects of the hypomorphs. These results demonstrate that the extent of the recombination checkpoint delay is dependent on the level of unrepaired DSBs. Two recent studies also proposed such a threshold effect on recombination checkpoint signaling in budding yeast. Callender and Hollingsworth found that the *rec8*Δ and *mek1-as* (a weak hypomorph) mutations synthetically contribute to checkpoint bypass in *dmc1*Δ. These authors hypothesized that the *mek1-as* allele raised the threshold number of DSBs required to trigger checkpoint arrest to a level above that produced in *rec8*Δ [38]. Similarly, Goldfarb and Lichten proposed that increased levels of Mek1 kinase activation occurs when there is an increased level of unrepaired DSBs, such as in *dmc1*Δ mutants and in haploid meiosis [26]. Evidence for a DSB threshold effect on checkpoint arrest has also been reported in *C. elegans*. Hermaphrodites heterozygous for a deletion that removes the pairing center on the X chromosome (*meDf2*/+) display unrepaired recombination intermediates that fail to trigger the recombination

checkpoint. However *syp-1* mutants, which have higher levels of unrepaired DSBs, trigger the checkpoint [54, 76].

A DSB threshold model for checkpoint activation (and therefore Mek1 activation) is sufficient to explain the synergistic effects on sporulation efficiency that the *pch2*Δ and *spo11-HA* mutations have in *dmc1*Δ cells. Through different mechanisms, both *pch2*Δ and *spo11-HA* mutations lower the level of unrepaired DSBs available to trigger the checkpoint (Figure 3-5). The resulting lower levels of checkpoint activation lead to less Mek1 signaling, which in turn leads to even less constraint on intersister DSB repair. This scenario creates a positive feedback loop where increased levels of DSBs are repaired and increased meiotic progression is allowed.

The requirement for a threshold level of unrepaired DSBs to trigger the recombination checkpoint is a stark contrast to the mitotic DNA damage checkpoint in which a single unrepaired DSB can prevent G2 to M phase cells cycle progression [77]. How can cells ensure that the MI division is delayed until all DSBs are repaired if the recombination checkpoint requires a threshold number of DSBs to halt cell cycle progression? One possible scenario is that proposed by Malone and colleagues of a "recombination initiation signal" (RIS) that delays the MI division [78]. The nature of the RIS is unknown, but the signal is not DSBs as DSB-deficient *rec103/ski8* mutants have wild-type MI division timing [78]. Perhaps the recombination checkpoint can induce a longer delay/arrest when the unrepaired DSB threshold is exceeded, but that the RIS is primarily responsible for wild-type MI division kinetics.

Pch2 acts to limit inappropriate recombination in meiosis. We demonstrate here that Pch2 acts in meiosis to suppress inappropriate DSB repair. Such a phenotype has been described for Pch2 in checkpoint-triggering mutants (*zip1*Δ and *rad17*Δ), but we find that Pch2 suppresses intersister recombination in wild-type

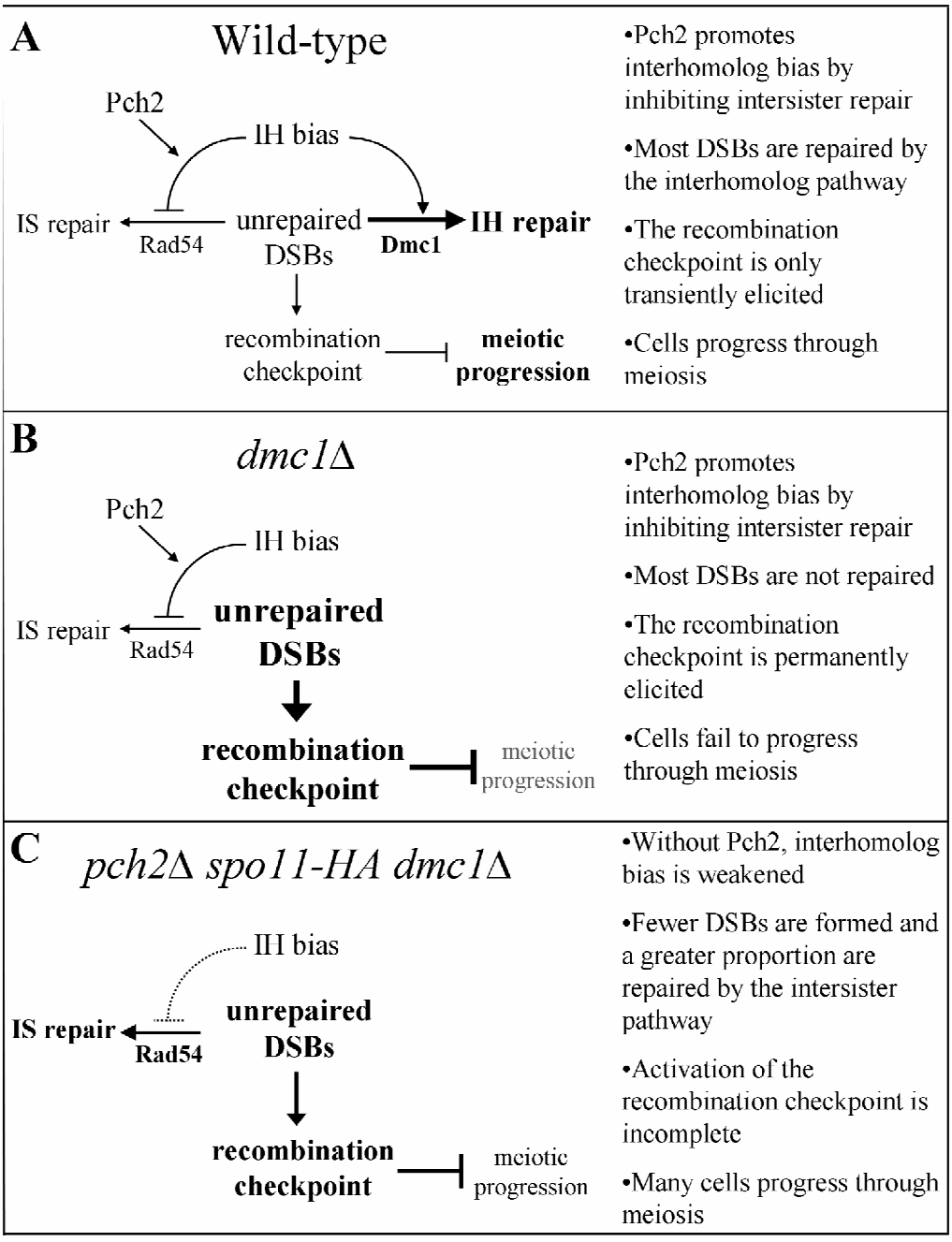

Figure 3-5. Model for DSB repair and meiotic progression in wild-type, *dmc1*Δ, and *pch2*Δ *spo11-HA dmc1*Δ meiosis.

IH, interhomolog; IS, intersister. See text for details.

meioses (Table 3-1; Figure 3-4; [49, 57]). This anti-recombination function of Pch2 promotes checkpoint-mediated delay/arrest of *dmc1*and *zip1* mutants by preventing DSB repair (Table 3-1; [57]). This repair is most likely intersister recombination because decreased DSB levels and sporulation in *pch2*Δ *dmc1*Δ mutants and spore viability in *pch2*Δ *dmc1*Δ *spo13* mutants were dependent on Rad54. However, it is important to note that lower than expected DSB levels were observed in *pch2*Δ *dmc1*Δ *rad54*Δ and *pch2*Δ *spo11-HA dmc1*Δ *rad54*Δ mutants (Table 3-1; Figure 3-1 [2]). It is, therefore, still formally possible that both Dmc1 and Rad54-independent DSB repair can occur in *pch2*Δ mutants and contribute to the low level of remaining DSBs observed in *pch2*Δ *spo11-HA dmc1*Δ and *pch2*Δ *spo11-HA dmc1*Δ *rad54*Δ mutants.

Pch2's role in suppressing intersister repair is certainly less crucial than seen for previously identified factors (i.e. Hop1, Red1, and Mek1; see Introduction). For example, in *hop1*Δ mutants interhomolog bias is lost, whereas interhomolog bias is only diminished in *pch2*Δ. However, our work suggests that the search for factors involved in regulation of DSB repair decisions should be expanded to include genes not required for high spore viability in budding yeast.

Links between meiotic interhomolog bias and the CO vs. NCO DSB repair decision. Pch2 acts in meiotic crossover control to limit crossover formation on large chromosomes and promote crossover interference [19, 20]. The mechanisms promoting interhomolog bias and the interference-regulated CO vs. NCO DSB repair decision are often considered separately. The increased level of intersister joint molecules and increased CO levels observed in *sgs1* mutants, however, suggest a link between the two [79, 80]. This work strengthens this connection by demonstrating that Pch2, in addition to its key role in crossover control, plays a role in promoting interhomolog bias. We propose that a Pch2-dependent chromosome structure, acting

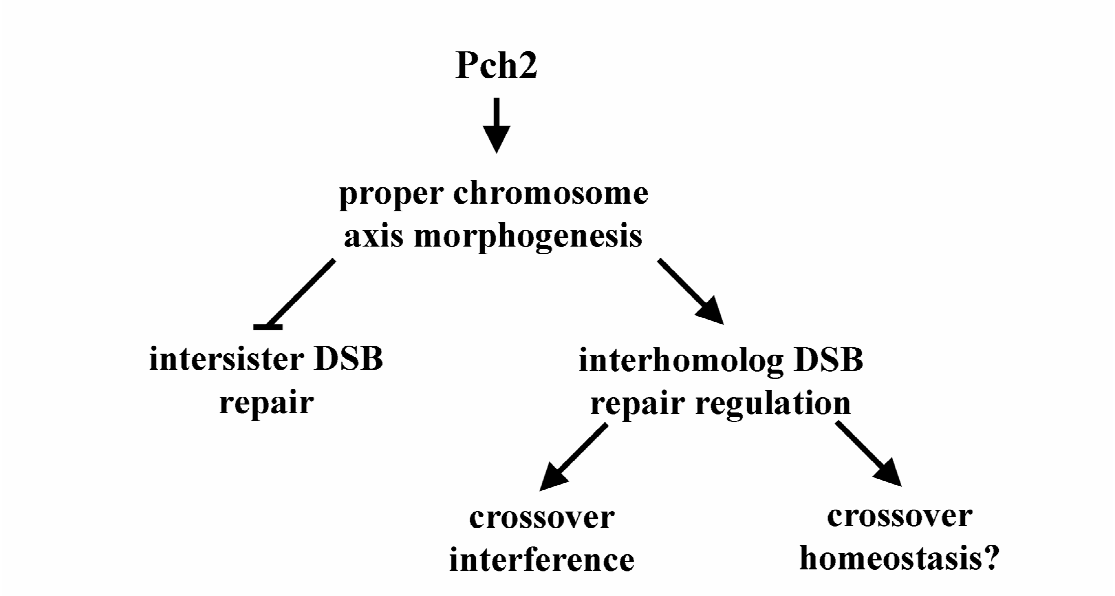

Figure 3-6. Model proposing Pch2-promoted chromosome axis organization both inhibits intersister DSB repair and regulates interhomolog DSB repair.

before or shortly after DSB formation, regulates both interhomolog DSB repair and inhibits intersister DSB repair (Figure 3-6; [20, 57]). Although the mechanism of Pch2 function is unknown, there are several avenues worthy of investigation. RTEL-1, the *C. elegans* homolog of the yeast *SRS2* helicase has recently been shown to be defective in CO interference and CO homeostasis [81]. Pch2's role in DSB repair could involve facilitating access of a helicase to inappropriate strand invasion events. Borner *et al*. [57] posit another attractive (and not mutually exclusive) hypothesis that Pch2 somehow promotes Mec1 regulatory action. Indeed, at least one downstream target of Mek1 (a Mec1 target) that promotes interhomolog bias is still unknown [8, 31]. Perhaps Pch2 is a Mek1 target and/or influences Mek1 signaling in some way. Experiments to test these hypotheses are underway.

Budding yeast Pch2 as a regulator of recombination. Pch2 has been characterized as a checkpoint factor based on the ability of the *pch2*Δ mutation to suppress the meiotic arrest/delay phenotypes of *dmc1*, *zip1*, *rad17*, *mms4*, and *sae2* mutants [48, 49, 50, 51, 57]. Although proteins can be both recombination and checkpoint factors [82], we argue that this is not the case for Pch2. First, the suppression of *dmc1*Δ*, zip1*Δ*,* and likely *rad17*Δ arrests/delay phenotypes by the *pch2*Δ mutation are accompanied by an excess of intersister DSB repair [this work; 49; 57]. Therefore, these *pch2*Δ phenotypes can be explained by a reduction in the checkpoint-eliciting lesions to sub-threshold levels, without Pch2 having checkpoint signaling capabilities. It is feasible that suppression of the *mms4*Δ delay by *pch2*Δ occurs via a similar mechanism [51]. Second, the *pch2*Δ mutation does not suppress all mutants such as *hop2*Δ, *mnd1*Δ, *sgs1*Δ, and *csm4*Δ, which have been demonstrated to elicit recombination checkpoint arrests/delays ([41, 52, 83-85]; our unpublished data). Finally, the existence of a synapsis checkpoint in budding yeast is challenged by 1) the numerous mutants which have synapsis defects, yet have wild-type or

accelerated MI division timing [i.e. 78] and 2) the fact that the *zip1* arrest/delay is mediated by the same factors as the recombination checkpoint, which are thought to recognize ssDNA recombination intermediates [reviewed in 53].

The only phenotype left unexplained by our intersister DSB repair model is the higher percentage of cells that complete the MI division in *pch2*Δ *sae2*Δ (~90%) as compared to *sae2*Δ (60-70%) [49]. The *sae2*Δ mutation is similar to *rad50S* in that no DSB processing or repair occurs [64, 86]. It is, therefore, formally possible that Pch2 is acting as a checkpoint factor to promote meiotic delay in response to what has been termed the *rad50S* checkpoint [41]. However, a more parsimonious explanation is that the same Pch2-dependent chromosome organization we propose regulates DSB repair could also facilitate recognition of lesions which trigger the *rad50S* checkpoint.

In *zip1*Δ mutants arrested in meiotic prophase, Pch2 accumulates in the nucleolus [48]. This nucleolar localization of Pch2 is likely required for its role in preventing meiotic progression in *zip1*Δ and *dmc1*Δ mutants because in a *dot1*Δ (and presumably *sir2*Δ) strain background, in which Pch2 fails to accumulate in the nucleolus, *zip1*Δ and *dmc1*Δ mutants repair DSBs and complete meiosis [48, 57, 87]. This phenotype can also be explained by Pch2's role in suppressing inappropriate recombination. The nucleolus houses rDNA, ~150 tandem repeats of the ribosomal RNA genes [88]. Recombination is normally inhibited in the rDNA to prevent expansions/contractions of the tandem repeats [89]. Sir2 and Pch2 are required to inhibit rDNA recombination, although the contribution of an anti-recombinase activity is unclear because *pch2*Δ and *sir2*Δ mutants also have increased DSB formation in or near the rDNA ([48, 90, 91]; A. Hochwagen personal communication). We interpret the whole of the yeast Pch2 literature to mean that Pch2 suppresses inappropriate recombination genome-wide and this role is especially needed in the highly repetitive rDNA region, where Pch2 is recruited in a Dot1 and Sir2-dependent manner. In the

absence of Zip1 or Dmc1, excess recombination intermediates trigger the recombination checkpoint to delay/arrest meiosis. Mutating *PCH2* can thus allow a greater proportion of the DSBs to be repaired and allow more cells complete meiosis/complete meiosis more quickly.

Functions of *PCH2* orthologs. In *C. elegans* and *D. melanogaster*, the checkpoint responses dependent upon *PCH2* orthologs are independent of DSB formation [49, 54, 55]. Thus, like the yeast *pch2*Δ *sae2*Δ mutant, the checkpoint bypasses provided by mutation of *PCH2* orthologs in these organisms cannot be caused by inappropriate DSB repair. The *PCH2* orthologs may have different roles in flies and worms, but similar chromosome organization roles could underlie the checkpoint phenotypes observed in these organisms [54, 55]. For example, the checkpoint elicitors described by Bhalla and Dernburg [54] and Joyce and McKim [55] could require Pch2-dependent chromatin organization in order to be recognized by checkpoint sensors. Without this Pch2-created chromatin context, the checkpoint trigger would go unnoticed. Thus, a *PCH2* mutation would lead to checkpoint bypass by preventing checkpoint activation, not checkpoint signaling ability, analogous to the situation we have proposed for yeast.

Our hypothesis that the repetitive nature of the rDNA explains the special role budding yeast Pch2 plays in the nucleolus could also help explain the more severe phenotype observed in mice mutants of the *PCH2* ortholog, *Trip13*. *pch2*Δ and *Trip13*$^{-/-}$ mutants both display altered crossover interference/crossover distribution and altered late-pachytene organization of HORMAD proteins and the SC central element, suggesting that the DSB repair and chromosome axis organization functions of the protein may be conserved between the two organisms. However, *pch2*Δ mutants have wild-type spore viability whereas *Trip13*$^{-/-}$ mice are completely sterile [48, 49, 58-60]. This difference could be caused by a greater dependence upon our proposed anti-

recombination function of *Trip13* due to the more complex, repetitive nature of the mouse genome.

MATERIALS AND METHODS

Media and yeast strains. All yeast strains (Table 3-2) were grown at 30°C on standard YPD (yeast peptone dextrose), synthetic complete, or synthetic complete – histidine [92]. The sporulation media was described previously [93, 85]. Geneticin (Invitrogen), nourseothricin (Hans-Knoll Institute fur Naturstoff-Forschung), and hygromycin B (Calbiochem) were added in standard concentrations to YPD media when required [93, 94].

All strains, except those used in the sister chromatid recombination assays (see below), are isogenic to the NHY943 SK1 strain described in de los Santos *et al*. [95]. The *spo11* hypomorphic mutants were described by Cha *et al*. [62], Diaz *et al*. [96] and Henderson and Keeney [61]. The NHY943 strains containing these alleles are described in Martini *et al*. [16]. As in Martini *et al*. [16], we refer to *spo11-HA3His6* as *spo11-HA* and *spo11(Y135F)-HA3His6* as *spo11yf-HA*. The *dmc1*Δ, and *zip1*Δ and *rad54*Δ alleles used in this work were all complete open reading frame (ORF) deletions. The *pch2*Δ allele contains a deletion of amino acids 17-587 [19]. All deletion cassettes were made via PCR and the deleted regions were replaced with *HPHMX4*, *KANMX4*, or *NATMX4* as shown in Table 3-2 [93, 94]. A *BamHI* fragment of pNKY58 was integrated into the genome to create the s*po13::hisG-URA3-hisG* mutation [64]. A *BglII* to *EcoRI* fragment of pNKY349 was used to replace *RAD50* with *rad50S::URA3* [64]. All mutations were initially integrated into the genome using standard transformation techniques [98]. Standard genetic crosses were used to

Table 3-2. Yeast strains.

The strains used are listed with all strains are isogenic to NH943 [95]. The strains are listed as diploids. The diploid strain names are composites of the haploid strains used to create them.

Diploid Strain Names	Genotype
NH943/EAY2580	*MATa/α*, homozygous for: *ho::hisG ade2Δ, ura3(ΔSma-Pst), leu2::hisG, CEN3::ADE2, lys5-P, cyh2^r, his4-B*
EAY2581/EAY2210	as NH943/EAY2580 except *pch2Δ::NATMX4*
EAY2582/SKY635	as NH943/EAY2580 except *spo11-HA3His6::KANMX4*
EAY2787/EAY2263	as NH943/EAY2580 except *pch2Δ::NATMX4, spo11-HA3His6::KANMX4*
EAY2637/EAY2638	as NH943/EAY2580 except *dmc1Δ::KANMX4*
EAY2639/EAY2640	as NH943/EAY2580 except *pch2Δ::NATMX4, dmc1Δ::KANMX4*
EAY2619/EAY2630	as NH943/EAY2580 except *spo11-HA3His6::KANMX4*, *dmc1Δ::KANMX4*
EAY2631/EAY2632	as NH943/EAY2580 except *pch2Δ::NATMX4, spo11-HA3His6::KANMX4, dmc1Δ::KANMX4*
EAY2582/SKY665	as NH943/EAY2580 except *spo11-HA3His6::KANMX4/spo11(Y135F)-HA3His6::KANMX4*
EAY2787/EAY2265	as NH943/EAY2580 except *pch2Δ::NATMX4*, *spo11-HA3His6::KANMX4/spo11(Y135F)-HA3His6::KANMX4*
EAY2620/EAY2800	as NH943/EAY2580 except *spo11-HA3His6::KANMX4/spo11(Y135F)-HA3His6::KANMX4, dmc1Δ::KANMX4*
EAY2622/EAY2802	as NH943/EAY2580 except *pch2Δ::NATMX4*, *spo11-HA3His6::KANMX4/spo11(Y135F)-HA3His6::KANMX5, dmc1Δ::KANMX4*
EAY2589/EAY2590	as NH943/EAY2580 except *spo13::URA3*
EAY2591/EAY2592	as NH943/EAY2580 except *pch2Δ::NATMX4, spo13::URA3*
EAY2595/EAY2596	as NH943/EAY2580 except *spo11-HA3His6::KANMX4*, *spo13::URA3*
EAY2593/EAY2594	as NH943/EAY2580 except *pch2Δ::NATMX4, spo11-HA3His6::KANMX4, spo13::URA3*
EAY2643/EAY2644	as NH943/EAY2580 except *dmc1Δ::KANMX4, spo13::URA3*
EAY2641/EAY2642	as NH943/EAY2580 except *pch2Δ::NATMX4, dmc1Δ::KANMX4, spo13::URA3*
EAY2633/EAY2634	as NH943/EAY2580 except *spo11-HA3His6::KANMX4, dmc1Δ::KANMX4, spo13::URA3*
EAY2635/EAY2636	as NH943/EAY2580 except *pch2Δ::NATMX4, spo11-HA3His6::KANMX4, dmc1Δ::KANMX4, spo13::URA3*
EAY2578/EAY2579	as NH943/EAY2580 except *rad50S::URA3*
EAY2585/EAY2586	as NH943/EAY2580 except *pch2Δ::NATMX4*, *rad50S::URA3*
EAY2587/EAY2588	as NH943/EAY2580 except *spo11-HA3His6::KANMX4*, *rad50S::URA3*
EAY2583/EAY2584	as NH943/EAY2580 except *pch2Δ::NATMX4*, *spo11-HA3His6::KANMX4*, *rad50S::URA3*

Table 3-2 continued

EAY2722/EAY2723	as NH943/EAY2580 except *rad54Δ::HPHMX4*
EAY2681/EAY2746	as NH943/EAY2580 except *pch2Δ::NATMX4, rad54Δ::HPHMX4*
EAY2740/EAY2741	as NH943/EAY2580 except *spo11-HA3His6::KANMX4*, *rad54Δ::HPHMX4*
EAY2726/EAY2727	as NH943/EAY2580 except *pch2Δ::NATMX4, spo11-HA3His6::KANMX4, rad54Δ::HPHMX4*
EAY2742/EAY2743	as NH943/EAY2580 except *rad54Δ::HPHMX4, dmc1Δ::KANMX4*
EAY2728/EAY2729	as NH943/EAY2580 except *pch2Δ::NATMX4, rad54Δ::HPHMX4, dmc1Δ::KANMX4*
EAY2738/EAY2739	as NH943/EAY2580 except *spo11-HA3His6::KANMX4, rad54Δ::HPHMX4, dmc1Δ::KANMX4*
EAY2724/EAY2725	as NH943/EAY2580 except *pch2Δ::NATMX4, spo11-HA3His6::KANMX4, rad54Δ::HPHMX4, dmc1Δ::KANMX4*
EAY2750/EAY2799	as NH943/EAY2580 except *zip1Δ::KANMX4*
EAY2749/EAY2798	as NH943/EAY2580 except *pch2Δ::NATMX4, zip1Δ::KANMX4*
EAY2873/EAY2874	as NH943/EAY2580 except *zip1Δ::KANMX4, spo13::URA3*
EAY2875/EAY2876	as NH943/EAY2580 except *pch2Δ::NATMX4, zip1Δ::KANMX4, spo13::URA3*
EAY2951/EAY2952	MATa/α homozygous for *ho::hisG*, *ura3*, and *his3Δ::KANMX4* hemizygous for *his3-Δ5' his3-Δ3'::URA3*
EAY2955/EAY2956	as EAY2951/2952 except *pch2Δ::NATMX4*

generate the various mutant combinations. Details on strain construction and primer sequences are available upon request.

To create the strains used in the sister chromatid exchange assays, the *HIS3* gene was deleted from a haploid segregant of the SK1 diploid EAY28 to create EAY2908. A cross of EAY2908 by EAY2209 (*pch2*Δ in NHY943) [19] generated EAY2910 and EAY2913. The *HIS3* sister chromatid recombination reporter assay contained on plasmid pNN287 (provided by Mike Fasullo) was integrated into the genome near *TRP1* in EAY2913 as described by Fasullo and Davis [75] to create EAY2918. Correct integration of the sister-chromatid recombination assay in EAY2918 was confirmed using Southern blot analysis. EAY2918 was then crossed to EAY2910 to generate strains EAY2951-EAY2952 (wild-type) and EAY2955-EAY2956 (*pch2*Δ*)* used in the sister chromatid recombination experiments.

Meiotic time courses and DSB Southern blotting. For the time courses to analyze meiotic DSB levels, 0.3 ml (for *RAD54* strains) or 0.6 ml (for *rad54*Δ strains) of a saturated YPD overnight culture from each strain to be analyzed was diluted into 200 ml YPA (2% potassium acetate) and grown for 17 hours. The YPA culture was then spun down, washed once in 1% potassium acetate, and resuspended in 100 ml 1% potassium acetate [98]. All strains were grown in the same batches of media and treated identically. DNA was isolated from meiotic cultures as in [10] for *dmc1*Δ strains and as in [99] for *rad50S* strains. Southern blotting was performed using standard techniques. The percent of DSB formation for four to six independent time courses (% of hybridizing bands +/- standard deviation, SD) was calculated using Image Quant software.

Meiotic sister-chromatid recombination assay. Saturated YPD overnight cultures were diluted into 22 ml YPA and grown for 17 hours. A sample of each YPA culture (0.4 to 2 ml) was plated on synthetic complete –HIS plates to detect early

mitotic sister-chromatid recombination events which would skew meiotic analyses. No such His^+ jackpots were observed in cells plated from YPA cultures (generally, fewer than 1 His^+ cell/ml plated was observed for all strains). After 17 hours, the YPA cultures were spun down, washed once in 1% potassium acetate, resuspended in 10 ml 1% potassium acetate and then allowed to sporulate 24 hours. Undiluted sporulated cells were then plated on synthetic complete –HIS and cell dilutions were plated on synthetic complete media. The frequency of His^+ cells was found by dividing the number of His^+ cells/ml by the total number of cells/ml. Experimental replicates in which fewer than 90% of cells sporulated were not included in the data presented.

ACKNOWLEDGEMENTS

We thank Andreas Hochwagen, Michael Lichten and Scott Keeney for providing unpublished data, Chip Aquadro, Heather Flores, Tamara Goldfarb, Nancy Hollingsworth, and Michael Lichten for DSB Southern blot advice, and Mike Fasullo for providing us with the *HIS3* sister chromatid exchange plasmid. We are also grateful to Nancy Hollingsworth for helpful discussions which significantly improved our presentation of this work. This work was supported by NIH grant GM53085 to EA. SZ was supported by a Cornell Presidential Fellowship and a Genetics and Development NIH training grant.

REFERENCES

1. Kadyk LC, Hartwell LH (1992) Sister chromatids are preferred over homologs as substrates for recombinational repair in *Saccharomyces cerevisiae*. Genetics 132: 387-402.

2. Arbel A, Zenvirth D, Simchen G (1999) Sister chromatid-based DNA repair is mediated by *RAD54*, not by *DMC1* or *TID1*. Embo J 18: 2648-58.

3. Shinohara M, Shita-Yamaguchi E, Buerstedde JM, Shinagawa H, Ogawa H *et al.* (1997) Characterization of the roles of the *Saccharomyces cerevisiae RAD54* gene and a homologue of *RAD54*, *RDH54*/*TID1*, in mitosis and meiosis. Genetics 147: 1545-56.

4. Krogh BO, Symington LS (2004) Recombination proteins in yeast. Annu Rev Genet 38: 233-71.

5. Roeder GS (1997) Meiotic chromosomes: it takes two to tango. Genes Dev 11: 2600-2621.

6. Dresser ME, Ewing DJ, Conrad MN, Dominguez AM, Barstead R, *et al*. (1997) *DMC1* functions in a *Saccharomyces cerevi*siae meiotic pathway that is largely independent of the *RAD51* pathway. Genetics 147: 533-44.

7. Klein HL (1997) *RDH54*, a *RAD54* homologue in *Saccharomyces cerevisiae*, is required for mitotic diploid-specific recombination and repair and for meiosis. Genetics 147: 1533-43.

8. Hollingsworth NM (2010) Phosphorylation and the creation of interhomolog bias during meiosis in yeast. Cell Cycle 9: 436-7.

9. Hassold T, Hall H, Hunt P (2007) The origin of human aneuploidy: where we have been, where we are going. Hum Mol Genet 16 Spec No. 2: R203-8.

10. Buhler C, Borde V, Lichten M (2007) Mapping meiotic single-strand DNA reveals a new landscape of DNA double-strand breaks in *Saccharomyces cerevisiae*. PLoS Biol 5: e324.

11. Blitzblau HG, Bell GW, Rodriguez J, Bell SP, Hochwagen A (2007) Mapping of meiotic single-stranded DNA reveals double-stranded-break hotspots near centromeres and telomeres. Curr Biol 17: 2003-12.

12. Mancera E, Bourgon R, Brozzi R, Huber W, Steinmetz LM (2008) High-resolution mapping of meiotic crossovers and non-crossovers in yeast. Nature 454: 479-85.

13. Chen SY, Tsubouchi T, Rockmill B, Sandler JS, Richards DR, *et al*. (2008) Global analysis of the meiotic crossover landscape. Dev Cell 15: 401-15.

14. Bishop DK, Zickler D (2004) Early decision; meiotic crossover interference prior to stable strand exchange and synapsis. Cell 117: 9-15.

15. Borner GV, Kleckner N, Hunter N (2004) Crossover/noncrossover differentiation, synaptonemal complex formation, and regulatory surveillance at the leptotene/zygotene transition of meiosis. Cell 117: 29-45.

16. Martini E, Diaz RL, Hunter N, Keeney S (2006) Crossover homeostasis in yeast meiosis. Cell 126: 285-95.

17. Berchowitz LE, Copenhaver GP (2010) Genetic Interference: Don't stand so close to me. Current Genomics 11: 91-102.

18. Jones GH, Franklin FC (2006) Meiotic crossing-over: obligation and interference. Cell 126: 246-8.

19. Zanders S, Alani E (2009) The *pch2Delta* mutation in baker's yeast alters meiotic crossover levels and confers a defect in crossover interference. PLoS Genet 5: e1000571.

20. Joshi N, Barot A, Jamison C, Borner GV (2009) Pch2 links chromosome axis remodeling at future crossover sites and crossover distribution during yeast meiosis. PLoS Genet 5: e1000557.

21. Haber JE, Thorburn PC, Rogers D (1984) Meiotic and mitotic behavior of dicentric chromosomes in *Saccharomyces cerevisiae*. Genetics 106: 185-205.

22. Jackson JA, Fink GR (1985) Meiotic recombination between duplicated genetic elements in *Saccharomyces cerevisiae*. Genetics 109: 303-32.

23. Game JC, Sitney KC, Cook VE, Mortimer RK (1989) Use of a ring chromosome and pulsed-field gels to study interhomolog recombination, double-strand DNA breaks and sister-chromatid exchange in yeast. Genetics 123: 695-713.

24. Schwacha A, Kleckner N (1994) Identification of joint molecules that form frequently between homologs but rarely between sister chromatids during yeast meiosis. Cell 76: 51-63.

25. Schwacha A, Kleckner N (1997) Interhomolog bias during meiotic recombination: meiotic functions promote a highly differentiated interhomolog-only pathway. Cell 90: 1123-35.

26. Goldfarb T, Lichten M (2010) The sister chromatid is frequently and efficiently used for DNA double-strand break repair during budding yeast meiosis. (submitted)

27. Wan L, de los Santos T, Zhang C, Shokat K, Hollingsworth NM (2004) Mek1 kinase activity functions downstream of *RED1* in the regulation of meiotic double strand break repair in budding yeast. Mol Biol Cell 15: 11-23.

28. Webber HA, Howard L, Bickel SE (2004) The cohesion protein ORD is required for homologue bias during meiotic recombination. J Cell Biol 164: 819-29.

29. Niu H, Wan L, Baumgartner B, Schaefer D, Loidl J, *et al.* (2005) Partner choice during meiosis is regulated by Hop1-promoted dimerization of Mek1. Mol Biol Cell 16: 5804-18.

30. Niu H, Li X, Job E, Park C, Moazed D, *et al*. (2007) Mek1 kinase is regulated to suppress double-strand break repair between sister chromatids during budding yeast meiosis. Mol Cell Biol 27: 5456-67.

31. Niu H, Wan L, Busygina V, Kwon Y, Allen JA, *et al.* (2009) Regulation of meiotic recombination via Mek1-mediated Rad54 phosphorylation. Mol Cell 36: 393-404.

32. Hollingsworth NM, Byers B(1989) *HOP1*: a yeast meiotic pairing gene. Genetics 121: 445-62.

33. Hollingsworth NM, Goetsch L, Byers B (1990) The *HOP1* gene encodes a meiosis-specific component of yeast chromosomes. Cell 61: 73-84.

34. Rockmill B, Roeder GS (1990) Meiosis in asynaptic yeast. Genetics 126: 563-74.

35. Carballo JA, Johnson AL, Sedgwick SG, Cha RS (2008) Phosphorylation of the axial element protein Hop1 by Mec1/Tel1 ensures meiotic interhomolog recombination. Cell 132: 758-70.

36. Tsubouchi H, Roeder GS (2006) Budding yeast Hed1 down-regulates the mitotic recombination machinery when meiotic recombination is impaired. Genes Dev 20: 1766-75.

37. Busygina V, Sehorn MG, Shi IY, Tsubouchi H, Roeder GS, *et al*. (2008) Hed1 regulates Rad51-mediated recombination via a novel mechanism. Genes Dev 22: 786-95.

38. Callender T, Hollingsworth NM (2010) Mek1 suppression of meiotic double strand break repair is specific to sister chromatids, chromosome autonomous and independent of Rec8 cohesin complexes. Genetics (in press)

39. De Massy B, Baudat F, Nicolas A (1994) Initiation of recombination in *Saccharomyces cerevisiae* haploid meiosis. Proc Natl Acad Sci USA 91: 11929-11933.

40. Hartwell LH, Weinert TA (1989) Checkpoints: controls that ensure the order of cell cycle events. Science 246: 629-34

41. Hochwagen A, Amon A (2006) Checking your breaks: surveillance mechanisms of meiotic recombination. Curr Biol 16: R217-28.

42. Bishop DK, Park D, Xu L, Kleckner N (1992) *DMC1*: a meiosis-specific yeast homolog of E. coli *recA* required for recombination, synaptonemal complex formation, and cell cycle progression. Cell 69: 439-56.

43. Lydall D, Nikolsky Y, Bishop DK, Weinert TA (1996) A meiotic recombination checkpoint controlled by mitotic checkpoint genes. Nature 383: 840-3.

44. Xu L, Weiner BM, Kleckner N (1997) Meiotic cells monitor the status of the interhomolog recombination complex. Genes Dev 11: 106-18.

45. BishopDK, Nikolski Y, Oshiro J, Chon J, Shinohara M, *et al*. (1999) High copy number suppression of the meiotic arrest caused by a *dmc1* mutation: *REC114* imposes an early recombination block and *RAD54* promotes a *DMC1*-independent DSB repair pathway. Genes Cells 4: 425-44.

46. Thompson DA, Stahl FW (1999) Genetic control of recombination partner preference in yeast meiosis. Isolation and characterization of mutants elevated for meiotic unequal sister-chromatid recombination. Genetics 153: 621-41.

47. Tsubouchi H, Roeder GS (2003) The importance of genetic recombination for fidelity of chromosome pairing in meiosis. Dev Cell. 5: 915-25

48. San-Segundo PA, Roeder GS (1999) Pch2 links chromatin silencing to meiotic checkpoint control. Cell 97: 313-24.

49. Wu HY, Burgess SM (2006) Two distinct surveillance mechanisms monitor meiotic chromosome metabolism in budding yeast. Curr Biol 16: 2473-9.

50. Mitra N, Roeder GS (2007) A novel nonnull *ZIP1* allele triggers meiotic arrest with synapsed chromosomes in Saccharomyces cerevisiae. Genetics 176: 773-87.

51. de los Santos T, Loidl J, Larkin B, Hollingsworth NM (2001) A role for *MMS4* in the processing of recombination intermediates during meiosis in *Saccharomyces cerevisiae.* Genetics 159: 1511-25.
52. Zierhut C, Berlinger M, Rupp C, Shinohara A, Klein F (2004) Mnd1 is required for meiotic interhomolog repair. Curr Biol 14: 752-62.

53. Hochwagen A, Tham WH, Brar GA, Amon A (2005) The FK506 binding protein Fpr3 counteracts protein phosphatase 1 to maintain meiotic recombination checkpoint activity. Cell 122: 861-73.

54. Bhalla N, Dernburg AF (2005) A conserved checkpoint monitors meiotic chromosome synapsis in Caenorhabditis elegans. Science 310: 1683-6.

55. Joyce EF, McKim KS (2009) Drosophila *PCH2* is required for a pachytene checkpoint that monitors double-strand-break-independent events leading to meiotic crossover formation. Genetics 181: 39-51.

56. Sym M, Roeder GS (1995) Zip1-induced changes in synaptonemal complex structure and polycomplex assembly. J Cell Biol 128: 455-66.

57. Borner GV, Barot A, Kleckner N (2008) Yeast Pch2 promotes domainal axis organization, timely recombination progression, and arrest of defective recombinosomes during meiosis. Proc Natl Acad Sci U S A 105: 3327-32.

58. Li XC, Schimenti JC (2007) Mouse pachytene checkpoint 2 (*trip13*) is required for completing meiotic recombination but not synapsis. PLoS Genet 3: e130.

59. Wojtasz L, Daniel K, Roig I, Bolcun-Filas E, Xu H, *et al*. (2009) Mouse HORMAD1 and HORMAD2, two conserved meiotic chromosomal proteins, are depleted from synapsed chromosome axes with the help of TRIP13 AAA-ATPase. PLoS Genet 5: e1000702.

60. Roig I, Dowdle JA, Toth A, de Rooj DG, Jasin M, Keeney S (2010) Mouse TRIP13/*PCH2* is required for recombination and normal higher order chromosome structure during meiosis. PLoS Genetics (in press)

61. Henderson KA, Keeney S (2004) Tying synaptonemal complex initiation to the formation and programmed repair of DNA double-strand breaks. Proc Natl Acad Sci U S A 101: 4519-24.

62. Cha RS, Weiner BM, Keeney S, Dekker J, Kleckner N (2000) Progression of meiotic DNA replication is modulated by interchromosomal interaction proteins, negatively by Spo11p and positively by Rec8p. Genes Dev 14: 493-503.

63. Bullard SA, Kim S, Galbraith AM, Malone RE (1996) Double strand breaks at the *HIS2* recombination hot spot in *Saccharomyces cerevisiae*. Proc Natl Acad Sci U S A 93: 13054-9.

64. Alani E, Padmore R, Kleckner N (1990) Analysis of wild-type and *rad50* mutants of yeast suggests an intimate relationship between meiotic chromosome synapsis and recombination. Cell 61: 419-36.

65. Klapholz S, Esposito RE (1980) Isolation of *SPO12*-1 and *SPO13*-1 from a natural variant of yeast that undergoes a single meiotic division. Genetics 96: 567-88.

66. Shonn MA, McCarroll R, Murray AW (2002) Spo13 protects meiotic cohesin at centromeres in meiosis I. Genes Dev 16: 1659-71.

67. Lee BH, Amon A, Prinz S (2002) Spo13 regulates cohesin cleavage. Genes Dev 16: 1672-81.

68. Katis Vl, Matos J, Mori S, Shirahige K, Zachariae W, *et al*. (2004) Spo13 facilitates monopolin recruitment to kinetochores and regulates maintenance of centromeric cohesion during yeast meiosis. Curr Biol 14: 2183-96.

69. Lee BH, Kiburz BM, Amon A (2004) Spo13 maintains centromeric cohesion and kinetochore coorientation during meiosis I. Curr Biol 14: 2168-82.

70. Hugerat Y, Simchen G (1993) Mixed segregation and recombination of chromosomes and YACs during single-division meiosis in *spo13* strains of *Saccharomyces cerevisiae*. Genetics 135: 297-308.

71. Malone RE, Esposito RE (1981) Recombinationless meiosis in *Saccharomyces cerevisiae*. Mol Cell Biol 1: 891-901.

72. Rockmill B, Roeder GS (1988) *RED1*: a yeast gene required for the segregation of chromosomes during the reductional division of meiosis. Proc Natl Acad Sci U S A 85: 6057-61.

73. Sym M, Engebrecht JA and Roeder GS (1993) *ZIP1* is a synaptonemal complex protein required for meiotic chromosome synapsis. Cell 72: 365-78.

74. Sym M, Roeder GS (1994) Crossover interference is abolished in the absence of a synaptonemal complex protein. Cell 79: 283-92.

75. Fasullo MT, Davis RW (1987) Recombinational substrates designed to study recombination between unique and repetitive sequences in vivo. Proc Natl Acad Sci U S A 84: 6215-9.

76. MacQueen AJ, Phillips CM, Bhalla N, Weiser P, Villeneuve AM, *et al*. (2005) Chromosome sites play dual roles to establish homologous synapsis during meiosis in *C. elegans*. Cell 123: 1037-50.

77. Bennett CB, Lewis AL, Baldwin KK, Resnick MA (1993) Lethality induced by a single site-specific double-strand break in a dispensable yeast plasmid. Proc Natl Acad Sci U S A 90: 5613-7.

78. Malone RE, Haring SJ, Foreman KE, Pansegrau ML, Smith SM, et al. (2004) The signal from the initiation of meiotic recombination to the first division of meiosis. Eukaryot Cell 3: 598-609.

79. Oh SD, Lao JP, Taylor AF, Smith GR, Hunter N (2008) RecQ helicase, Sgs1, and XPF family endonuclease, Mus81-Mms4, resolve aberrant joint molecules during meiotic recombination. Mol Cell 31: 324-36.

80. Jessop L, Lichten M (2008) Mus81/Mms4 endonuclease and Sgs1 helicase collaborate to ensure proper recombination intermediate metabolism during meiosis. Mol Cell 31: 313-23.

81. Youds JL, Mets DG, McIlwraith MJ, Martin JS, Ward JD, *et al*. RTEL-1 enforces meiotic crossover interference and homeostasis. Science 327: 1254-8.

82. Grushcow JM, Holzen TM, Park KJ, Weinert T, Lichten M, *et al*. (1999) *Saccharomyces cerevisiae* checkpoint genes *MEC1*, *RAD17* and *RAD24* are required for normal meiotic recombination partner choice. Genetics 153: 607-20.

83. Rockmill B, Fung JC, Branda SS, Roeder GS (2003) The Sgs1 helicase regulates chromosome synapsis and meiotic crossing over. Curr Biol 13: 1954-62.

84. Roeder GS, Bailis JM (2000) The pachytene checkpoint. Trends Genet 16: 395-403.

85. Wanat JJ, Kim KP, Koszul R, Zanders S, Weiner B, *et al.* (2008) Csm4, in collaboration with Ndj1, mediates telomere-led chromosome dynamics and recombination during yeast meiosis. PLoS Genet 4: e1000188.

86. San-Segundo PA, Roeder GS (2000) Role for the silencing protein Dot1 in meiotic checkpoint control. Mol Biol Cell 11: 3601-15.

87. Warner JR (1999) The economics of ribosome biosynthesis in yeast. Trends Biochem Sci 24: 437-40.

88. Petes TD, Botstein D (1977) Simple Mendelian inheritance of the reiterated ribosomal DNA of yeast. Proc Natl Acad Sci U S A 74: 5091-5.

89. Gottlieb S, Esposito RE (1989) A new role for a yeast transcriptional silencer gene, *SIR2*, in regulation of recombination in ribosomal DNA. Cell 56: 771-6.

90. Mieczkowski PS, Dominska M, Buck MJ, Lieb JD, Petes TD (2007) Loss of a histone deacetylase dramatically alters the genomic distribution of Spo11p-catalyzed DNA breaks in *Saccharomyces cerevisiae*. Proc Natl Acad Sci U S A 104: 3955-60.

91. Rose MD, Winston F, Hieter P(1990) Methods in yeast genetics: A laboratory course manual. Cold Spring Harbor, NY: Cold Spring Harbor Laboratory Press.

92. Argueso JL, Wanat J, Gemici Z, Alani E (2004) Competing crossover pathways act during meiosis in *Saccharomyces cerevisiae*. Genetics 168: 1805-16.

93. Wach A, Brachat A, Pohlmann R, Philippsen P (1994) New heterologous modules for classical or PCR-based gene disruptions in *Saccharomyces cerevisiae*. Yeast 10: 1793-808.

94. Goldstein AL, McCusker JH (1999) Three new dominant drug resistance cassettes for gene disruption in *Saccharomyces cerevisiae*. Yeast 15: 1541-53.

95. de los Santos T, Hunter N, Lee D, Larkin B, Loidl J, *et al.* (2003) The Mus81/Mms4 endonuclease acts independently of double-Holliday junction resolution to promote a distinct subset of crossovers during meiosis in budding yeast. Genetics 164: 81-94.

96. Diaz RL, Alcid AD, Berger JM, Keeney S (2002) Identification of residues in yeast Spo11p critical for meiotic DNA double-strand break formation. Mol Cell Biol 22: 1106-15.

97. Gietz RD, Schiestl RH, Willems AR, Woods RA (1995) Studies on the transformation of intact yeast cells by the LiAc/SS-DNA/PEG procedure. Yeast 11: 355-60.

98. Galbraith AM, Bullard SA, Jiao K, Nau JJ, Malone RE (1997) Recombination and the progression of meiosis in *Saccharomyces cerevisiae*. Genetics 146: 481-9.

99. Goyon C, Lichten M (1993) Timing of molecular events in meiosis in *Saccharomyces cerevisiae*: stable heteroduplex DNA is formed late in meiotic prophase. Mol Cell Biol 13: 373-82.

100. Yamashita K, Shinohara M, Shinohara A (2004) Rad6-Bre1-mediated histone H2B ubiquitylation modulates the formation of double-strand breaks during meiosis. Proc Natl Acad Sci U S A. 101:11380-5.

CHAPTER 4

Identification of mutagenesis patterns in mismatch repair defective diploid yeast by whole-genome sequencing[1].

[1]This chapter has been submitted for publication by Zanders S, Ma X, RoyChoudhury A, Hernandez R, Demogines A, Baker B, Gu Z, Bustamante C, Alani E. Contributions to this work were as follows: All authors aided in the conception and design of experiments. A Demogines isolated a subset of the genomic DNA that was sequenced; X Ma and A RoyChoudhury carried out the simulation, sequence alignments and mutation calling; E Alani created the plasmids used for the mutational reporter assays; all other work was completed by S.E. Z.

ABSTRACT

DNA replication errors that escape polymerase proofreading and mismatch repair (MMR) can lead to base substitution and frameshift mutations. Such mutations can disrupt gene function, reduce fitness, and promote diseases such as cancer, and are also the raw material of molecular evolution. To analyze with limited bias genomic features associated with DNA polymerase errors, we performed a genome-wide analysis of the mutations that accumulated in MMR-deficient diploid lines of *Saccharomyces cerevisiae*. These lines were derived from a common ancestor and were grown for 160 generations, with bottlenecks reducing the population to one cell every twenty generations. We sequenced to between eight and twenty-fold coverage one wild-type and three mutator lines using Illumina Solexa 36-bp reads. Using an experimentally aware Bayesian genotype caller to pool experimental data across sequencing runs for all strains, we detected a combined 28 heterozygous single-nucleotide polymorphisms (SNPs) and 48 single nt insertion/deletions (indels) in the mutator lines. No mutations were detected in the wild-type line. The genotype caller was evaluated on simulated data sets and found to have a very low false positive rate (~6×10^{-5}) and a false negative rate of 0.08 within the unique mapping regions of the genome that contained at least seven-fold coverage. The method was also confirmed by Sanger sequencing the detected mutations. All of the mutations were unique to a given line, except for a single nt deletion mutation which occurred independently in two lines. All 48 indels, comprised of 46 deletions and two insertions, occurred in homopolymer tracts (i.e., 47 poly A or T tracts, 1 poly G or C tract) between five and thirteen base pairs long. Furthermore, we found that insertion/deletion (indel) mutations within homopolymeric (HP) tracts appear more likely to occur when present in 50-500 bp windows that contain additional HP tracts ($p < 0.05$, Mann-Whitney U-

test). Importantly, no such enrichment is seen for SNPs. Our findings are of interest because HP tracts are present at high levels in the yeast genome (> 77,400 for five to twenty nt HP tracts), and frameshift mutations in these regions are likely to disrupt gene function. Also, the Bayesian method provides a robust tool to detect heterozygous mutations in diploid organisms from short read sequencing data.

INTRODUCTION

Mutation rates in prokaryotic and eukaryotic organisms are typically determined by measuring reversion or forward mutation for specific marker alleles. These values are then extrapolated to obtain genome-wide estimates. Mutation rates in higher eukaryotes are also estimated by analyzing sequence divergence between different strains or species, followed by reconstructing the accumulation of mutations since divergence (reviewed in [1]). These approaches suffer from two main limitations. First, recent studies have shown that mutation rate and repair efficiency vary across the genome and are affected by parameters that include base composition, local recombination rate, gene density, transcriptional activity, repair efficiency, chromatin structure, nucleosome position, and replication timing [2-10]. Second, genomic comparisons can yield inaccurate rate measurements because DNA repair and subsequent purifying natural selection can bias the number and type of mutations that remain in the population, especially for mutations that occur in coding regions (reviewed in [1]).

Our goal in this study was to analyze with limited bias the rate at which mutations occur due to DNA polymerase errors during DNA replication, and to identify novel genomic features associated with these errors. This was accomplished by whole genome sequence analyses of diploid DNA mismatch repair (MMR)-

defective strains which had previously been allowed to accumulate mutations for 160 generations [11]. These lines contain a temperature sensitive mutation in the *mlh1* MMR gene (*mlh1-7*, referred to here as *mlh1*^{ts}; [11]). Mlh1 is an essential component of the DNA mismatch repair machinery that acts to repair base-base and insertion/deletion loop mismatches (indels) that occur as the result of DNA polymerase errors during DNA replication [12]. The sequenced lines were created by allowing one wild-type and three *mlh1*^{ts} diploids to grow for 160 generations at the non-permissive temperature with a bottleneck that reduced the population size to one cell every 20 generations. A conditional *mlh1* allele was chosen instead of a null so that mutation accumulation in the absence of MMR could be limited to 160 generations by shifting cells at generation 160 to the permissive temperature for MMR function. Unlike *mlh1*Δ strains that display poor spore viability due to defects in meiotic crossing over, *mlh1-7*^{ts} lines display wild-type spore viability at the permissive temperature. Such a phenotype allowed us to easily identify recessive lethal mutations [11]. At the non-permissive temperature, the *mlh1-7*^{ts} mutation conferred a phenotype similar to the null in the canavanine resistance mutation assay and a mutator phenotype in the *lys2-A14* reversion assay that was 1000-fold higher than *MLH1* but four-fold lower than the null ([11]; Julie Heck, and E. A., unpublished observations).

Tetrad analysis showed that the *mlh1-7*^{ts} bottleneck lines would be ideally suited for a high-throughput DNA sequencing approach that would identify mutagenesis patterns. First, the wild-type line maintained high spore viability (~94%) at generation 160. In contrast, the *mlh1-7*^{ts} lines sequenced displayed reduced spore viabilities demonstrating that the lines had accumulated mutations. Second, comparative genome hybridization (CGH) and pulse-field (PFGE) analyses of the *mlh1-7*^{ts} strains indicated that they did not undergo major genome rearrangements [11]. Third, because the lines were grown as diploids for a limited number of

generations, secondary mutations should rarely occur that alter the rate or type of mutagenesis. Also, because there is no sexual reproduction and mutations should clonally propagate after escaping the initial bottleneck, newly arising mutations should appear as heterozygous sites. Finally, the above strategy should limit biases in mutation accumulation because the diploid cells were grown in rich media under minimal selection pressure where deleterious mutations could accumulate [11].

As described below, a Bayesian method was developed to detect heterozygous mutations in one wild-type and three *mlh1-7*^{ts} lines using whole-genome sequencing. We detected 28 heterozygous single-nucleotide polymorphisms (SNPs) and 48 single nt insertion/deletion (indels) in the mutator lines, all of which mapped to homopolymeric runs of nucleotides (HP tracts). The mutation spectra matches closely with that predicted by previous mutational analysis of different reporter constructs. In addition, we were able to correlate genotype to phenotype for one locus in one mutator line and provided bioinformatics evidence that regions of the genome enriched for polymeric runs can alter DNA polymerase fidelity. Together this work provides new insights into how sequence context can shape genome evolution.

MATERIALS AND METHODS

Whole-genome sequencing analysis of Mut lines: Bottleneck experiments involving ten independent wild-type (*MATa/MATalpha*, *his3/HIS3*, *LEU2/leu2*, *cyh*^{r}*/cyh*^{s}, *ade2/ADE2*, *ura3/ura3*, *trp1/trp1*) and isogenic *mlh1-7*^{ts} (*MATa/MATalpha*, *mlh1-7::KanMX4/mlh1-7::KanMX4*, *his3/HIS3*, *LEU2/leu2*, *cyh*^{r}*/cyh*^{s}, *ade2/ADE2*, *ura3/ura3*, *trp1/trp1*) lines were performed previously [11]. Three of the ten *mlh1-7*^{ts} lines at generation 160 were analyzed by whole genome sequencing. These lines were chosen to ensure a reasonable sample set of mutations, and displayed a lower range of

spore viabilities (2.5-15.6%) following tetrad dissection compared to the entire set (1.1-77%).

Whole-genome sequencing was performed at the Cornell University Life Sciences Core Laboratory Center (CLC) using an Illumina Genome Analyzer (http://www.illumina.com). Yeast genomic DNA for whole genome sequencing was prepared using a Qiagen genomic DNA preparation kit (www.qiagen.com). Sequencing was performed using the Illumina pipeline for 36 bp single-end reads. Reads were aligned onto the S288c genome (http://genome.ucsc.edu/cgi-bin/hgGateway) using Novoalign (www.novocraft.com), a program that performs a gapped alignment with high specificity and sensitivity.

Detection of DNA sequence heterozygosity using a Bayesian approach: We analyzed five diploid strains in this study: a wild-type strain at generations 0 and 160 (Wt0, Wt160) and three derived *mlh1-7*^{ts} mutator lines grown vegetatively (i.e., no meiosis) and bottlenecked to one cell every twenty generations until generation 160 (Mut2, Mut3, Mut4). Several aspects of the experiment required us to develop a novel approach for calling genotypes from the sequencing data. First, the initial wild-type strain (Wt0) likely contained SNPs and indels that distinguish it from the reference yeast genome. Because all lines were grown vegetatively, they were all expected to have the "propagated" SNPs and indels. Thus reads from the five sequenced lines were used to identify these variants. Furthermore, we expect new mutations (i.e., those occurring in Wt160, Mut2, Mut3, or Mut4 during generations 1-160) to be heterozygous at the end of the experiment and few, if any, variants expected to be shared (i.e., would require independent hits in replicate lines). Lastly, the sequencing depth (~8-20X) suggests moderate but not exceptional power to detect heterozygous mutations from the sequence of a single line on its own. Therefore, we developed a

Bayesian SNP caller that (1) aligns all reads to the genome, (2) uses read depth and quality scores at a given position to call genotypes for all five lines simultaneously. Importantly, our Bayesian model allows us to distinguish between a propogated mutation, (defined as a variant seen in all five strains in either heterozygous or homozygous state from Wt0) and a derived mutation, defined as a DNA sequence variant that arose in only a single line. First, we indexed the five diploid strains as s = 1, 2, 3, 4, 5 for Wt0, Wt160, Mut2, Mut3, Mut4 respectively. We set the prior probability of strain s being heterozygous as $\text{Prior}_s = 10^{-7}, 10^{-8}, 10^{-5}, 10^{-5}, 10^{-5}$ for s = 1, 2, 3, 4, and 5, respectively, according to mutation rates previously determined in wild-type and mismatch repair defective organisms [1, 12, 13]. At a given locus, let A and a be the major and minor allele types, respectively, based on the allele counts from all the strains. Let N_s be the total number of alleles observed for strain s; let $A_{j,s}$ be the type of the j^{th} allele copy among these N_s alleles, $j = 0, 1, \ldots N_s$. Let e_j be the probability that the j^{th} allele has been assigned the wrong allele-type. We estimated e_j from the error rates given by Dohm et al. [14] for 36 bp Solexa reads as a function of read position.

In order to call SNPs and indels in Wt0, we used the allele count data from Wt0 along with that from the other four strains. The posterior probabilities of a given genomic position being homozygous or heterozygous in Wt0 are:

$$\begin{aligned}
\mathbf{P}_1(\text{Heter.} \mid \text{Data}) &= \frac{\mathbf{P}_1(\text{Data} \mid \text{Heter.}) \times \mathbf{P}_1(\text{Heter.})}{\mathbf{P}(\text{Data})} \\
&\propto \text{Prior}_1 \times (0.5)^{\sum_{s=1}^{5} N_s} \\
\mathbf{P}_1(\text{Homo.} \mid \text{Data}) &= \frac{\mathbf{P}_1(\text{Data} \mid \text{Homo.}) \times \mathbf{P}_1(\text{Homo.})}{\mathbf{P}(\text{Data})} \\
&\propto (1 - \text{Prior}_1) \times \prod_{j=1}^{N_1} (1 - e_j)^{1(A_j = A)} \times e_j^{1(A_j = a)} \\
&\times \prod_{s=2}^{5} \left((1 - \text{Prior}_s) \prod_{j=1}^{N_s} (1 - e_j)^{1(A_j = A)} (e_j)^{1(A_j = a)} + \text{Prior}_s \times (0.5)^{N_s} \right)
\end{aligned}$$

where $P_s(.)$ denotes the probability in the context of strain s. Based on the posterior probabilities above, we classified each locus as homozygous or heterozygous for Wt0. If a locus was classified as heterozygous for Wt0, then it was assumed to have a propagated mutation in the rest of the strains. To call derived mutation in strains s = 2, 3, 4, 5, we use similar logic:

$$\mathbf{P}_s(\text{Heter.} \mid \text{Data}) = \frac{\mathbf{P}_s(\text{Data} \mid \text{Heter.}) \times \mathbf{P}_s(\text{Heter.})}{\mathbf{P}_s(\text{Data})} \propto \text{Prior}_s \times (0.5)^{N_s}$$

$$\mathbf{P}_s(\text{Homo.} \mid \text{Data}) = \frac{\mathbf{P}_s(\text{Data} \mid \text{Homo.}) \times \mathbf{P}_S(\text{Homo.})}{\mathbf{P}_s(\text{Data})} \propto (1 - \text{Prior}_s) \times \prod_{j=1}^{N_s} (1 - e_j)^{1_{(A_j = A)}} \times e_j^{1_{(A_j = a)}}$$

We use the posterior probabilities calculated above, to make a decision as to whether a site is called as heterozygous for a new mutation, heterozygous for a propagated mutation, or invariant for the four evolved strains: s = 2, 3, 4, 5. Specifically, if the posterior probability of heterozygosity was greater than 50% at a given position, then we classified the site as containing a SNP or indel. Visual inspection of the alignments for some of the inferred indel positions revealed that pair wise alignment of reads could induce false positives across multiple lines due to variations on how the alignment software interprets the alignment of different reads around a given position. These are characterized by one allele count being much smaller (but non-zero) compared to the other, across multiple strains. To bioinformatically cull such sites from our data set, we carried out an additional Likelihood Ratio Test for the allele frequencies to be equal (i.e., a propagated SNP had to have statistical support for the model of 50% frequency across Wt0, Wt160, Mut2, Mut3, and Mut4; a derived SNP had to have statistical support for 50% in one of the

evolved lines and 0% in all the others). If the hypothesis of equality was rejected for an indel, we flagged it as low-confidence (Figure 4-1).

We expected, based on previous estimates of mutation rate in MMR defective strains, to find ~125 mutations for each of the MMR deficient strains (~one mutation per line generation). This corresponds to a prior mutation rate of 10^{-5} mutations per site per generation. However, we detected 12, 24, 40 mutations for each of the MMR deficient strains, which yield mutation rates of 1×10^{-6}, 2×10^{-6} and 3×10^{-6} in each line, respectively. Although our estimated prior values differ somewhat from the real data, the alignment analysis allowed us to calculate very accurate posterior subjective probabilities. This accuracy is due to the large number of observations and has in practice made the influence of the prior negligible. Thus given the high coverage for the Mut lines, the difference in our prior estimates does not influence our analysis. Even with low coverage data where accurate estimates of prior are critical, a higher prior value would yield a larger number of false positives. The majority of mutations (and all low confidence mutations) were verified by Sanger sequencing, suggesting that false positives were rare, but we may have false negatives (i.e., missed variants) due to the medium coverage (~8-20X) of the lines.

Simulation study: To estimate the False Positive (FP) and False Negative (FN) rates (as well as to check our bioinformatics and SNP/indel calling pipelines), we set up a simulation to test the accuracy of our Bayesian approach. We started with a complete genome of a yeast S288c strain (http://genome.ucsc.edu/cgi-bin/hgGateway; June 2008 assembly from the SGD (http://www.yeastgenome.org/) and introduced SNPs and indels to simulate five strains: Wt0, Wt160, Mut2, Mut3 and Mut4. To simulate Wt0, we duplicated the S288c genome to create a diploid. We then randomly selected n_μ and n_d positions for SNPs and indels respectively. ($n_\mu = 2$, $n_d = 8$; the values of n_μ and n_d were chosen to mimic changes between S288c and the Wt0

Figure 4-1. Flow chart describing bioinformatic methods used to identify heterozygous mutations from Illumina GA whole-genome sequencing.

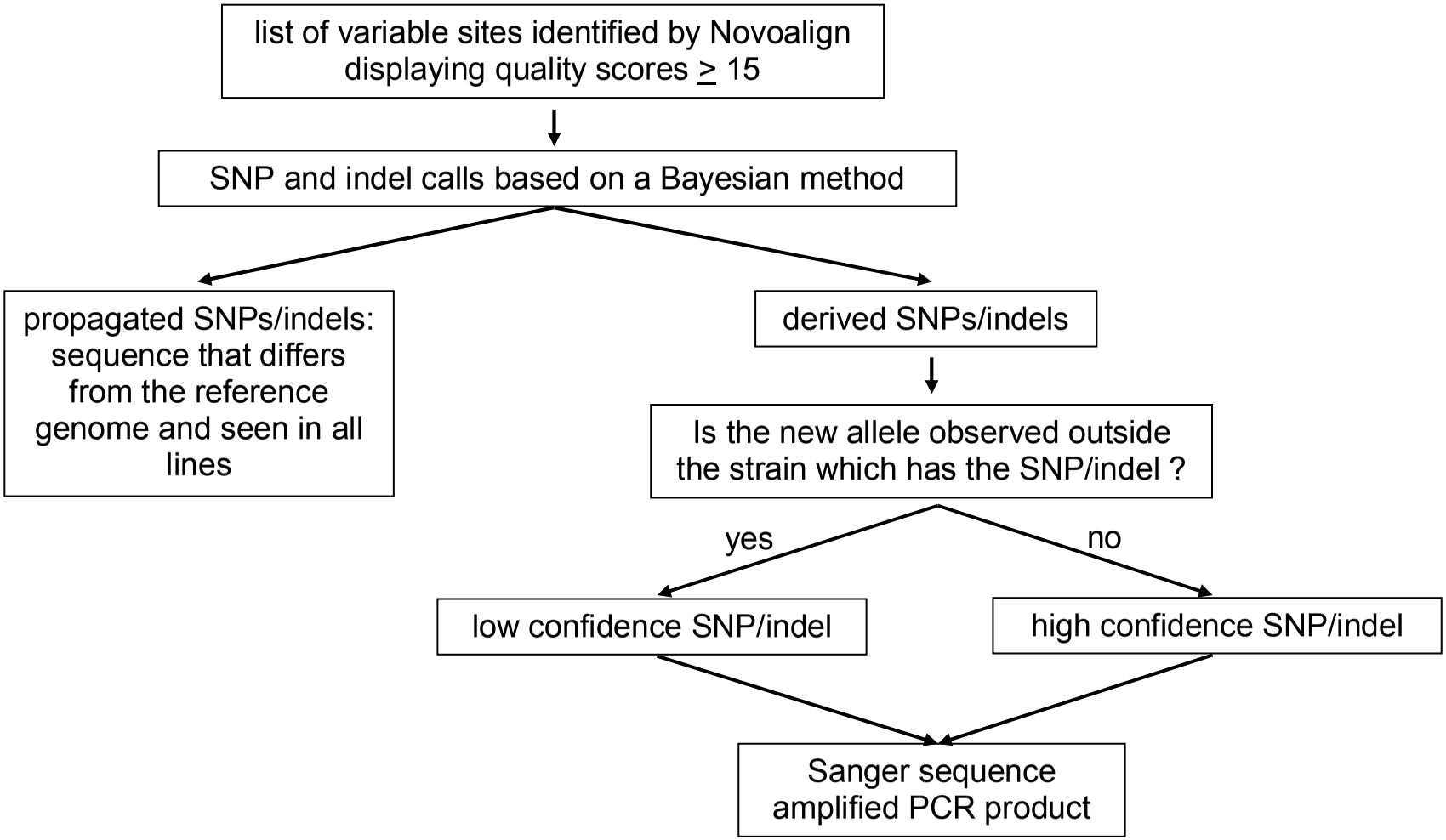
list of variable sites identified by Novoalign displaying quality scores ≥ 15
SNP and indel calls based on a Bayesian method
propagated SNPs/indels: sequence that differs from the reference genome and seen in all lines
derived SNPs/indels
Is the new allele observed outside the strain which has the SNP/indel ?
yes
no
low confidence SNP/indel
high confidence SNP/indel
Sanger sequence amplified PCR product

strainused in the bottleneck experiment). One of the two copies of S288c was randomly selected to incur each SNP or indel. For an indel mutation, the nt in that copy was deleted, or a new randomly chosen allele was inserted after it. For a SNP position, the nt was randomly changed to another nt. The resulting two copies of the genome were defined as the Wt0 diploid. The other four strains were all simulated directly from Wt0 by introducing SNPs and indels in the two copies of Wt0. The mechanism of adding SNPs and indels was exactly as described above. The values of n_μ and n_d for each of the simulations are given below. These values mimic the number of mutations that were expected in the bottleneck experiments. One distinction between the simulations and the real data is that the SNPs and indels in the simulations were not introduced into HP tracts. As described below, we believe that our ability to detect indels in HP tracts is lower because indels in HP tracts can be identified only if the entire tract and sequence flanking both sides are present in a 36 nt read.

	0 →Wt0	Wt0 →Wt160	Wt0→Mut2	Wt0→Mut3	Wt0 →Mut4
n_μ	2	1	25	25	25
n_d	1	1	100	100	100

Next, we simulated 32 nt Illumina GA reads from each of the five strains by randomly choosing read-start positions and copying 32 nt of strain s starting from that position. For each strain, the number of reads simulated matches the coverage achieved in the real sequencing experiment. We also simulated a quality score for each position of each read, following the error rate distribution given in Dohm et al. [14]. The reads were aligned with S288c using Novoalign (www.novocraft.com). Based on the alignment, we listed the allele-counts and associated quality scores in each of the variable, potentially heterozygous, positions. We used this list as the input

to a computer-program created based on our method of heterozygosity detection, which went through all the steps described in the last section. The rates of false positives and negatives (based on the output of the program) are given in Table 4-1. We believe that these rates are similar to those seen in the bottleneck experiment.

Verifying mutations identified using Bayesian method: Our method for heterozygous mutation calling from the whole-genome sequencing data yielded both low and high confidence predictions (see above). All low confidence predictions (ten in total) were verified and either validated (n = 4) or disproved (n = 6) using Sanger sequencing. Briefly, to assay heterozygous mutations predicted from the whole-genome sequence data, genomic DNA was prepared from wild-type generation zero, and mutation accumulation lines Mut2, Mut3, and Mut4 using standard techniques. Approximately 400 bases-pairs of DNA flanking the predicted mutated site was amplified in all lines using PCR and Sanger sequenced at the Cornell CLC using an Applied Biosystems Automated 3730 DNA Analyzer. The sequencing traces were all analyzed visually. A heterozygous base change mutation was confirmed if a doublet representing both alleles was observed only in the sequencing trace of the predicted Mut line, but all other lines showed only a singlet representing the parental allele. A heterozygous indel mutation was confirmed if the sequencing reaction failed (i.e. tall singlet peaks fall to small doublet peaks or random noise) at the predicted location only in the predicted Mut line, but the sequencing reactions in all other lines were able to successfully sequence past the site.

For the high confidence predictions, 31 (out of 65) were sequenced and verified using the methods described above. Of those 31 mutations, ten were further verified by genotyping the haploid progeny of the diploid containing the heterozygous mutation via Sanger sequencing. Both alleles comprising the heterozygote were observed in the haploid progeny with the exception of the frameshift mutation in the

essential *MDN1* gene. Six additional high confidence predictions were also verified by genotyping the haploid progeny of the heterozygous diploid.

We also found and verified by Sanger sequencing of the diploid lines (see above) four heterozygous mutations that were detected in earlier, less accurate prediction protocols that were not found using the final more stringent prediction method.

Yeast indel and SNP window analysis: One intriguing result of our experiment was that all indels occurred in homopolymer (HP) runs of at least five bases (e.g., AAAAA or TTTTT). To assess whether clustering of homopolymer runs (which we termed "HP tracts") conferred an additional increase for mutability, we analyzed the distribution of HP tracts in the yeast genome. This was accomplished by testing whether regions containing an indel tended to have additional HP tracts as compared to regions that did not contain an indel. All analyses were conditioned on comparing regions with at least one homopolymer run, since all indels occurred in HP tracts of at least 5 nt in size. Since we were also interested in the scale at which this phenomenon might occur, we varied window size in the analysis.

Specifically, we quantified the distribution of the number of 5-20 bp HP tracts in 50-2000 bp windows, each containing a 5-20 bp HP tract with an indel (Population 1). We then quantified the distribution of the number of 5-20 bp HP tracts in 50-2000 bp windows that each contained a non-mutated 5-20 bp HP tract (Population 2). We then performed a Mann-Whitney U test to compare these two populations, with the null hypothesis that the distribution of the number of nearby HP tracts is the same for indel-containing vs. non-mutated HP tracts. We repeated the same analysis for base substitutions (instead of indels), and performed the same test as described above. For both sets of analyses, HP tracts were considered within the window if any part of the tract fell within the window. Statistical significance was assessed using the two-sided

Mann-Whitney U tests. A Goodness-of-Fit test was also performed (see Table 4-4) to compare the distribution of "additional HP tracts" for windows with (n = 47) and without indels (monomorphic), and windows with (n = 28) and without SNPs (monomorphic). The G-statistic and associated p-value with degrees of freedom (df) used to bin the data are presented.

Analysis of hotspot function in yeast: To test whether regions with multiple homopolymer runs have higher mutation rates than those with a single HP run, we constructed plasmids with varying predicted mutation rates based on our bioinformatics results. pEAA533 is a *TRP1 ARS CEN* vector bearing a *URA3* fusion construct. In this construct the *GAL1* promoter drives expression of a chimeric protein consisting of 28 amino acids of Gal1, 93 amino acids of His4, and amino acids 6-267 of Ura3 [15]. *ura3* mutants containing pEAA533 display Ura^+ and Ura^- phenotypes when grown in minimal yeast media containing galactose + sucrose and glucose, respectively [15, 16].

Derivatives of pEAA533 were constructed in which 55 bp duplexes containing an A10 run (creating a +1 frameshift mutation; DNA sequences shown in Figure 4-4A) were inserted immediately after the *GAL1* ORF. pEAA534 also contained A8 and A7 runs within the 55 bp insertion. A stop codon was introduced out of frame immediately after the A8 and A7 runs so that -1 frameshifts in these runs would not result in reversion to Ura^+. The hotspot insertion in pEAA534 was modeled after the HP tract pattern observed in Figure 4-3. Three control duplexes (1-3) were inserted into pEAA533 to create pEAA535-537, respectively. Control Insertion 1 does not contain the nearby A8 and A7 runs but encodes the same amino acids as the hotspot insertion. Control Insertion 2 contains the same AT content present in the nearby A8 and A7 runs of the hotspot insertion, and Control Insertion 3 is matched for the amino acid sequence of Control Insertion 2. Derivatives of pEAA533-537, pEAA538-

pEAA542, respectively, were constructed in which the methionine codon at position 91 (relative to the *gal1-his4-URA3* reporter in pEAA533) was changed to alanine. These mutations were constructed by overlap PCR [17].

pEAA533-pEAA542 were transformed into FY23 (*MATa*, *ura3-52*, *leu2*Δ*1*, *trp1*Δ*63*) using previously described methods [18, 19]. For the transcription induction experiments (Figure 4-4B), transformants were replica plated on minimal yeast media containing 2% galactose + 2% sucrose or 2% glucose. Cells were grown for 2 days at 30^{o}C and then photographed. For the Ura^{+} reversion experiments, FY23 containing pEAA539 or pEAA540 were streaked to single colonies on selective (Trp dropout) minimal glucose media. Single colonies were used to set up ten independent minimal media cultures grown in tryptophan dropout minimal sucrose media. 1 ml of each overnight culture was plated to tryptophan and uracil dropout media containing 2% sucrose + 2% galactose and dilutions of the same culture were plated to tryptophan dropout media containing 2% sucrose + 2% galactose. The median rate of Ura^{+} reversion was determined using the method of Lea and Coulson [20].

RESULTS AND DISCUSSION

Identification of mutations in diploid bottleneck lines using maximum likelihood and Bayesian methods: One wild-type and three *mlh1-7^{ts}* lines (Mut2, Mut3, and Mut4) allowed to accumulate mutations for 160 generations were sequenced using the Illumina Genome Analyzer technology (Materials and Methods; http://www.illumina.com). The wild-type progenitor of all the strains was also sequenced. The analysis was performed with three independent *mlh1-7^{ts}* lines to control for chance associations within an individual line and for mutations that could alter the mutation rate of a given line. The Mut2, Mut3, and Mut4 lines at generation

160 displayed 15.6, 7.1, and 2.5 % spore viability, respectively [11]. As shown below and in Tables 4-2 and 4-3, our data analysis indicated that the mutation spectra and rates in the three *mlh1-7*^{ts} lines were indistinguishable. In total, 25 million, out of 35 million sequenced, 36 nt sequence reads were uniquely mapped to the yeast genome, allowing up to two mismatches per read (Materials and Methods). The wild-type and Mut2 generation 160 strains were sequenced to 9X and 8X average genome coverage depth, respectively. Mut3 (160) and Mut4 (160) were sequenced to average depths of 18X and 22X, respectively. We then developed and employed an "experiment aware" probabilistic framework using maximum likelihood and Bayesian methods that utilized sequence coverage of the entire data set (~70-fold; Figure 4-1; Materials and Methods; [14]). Briefly, the approach classifies each site in the yeast genome with uniquely mapping reads into one of three categories: (1) invariant across all strains, (2) heterozygous in the wild-type (and all derived strains) which we term "propagated" SNPs or indels, or (3) heterozygous in one of the mutant strains which we term "derived" SNPs or indels. As described below, this method allowed us to pool experimental data across sequencing runs for all strains and detect with high reliability heterozygous single-nucleotide polymorphisms (SNPs; 28 identified) and single nt indels (48 identified) from the 36 nt read data set. This method was evaluated on simulated data sets and found to have a very low false positive rate (~6 x 10^{-5}) and a false negative rate of 0.08 within the unique mapping regions of the genome that contained at least seven-fold coverage (Table 4-1). The low false positive rate was verified by PCR amplifying genomic fragments covering a specific mutation site and then confirming the presence of a heterozygous mutation by Sanger sequencing the fragment (Materials and Methods). Based on simulations, we estimated that the method, as applied to regions with at least seven-fold sequencing coverage, allowed us to detect heterozygous mutations in 60%, 41%, 69%, and 84 %

Table 4-1. False positive and negative rates based on the simulation analysis.

Mutation Type	False-positive rate	False-negative rate
Base Substitution	6×10^{-5}	0.030
Indel	0	0.089
Propagated	0	0
Derived	6×10^{-5}	0.091
Total	6×10^{-5}	0.078

of the total genome for the generation 160 wild-type, Mut2, Mut3, and Mut4 lines, respectively.

We did not detect any mutations in the wild-type generation 160 line, which was predicted based on the previously calculated mutation rate of 3.3×10^{-10} mutations per base per generation (< 1 expected; [21]). As shown in Tables 4-2 and 4-3, only heterozygous mutations, comprised of 28 base substitution and 48 single nt indel mutations, were detected in the three MMR-defective lines. All of the mutations were unique between lines except for a single nt deletion mutation between Saccharomyces Genome Database (SGD; http://www.yeastgenome.org) coordinates 92,271-92,279 on chromosome 2, which occurred independently in both Mut2 and Mut3 (Table 4-2). All 48 indels, comprised of 46 deletions and 2 insertions, occurred in HP tracts (47 poly A or T tracts, 1 poly G or C tract) between 5-13 base pairs long (Table 4-2). Due to the constraints of using 36 nt Illumina GA reads, we do not have the power to detect mutations in HP tracts larger than 13 nt, but less than 400 such tracts are present in the yeast genome.

Our analysis permitted the detection of up to two single nt indels in a 36 nt reads; these indels can be right next to each other to create a two nt indel or separated. We assigned this limit because creating high quality and unique alignments became very difficult when allowing indels larger than two nt. We were unable to detect indels of two nt in any of the lines. Such a result is not surprising based on previous studies of wild-type and MMR mutants analyzed for reversion of frameshift mutations in HP runs. In these studies the overwhelming majority of mutations involved single nt deletions. For example Tran et al. [22] found that 225 of 227 reversions in +1 HP tracts in wild type, polymerase proofreading, and mismatch repair mutants were due to deletions of a single nt. For -1 HP tracts, they found that 206 of 218 reversions were

Table 4-2. Genome location of mutations detected in the Mut2, 3, and 4 lines.

The type of mutation is shown, as well as the length of the HP tracts containing an indel. The specific Mut line (2, 3, or 4) is indicated under "strain." All HP tracts were polyA or polyT except for the mutation in Chromosome 3 at 212,451-212,457, which involved a polyC tract. For mutations that occurred within an open reading frame, both the systematic gene name and predicted amino acid (aa) changes (fs; frameshift) are provided. NA; not applicable. Coordinates are presented as shown in the SGD http://www.yeastgenome.org/).

Chromosome	SGD position	HP Tract Length	Strain	Gene	Mutation type	Protein Change
I	139349-139358	10	Mut4		deletion	
II	275549-275557	9	Mut2		deletion	
II	92271-92279	9	Mut2 and 3		deletion	
II	423462-423469	8	Mut3		insertion	
II	662560-662569	10	Mut4	YBR219C	deletion	fs between aa 103-106
II	653035-653045	11	Mut4		deletion	
III	212451-212457	7 (poly G/C)	Mut3	YCR048W	deletion	fs between aa 176-178
III	275289	NA	Mut4	YCR091W	G to A transition	aa 297 V to I
IV	512796	NA	Mut2		A to T transversion	
IV	814336	NA	Mut2		G to A transition	
IV	929182-929193	12	Mut3		deletion	
IV	963768	NA	Mut3	YDR252W	T to G transversion	aa 120 G to V
IV	231908-231914	7	Mut4		deletion	
IV	1386657-1386664	8	Mut4		deletion	
IV	470576-470584	9	Mut4		deletion	
IV	832716-832726	11	Mut4		deletion	
IV	50592-50603	12	Mut4		deletion	
IV	1054759	NA	Mut4		A to T transversion	
V	305972	NA	Mut2		C to A transversion	
V	479369	NA	Mut2	YER155C	T to A transversion	aa 1159 S to C
V	225319-225327	9	Mut3		deletion	
V	403576	NA	Mut3	YER122C	G to T transversion	aa 258 A to E
V	34325-34333	9	Mut4		deletion	
V	402832-402843	12	Mut4		deletion	
VI	223108-223118	11	Mut3		deletion	
VI	114200-114210	11	Mut4		deletion	
VI	88832	NA	Mut4	YFL024C	G to T transversion	aa 504 D to E
VI	225229	NA	Mut4	YFR034C	G to C transversion	aa 240 R to G
VII	194092-194098	7	Mut3	YGL163C	deletion	fs between aa 771-773
VII	878690-878701	12	Mut3		deletion	
VII	653363-653369	7	Mut4		deletion	

Table 4-2 (Continued).

Chromosome	SGD position	HP Tract Length	Strain	Gene	Mutation type	Protein Change
VII	882549-882558	10	Mut4		deletion	
VII	20017-20027	11	Mut4		deletion	
VII	678172-678182	11	Mut4		deletion	
VIII	150380-150386	7	Mut3		deletion	
VIII	472612-472624	13	Mut3		deletion	
VIII	288299	NA	Mut3	YHR092C	C to T transition	aa 172 K to K
VIII	370253	NA	Mut3	YHR132W-A	A to T transversion	aa 46 Y to F
IX	270327	NA	Mut2	YIL046W	G to T transversion	aa 560 A to S
IX	375856	NA	Mut3	YIR010W	G to A transition	aa 143 M to I
IX	199995	NA	Mut4	YIL087C	G to A transition	aa 41 T to I
X	445012-4450220	9	Mut3		deletion	
X	131051-131059	9	Mut4		deletion	
X	469684-469694	11	Mut4		deletion	
XI	162688-162695	8	Mut4		deletion	
XI	403466	NA	Mut4	YKL018C-A	C to T transition	aa 19 S to S
XII	405712-405719	8	Mut2	YLR131C	deletion	fs between aa 369-371
XII	32320-32330	11	Mut3		deletion	
XII	964065	NA	Mut3	YLR420W	G to A transition	aa 95 R to H
XII	1009007	NA	Mut3	YLR436C	T to C transition	aa 746 I to V
XII	363531-363537	7	Mut4	YLR106C	deletion	fs between aa 68-70
XII	201846-201856	11	Mut4		deletion	
XII	1047741	NA	Mut4	YLR454W	A to G transition	aa 1249 D to G
XIII	763010-763016	7	Mut2	snR86	insertion	small nucleolar RNA
XIII	241855-241867	13	Mut3		deletion	
XIII	311843	NA	Mut3		C to T transition	
XIII	139705-139709	5	Mut4	YML067C	deletion	fs between aa 138-139
XIII	816457-816463	7	Mut4	YMR275C	deletion	fs between aa 706-708
XIV	761792	NA	Mut2	YNR069C	C to T transition	aa 267 V to V
XIV	222733	NA	Mut3	YNL225C	C to T transition	aa 580 V to M
XIV	435595-435601	7	Mut4	YNL101W	deletion	fs between aa 199 to 201

Table 4-2 (Continued).

Chromosome	SGD position	HP Tract Length	Strain	Gene	Mutation type	Protein Change
XIV	481123-481129	7	Mut4		deletion	
XIV	685574-685582	9	Mut4		deletion	
XIV	575616-575626	11	Mut4		deletion	
XIV	400002	NA	Mut4	YNL121C	C to A transversion	aa 180 G to STOP
XIV	734321	NA	Mut4	YNR058W	A to G transition	aa 77 L to L
XV	854146-854153	8	Mut2		deletion	
XV	874052-874057	6	Mut3	YOR296W	deletion	fs between aa 1284 1286
XV	767667-767673	7	Mut3	YOR228C	deletion	fs between aa 36-38
XV	822829-822835	7	Mut3	YOR267C	deletion	fs between aa 678-680
XVI	146421-146427	7	Mut2	YPL216W	deletion	aa 868-870
XVI	22677	NA	Mut4		C to T transition	
XVI	131583	NA	Mut4	YPL222W	G to A transition	aa 475 A to T
XVI	509632	NA	Mut4	YPL022W	G to T transversion	aa 980 A to S
XVI	570131	NA	Mut4	YPR007C	G to A transition	aa 415 S to M

Table 4-3. Mutation rates for Mut2, Mut3 and Mut4 lines grown in bottlenecks for 160 generations.

The base substitution mutation rate was determined by first calculating the percentage of the genome in which at least seven-fold DNA sequencing coverage to unique regions was obtained. This was done because our statistical analysis did not have sufficient power to reliably detect heterozygous mutations in regions with lower coverage. This information was used to calculate the mutation rate based on the following formula: (number of mutations)/(160 generations)/(adjusted genome size), with the diploid *S. cerevisiae* genome size determined as 24,141,794 bp (http://www.yeastgenome.org/). To obtain indel mutation rates, we first determined the number of HP tracts of a given length in unique regions of the genome which had ≥ seven-fold sequence coverage. We then used the following equation to calculate mutation rate: (number of indels)/(160 generations)/(number of HP tracts with ≥ seven-fold coverage).

Base substitution mutations

Strain	# mutations	% genome ≥ 7X coverage	Genome Size (bp) adjusted	Mutation rate (per base/gen x10^{-9}
Mut2	6	41	9,898,136	3.8
Mut3	9	69	16,657,838	3.4
Mut4	13	84	20,279,107	4.0
average				**3.7**

Single nucleotide indel mutations in 5-13 nt HP tracts

Strain	# mutations	#HP tracts ≥ 7X coverage	Mutation rate (per HP tract/generation x 10^{-7})
Mut2	6	57,502	6.5
Mut3	15	99,714	9.4
Mut4	27	122,816	14
average			**10**

Single nucleotide indel mutations in 8-13 nt HP tracts

Strain	# mutations	#HP tracts ≥ 7X coverage	Mutation rate (per HP tract/generation x 10^{-7})
Mut2	4	2,820	89
Mut3	10	7,054	89
Mut4	19	8,696	140
average			**110**

due to additions of a single nt. The remaining evertants in both HP tracts involved expansions or contractions of no greater than two nt in size.

The predominance of single nt deletions over single nt insertions and base substitutions was similar to previous reports for the mutational spectra in reporter genes in MMR null mutants [13, 22-24]. The average mutation rate in the 5-13 bp HP tracts was 1.0×10^{-6} per HP tract per generation (Table 4-3). The rate was an order of magnitude greater (1.1×10^{-5}) if only runs between 8-13 base pairs long were considered (Table 4-3). These values approach the rates seen in MMR-defective yeast (*mlh1*, *msh2*) containing reporters bearing 10 bp poly T (2.8×10^{-4}; [22]) and 10 bp poly A (7.3×10^{-5}; [25]) tracts. Low sequence coverage provides one explanation for why the rate is lower than seen previously in reporter assays. In our analysis, indels in HP tracts can be identified only if the entire tract and sequence flanking both sides are present in a 36 nt read; the longer the HP tract, the less likely it is to obtain reads that cover the entire tract. Thus higher sequence coverages are required to identify indels in HP tracts. Consistent with this, a higher indel mutation rate was seen in lines that had higher sequencing coverage (Table 4-3). In contrast, SNPs that occur outside of an HP tract should not be as affected by sequence coverage (aside from the relationship between coverage and probability of detecting sufficient copies of the alternate base in order to reliably make a call). This was seen for the analysis of base substitutions (Table 4-3).

The average rate of base substitution mutations was 3.7×10^{-9} mutations per base per generation (Table 4-3), which is eleven-fold higher than the base substitution rate observed in wild-type haploid strains [21]. Of the 28 base substitution mutations detected in the Mut2-4 lines, sixteen were transitions and twelve were transversions (Table 4-2). Nineteen of these mutations resulted in a change from a G-C to an A-T base pair, whereas only four were in the opposite direction. This overall mutational

bias towards A-T base pairs was seen and discussed previously [21, 26-27]. The modest increase that we observed in the base substitution rate in MMR defective strains is significantly lower than predicted (~100 fold increase for base substitutions and frameshifts; [12, 13]. We suggest two reasons for these differences. First, our measurements were determined from a genome-wide measurement rather than by extrapolation from a few marker loci. Second, the *mlh1-7*^{ts} allele is not a complete null mutation. It phenocopies the *mlh1*Δ phenotype in the *CAN1* mutational assay, but has a four-fold lower mutation rate than *mlh1*Δ in the *lys2-A14* reversion assay ([11]; data not shown). Because *mlh1-7*^{ts} strains display residual DNA repair, it is possible that there is a bias towards the repair of specific mismatches in these strains. While we cannot rule this out, the fact that the mutation signature seen in *mlh1-7*^{ts} appeared indistinguishable from *mlh1* null strains argues against such a possibility [22-24].

Because the three lines showed viability that ranged from 2.5 to 15.6%, we expected to identify mutations that conferred a lethal phenotype. We examined whether any of the mutations that mapped to open reading frames in the Mut4 line (2.5% viability) were not detected in haploid progeny. This was done by sequencing the DNA surrounding a particular mutation in twenty viable spore clones obtained by sporulating the Mut4 generation 160 line. Of these fourteen mutations, only the frameshift mutation in *MDN1* was not detected, consistent with previous work showing that *mdn1*Δ mutants are inviable [28]. While it is unclear how many mutations would confer lethality in the absence of other mutations, the assortment of five independent lethal mutations would result in 3% spore viability, similar to that seen in the Mut4 line. We hypothesize that other lethal mutations were not identified in Mut4 and other lines because: 1. A large number of frameshift mutations in HP tracts may not have been detected because indels can be identified only if the entire tract and sequence flanking both sides are present in a 36 nt read. Identifying indels in

HP tracts is very challenging using short read sequencing. However, increasing sequence coverage and using paired-end reads of a larger size (~180 bp) should provide a good test of this idea. 2. Our sequence analysis did not cover the entire genome (84% for Mut4). 3. While previous CGH and PFGE analyses (~ 1 KB resolution; [11]) did not reveal rearrangements, it is possible that mutations occurred that involved indels larger than two nt and smaller than 1 KB. However, we find this to be less likely because a previous analysis of mutation spectra in MMR mutants indicate that indels greater than two nt are extremely rare [17].

Identification of a hotspot pattern for mutagenesis in the *S. cerevisiae* genome: Visual inspection of the DNA sequences surrounding the indel mutations (~400 bp; Figure 4-2) suggested that they were enriched for HP runs. These are primarily poly(dA:dT) tracts that are present in the yeast genome at a 20-fold higher frequency than poly(dG:dC) tracts. Consistent with this, the AT content of the genomic regions surrounding the indel mutations was significantly higher than for unmutated HP regions (windows up to 500 bp; data not shown). We found that mutations in the intergenic regions tend to be associated with highly expressed genes, consistent with the idea that transcription confers a mutagenic effect on the surrounding regions [7]. However, this correlation was marginally significant and would require a larger data set to be confirmed (data not shown).

We performed an increasing window size analysis comparing the sequence context of our mutated HP tracts to all similar-sized HP tracts (5 to 13 nt in length) in which a mutation was not detected (Materials and Methods). Genomic regions surrounding the mutated HP tracts contained significantly more HP tracts than regions surrounding unmutated HP tracts, but no apparent asymmetry or bias towards the same tract was seen for these tracts with respect to the indel position. This difference was marginally significant (p values of 0.054 to 0.084 for 50 to 500 bp windows) when the

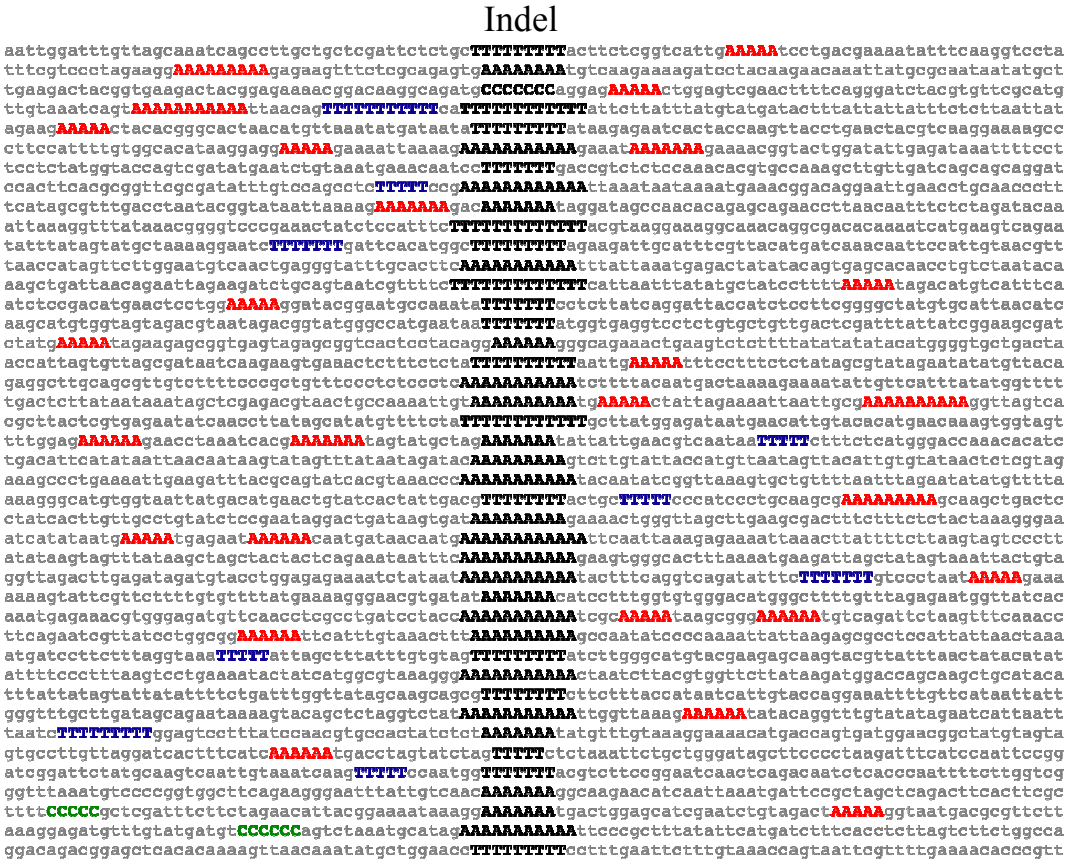

Figure 4-2. 100 bp region surrounding indel mutations in the Mut3 and Mut4 lines.

The locations of the indel mutations are indicated in black bold font. HP runs of ≥ 5 in this window are color coded as shown.

minimum size required to designate a tract was increased to 7 nt. If the 50 bp surrounding the mutated HP tract is excluded, the genomic context of the mutated HP tracts still contains significantly more HP tracts (5 to 20 nt in length) than unmutated HP tracts for window sizes of 200 and 500 bp ($p=0.034$ and 0.00078, respectively). This shows that the significance is not driven solely by sequences immediately flanking an HP site; a larger genomic context, ~500 bp, is also playing a role. Significantly more HP tracts (5 to 20 nt in length) were also observed surrounding mutated as compared to unmutated HP tracts for the same window sizes (50, 100, 200 and 500 bp) when the Mut3 and Mut4 lines were analyzed individually; this could not be done for Mut2 because of low levels of sequence coverage and mutation detection (data not shown).

No significant association was found with any of the mutant lines (together or separately) when a similar window analysis was performed to examine a correlation between HP tracts and SNPs (Figure 4-3). This observation is of interest because Tian et al. [29] examined the distribution of base substitutions near indels in six different genomes and found an increased base substitution rate in regions close to indels. Their work suggests that indels are mutagenic to surrounding areas or that mutational processes that cause indels result in an increased nearby base substitution rate. We did not see a correlation between increased base substitution rate and HP runs (Figure 4-3). However, because our data sets are limited we were unable to ask the question of whether indels in HP tracts were associated with increased nearby base substitutions. Such questions will likely be answered in follow up studies that include larger data sets.

To assess the robustness of our results with regards to assumptions of the Mann-Whitney U test, we used a G-test (goodness-of-fit) to compare the distribution of additional HP tracts for windows with an indel to the expected frequency

Figure 4-3. Window analyses for indel (A) and base substitution mutations (B) in the Mut2, 3 and 4 lines.

The number of 5-20 nt HP tracts was counted under different window sizes (W; 50-2000 bp). This was determined for windows centered on indel mutations in HP tracts (A, red bars) or on base substitution mutations (B, red bars). The mutated sites were excluded from the counting analysis. The genomic context of the mutated sites was compared to an HP tract length-matched set of unmutated tracts (A, blue bars) or to a set of unmutated sequence (B, blue bars). The X-axis displays the number of HP tracts contained within each window. The Y-axis, left, shows the frequency at which each HP tract was observed. The Y-axis, right, shows the total counts/events for which each HP tract was observed in the Mut2-4 lines (Population 1). This was compared to the distribution in the genome of the number of 5-20 bp HP tracts in 50-2000 bp windows that each contained a non-mutated 5-20 bp HP tract (Population 2). Mann-Whitney U p-values (Materials and Methods) are shown for each window indicating the statistical significance for a distribution containing a mutation (red bars) versus one that lacks a mutation (blue bars).

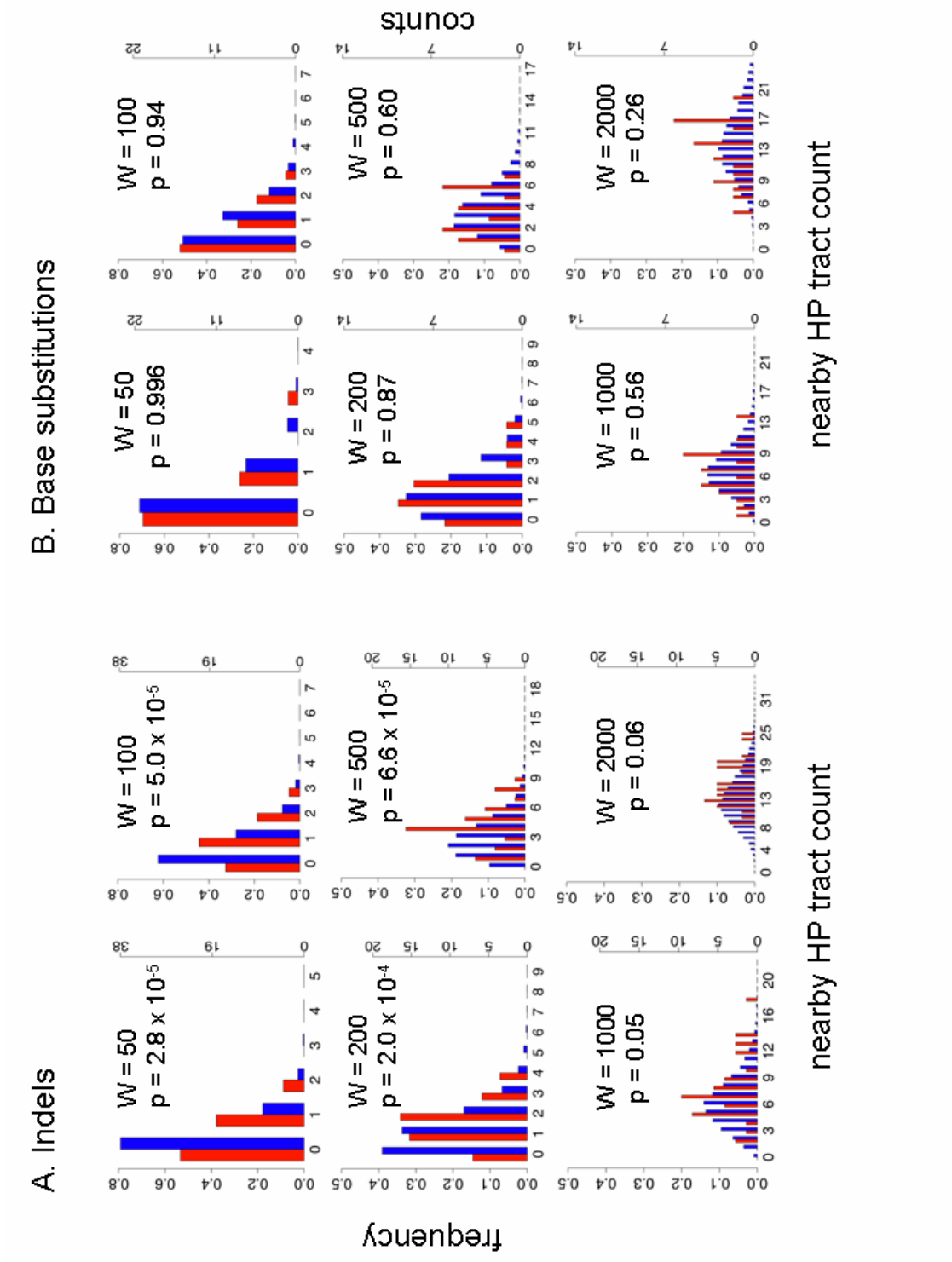
A. Indels
B. Base substitutions
frequency
counts
W = 50
p = 2.8 x 10-5
W = 100
p = 5.0 x 10-5
W = 200
p = 2.0 x 10-4
W = 500
p = 6.6 x 10-5
W = 1000
p = 0.05
W = 2000
p = 0.06
W = 50
p = 0.996
W = 100
p = 0.94
W = 200
p = 0.87
W = 500
p = 0.60
W = 1000
p = 0.56
W = 2000
p = 0.26
nearby HP tract count
nearby HP tract count

distribution given by windows of the same size without an indel. Similarly, we used the G-test to compare the distribution of additional HP tracts for windows with a SNP to the expected frequency distribution for windows without one (Table 4-4). Essentially, these analyses compared the distribution of the "red bars" in Figure 4-3 to the frequency distribution of the "blue bars" for six different window sizes (w = 50, 100, 200, 500, 1000, 2000). Similar to the two-sided Mann-Whitney U analysis shown in Figure 4-3, for window sizes of 50 to 500 bp, the goodness-of-fit test strongly rejected ($p < 5 \times 10\text{-}4$) the model of homogeneity among the distribution of indel vs. non-indel containing windows in terms of number of additional HP tracts. Specifically, there was a shift towards a higher mean number of HP tracts for windows with an indel. This was not observed for the window size of 2000 ($p = 0.376$). Also, the distributions of HP tracts for SNP and non-SNP windows were similar, with no window size having a p-value less than 0.444.

A hotspot motif can induce transcription in yeast: Individual HP tracts have long been known to be sensitive to indel mutations, which are most likely caused by DNA slippage during DNA replication [13, 22, 25, 30, 31]. Why would clusters of HP sites be especially prone to mutation? One possibility is that clusters of HP tracts form a secondary structure such as bent or flexible DNA that would predispose DNA polymerase to slippage [32-33]. If such structures exist, they are likely to be unstable, because we were unable to detect in acrylamide gels a change in the expected mobility of ~400 bp DNA fragments containing the DNA sequence in which indels were detected (data not shown). A second possibility is that DNA polymerase stalling at HP tracts facilitates polymerase switching, perhaps to a DNA polymerase thatreplicates adjoining HP tract with lower fidelity [34]. Work by Kim et al. [35] support such an idea. They found that frameshift mutations in HP tracts under high-

Table 4-4. Goodness of fit test for indel and SNP mutations in HP tracts from the yeast Mut2-4 lines.

A Goodness-of-Fit test was performed that compares the distribution of "additional HP tracts" for windows with (n=47) and without indels (monomorphic), and windows with (n = 28) and without SNPs (monomorphic). The G-statistic and associated p-value with degrees of freedom (df) used to bin the data are presented. Because cell counts are often below five, we pooled the bins to ensure enough observations per cell.

Window length (bp)	Type of allele	mean additional HP tracts	p-value
Window with an indel vs. windows without one			
50	indel	0.57	
	monomorphic	0.24	1.02×10^{-4} (G=18, df=2)
100	indel	0.98	
	monomorphic	0.50	2.09×10^{-5} (G=22, df=2)
200	indel	1.66	
	monomorphic	1.03	2.46×10^{-4} (G=22, df=4)
500	indel	4.09	
	monomorphic	2.81	5.13×10^{-4} (G=24, df=6)
1000	indel	7.45	
	monomorphic	5.99	0.042 (G=13, df=6)
2000	indel	14.53	
	monomorphic	12.73	0.376 (G=8.6, df=9)
Window with a SNP vs. windows without one			
50	SNP	0.39	
	monomorphic	0.35	0.964 (G=0.002, df=1)

Table 4-4 (Continued)

Window length (bp)	Type of allele	mean additional HP tracts	p-value
Window with a SNP vs. windows without one			
100	SNP	0.74	
	monomorphic	0.71	0.599 (G=1.0, df=2)
200	SNP	1.48	
	monomorphic	1.40	0.444 (G=2.7, df=3)
500	SNP	3.39	
	monomorphic	3.54	.745 (G=1.2, df=3)
1000	SNP	6.75	
	monomorphic	7.00	0.651 (G=1.6, df=3)
2000	SNP	12.72	
	monomorphic	13.63	0.562 (G=2.0, df=3)

transcription conditions were partially dependent on the function of polymerase zeta, an error-prone translesion DNA polymerase. A third possibility is that a cluster of HP tracts confers an increased mutation rate through increased transcription.

To test possible roles for the hotspot pattern identified in Figure 4-3 in mutagenesis, we constructed a *URA3* DNA slippage reporter bearing an insertion of a predicted hotspot in the open reading frame (Figure 4-4; Materials and Methods). In this reporter the *GAL1* promoter drives expression of a chimeric protein consisting of 28 amino acids of Gal1, 93 amino acids of His4 and amino acids 6-267 of Ura3 [15]. The hotspot sequence was inserted immediately after the *GAL1* ORF. It contains an A10 run that creates a +1 frameshift mutation and nearby A8 and A7 runs. Control insertions that lack the nearby A8 and A7 runs and either maintain or change AT content were also analyzed.

As shown in Figure 4-4B, *ura3* strains containing the *URA3* reporter without the hotspot insertion displayed a Ura^+ phenotype when grown in minimal media containing galactose + sucrose but a Ura^- phenotype when grown in media containing glucose. In contrast, *ura3* strains bearing the *URA3* reporter with the control insertions displayed an Ura^- phenotype in both carbon source conditions. However, Ura^+ revertants appeared in these strains on galactose + sucrose media that were likely to arise as the result of DNA slippages that restore the reading frame [22]. The *URA3* reporter bearing the hotspot insertion conferred an Ura^+ phenotype in *ura3* strains grown in either carbon source condition (Figure 4-4). This observation is consistent with previous work showing that poly(dA:dT) and poly(dG:dC) tracts present in either orientation increase the accessibility to transcription factors and are considered ubiquitious promoter elements [36, 37]. Additional studies have shown that poly(dA:dT) tracts are stiff, resist bending, and exclude nucleosomes [38].

Figure 4-4. **Multiple HP tracts act as a constitutive promoter.**

A) Map of the *URA3* slippage plasmid pEAA533. In this *TRP1 ARS CEN* plasmid the *GAL1* promoter drives expression of a chimeric protein consisting of 28 amino acids of GAL1, 93 amino acids of HIS4 and amino acids 6-267 of URA3. pEAA534 is a derivative of pEAA533 containing a 55 bp hotspot that is modeled based on the bioinformatic analysis shown in Figure 3. It is inserted immediately after the *GAL1* ORF. This hotspot contains a +1 frameshift mutation in the A_{10} run that disrupts the open reading frame as well as nearby A_8 and A_7 runs. Control insertion plasmids (pEAA535-537) contain the A_{10} run but lack the nearby A_8 and A_7 runs (Materials and Methods). B) FY23 (*ura3*) derivatives bearing pEAA533 to 537 were plated onto tryptophan and uracil dropout plates containing the indicated carbon sources.

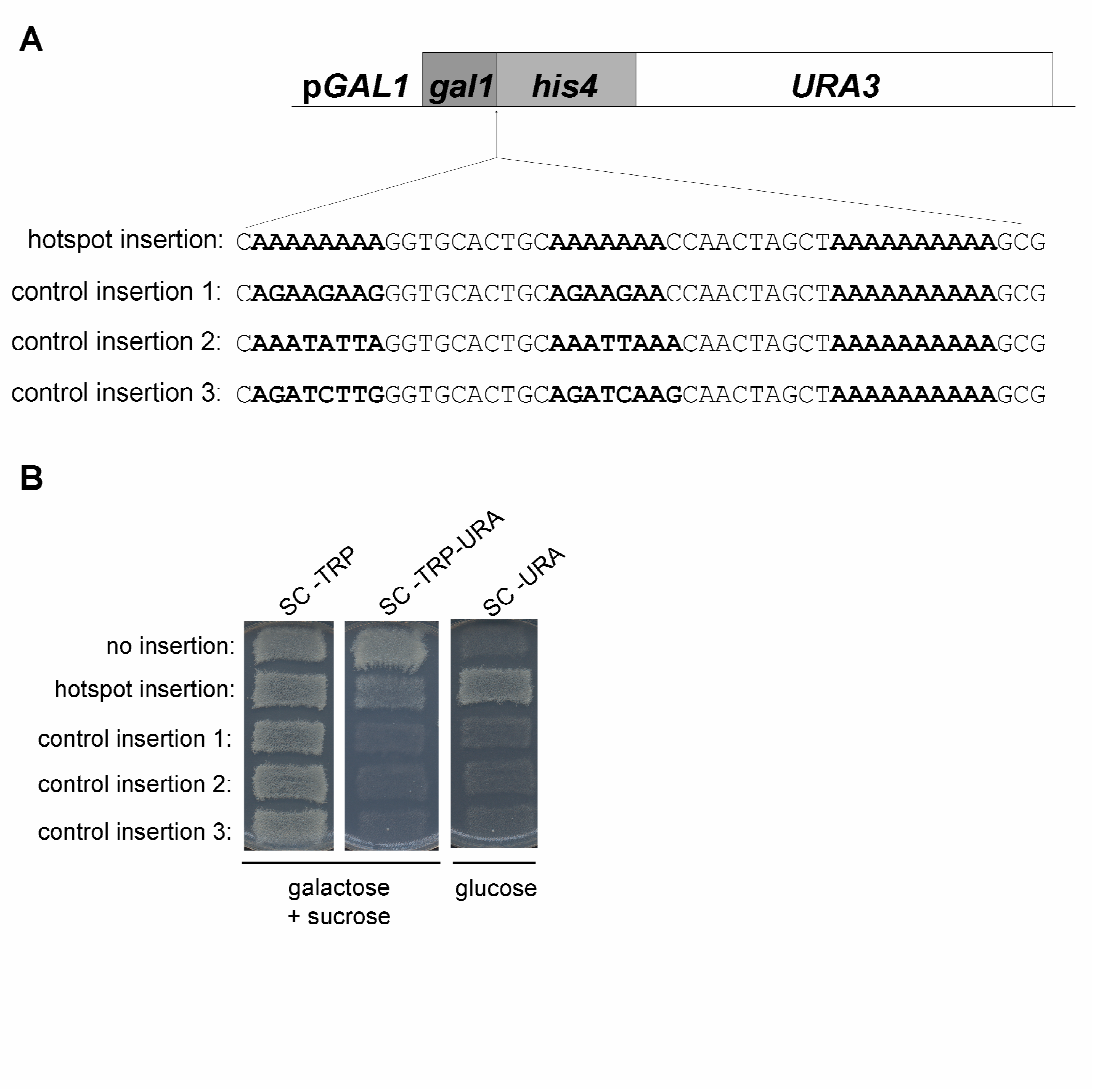
A
pGAL1
gal1
his4
URA3
hotspot insertion: CAAAAAAAAGGTGCACTGCAAAAAAACCAACTAGCTAAAAAAAAAAGCG
control insertion 1: CAGAAGAAGGGTGCACTGCAGAAGAACCAACTAGCTAAAAAAAAAAGCG
control insertion 2: CAAATATTAGGTGCACTGCAAATTAAACAACTAGCTAAAAAAAAAAGCG
control insertion 3: CAGATCTTGGGTGCACTGCAGATCAAGCAACTAGCTAAAAAAAAAAGCG
B
SC -TRP
SC -TRP-URA
SC -URA
no insertion:
hotspot insertion:
control insertion 1:
control insertion 2:
control insertion 3:
galactose
+ sucrose
glucose

The above data suggest that the hotspot sequence can act as a constitutive promoter element. Such an observation is of interest because previous studies have shown that high levels of transcription confer a modest (four to nine-fold) mutagenic effect on surrounding regions that include HP runs and simple repetitive DNA sequences [7, 35, 39]. This observation is also consistent with our finding that mutations mapping to intergenic regions associated with highly expressed genes. The mechanisms by which increased transcription increase mutation rate are not completely known, though genetic studies have shown that mutations in nucleotide excision repair and translesion polymerase factors affect this process [35, 40].

To test whether the hotspot created in the *URA3* reporter construct caused an increase in DNA slippage, we mutated the methionine codon at position 91 in the *gal1-his4-URA3* reporter and the equivalent positions in the four insertion constructs (Figure 4-4) to alanine codons. This was done because we hypothesized that methionine 91 served as the initiation codon for translation of the *URA3* reporter in the hotspot insertion construct in conditions where galactose was not included. This ATG codon is located 42 bp downstream of a TATA sequence and is in frame with the *URA3* coding region. The next ATG codon is 29 bp downstream from the methionine 91 codon and is out of frame with the *URA3* coding region. The *pGAL1-gal1-his4-URA3* reporter containing this mutation complemented *ura3* strains in the presence of galactose, indicating that the alanine substitution did not affect function of the reporter. The hotspot insertion construct did not complement *ura3* strains grown in glucose, indicating that mutating this codon prevented *URA3* translation initiation downstream of the hotspot insertion site. The modified hotspot and control insertion 1 constructs were introduced into *ura3* strains to measure the rate of reversion to Ura^+. The reversion rate (Ura^+ per cell per generation) for the hotspot insertion construct was 1.7 (1.0-2.4, 95% confidence interval) x 10^{-7}; the rate for control 1 was 2.1 (1.1-

2.9, 95% confidence interval) x 10^{-7}. These data indicate that the hotspot insertion did not increase the DNA slippage rate in mismatch repair proficient cells. Two possibilities are: 1. The level of transcription seen in the hotspot construct is modest relative to the high levels that appear to be required to affect the DNA slippage rate of a reporter but might be significant for instability in a while genome context [39]. In support of this idea, Iyer and Struhl [43] showed that the effect of a poly(dA:dT) tract on stimulating transcription in the absence of *GCN4* function is quite modest. 2. Alternatively, a larger genome context involving HP tracts that is missing from our plasmid reporters may be required to observe genomic stability. 3. Lastly, because the *mlh1-7*^{ts} allele is not a complete null at the non-permissive temperature, it is formally possible that the pattern that we observed is specific to the mutant allele.

Closing thoughts: In the *S. cerevisiae* S288c haploid genome there are over 77,425 HP tracts five nt or greater. More importantly, there are over five thousand 200 bp windows containing three HP tracts that we predict are hotspots (Figures 4-2, 4-3) for frameshift mutations. Frameshift mutations in coding regions that disrupt protein function are likely to have significant effects on organism fitness. In wild-type yeast, insertion/deletion mutations appear to be relatively rare compared to base substitutions; comparative analyses of multiple domestic and wild yeast strains identified ~14,000 indels compared to ~235,000 SNPs [41, 42]. In contrast, MMR mutants display a strong bias towards frameshifts over base substitutions in the genome. Thus our data, together with previous work, illustrate the critical role that MMR plays in preventing frameshifts in HP tracts across the genome.

ACKNOWLEDGMENTS

We thank Amit Indap and the Cornell CLC, especially Peter Schweitzer, James VanEe, and Tom Stelick, for preparing samples for Illumina GA sequencing and bioinformatic analyses, and Julie Heck, and K. T. Nishant for technical advice and providing unpublished data, and the Alani, Bustamante and Aquadro laboratories and Nadia Singh and Dan Barbash for comments on the manuscript. We also thank Zhenglong Gu, Brandon Barker and Ryan Hernandez for helpful discussions and for providing analyses not presented in this text. E. A., S. Z., and A. D. were supported by NIH GM53085. S. Z. was also supported by a Cornell Presidential Fellowship and an NIH training grant in Genetics and Development. A. D. was also supported by an NIH training grant in Biochemistry, Molecular and Cell Biology. X. M. and C. D. B were supported by NSF 0606461 and NSF 0701382. A. R. was supported by NIH grant RO1 HG003229.

REFERENCES

1. Nishant KT, Singh ND, Alani E (2009) Genomic mutation rates: what high-throughput methods can tell us. Bioessays 31: 912-20.

2. Hawk JD, Stefanovic L, Boyer JC, Petes TD, Farber RA (2005) Variation in efficiency of DNA mismatch repair at different sites in the yeast genome. Proc Natl Acad Sci U S A 102: 8639-43.

3. Wolfe KH, Sharp PM, Li WH (1989) Mutation rates differ among regions of the mammalian genome. Nature 337: 283-5.

4. Matassi G, Sharp PM, Gautier C (1999) Chromosomal location effects on gene sequence evolution in mammals. Curr Biol 9: 786-91.

5. Arndt PF, Hwa T, Petrov DA (2005) Substantial regional variation in substitution rates in the human genome: importance of GC content, gene density, and telomere-specific effects. J Mol Evol 60: 748-63.

6. Hardison RC, Roskin KM, Yang S, Diekhans M, Kent WJ, et al. (2003) Covariation in frequencies of substitution, deletion, transposition, and recombination during eutherian evolution. Genome Res 13: 13-26.

7. Datta A, Jinks-Robertson S (1995) Association of increased spontaneous mutation rates with high levels of transcription in yeast. Science 268: 1616-9.

8. Teytelman L, Eisen MB, Rine J (2008) Silent but not static: accelerated base-pair substitution in silenced chromatin of budding yeasts. PLoS Genet 4: e1000247.

9. Washietl S, Machne R, Goldman N (2008) Evolutionary footprints of nucleosome positions in yeast. Trends Genet 24: 583-7.

10. Stamatoyannopoulos JA, Adzhubei I, Thurman RE, Kryukov GV, Mirkin SM, et al. (2009) Human mutation rate associated with DNA replication timing. Nat Genet 41: 393-5.

11. Heck JA, Gresham D, Botstein D, Alani E (2006) Accumulation of recessive lethal mutations in Saccharomyces cerevisiae mlh1 mismatch repair mutants is not associated with gross chromosomal rearrangements. Genetics 174: 519-23.

12. Iyer RR, Pluciennik A, Burdett V, Modrich PL (2006) DNA mismatch repair: functions and mechanisms. Chem Rev 106: 302-23.

13. Denver DR, Feinberg S, Estes S, Thomas WK, Lynch M (2005) Mutation rates, spectra and hotspots in mismatch repair-deficient Caenorhabditis elegans. Genetics 170: 107-13.

14. Dohm JC, Lottaz C, Borodina T, Himmelbauer H (2008) Substantial biases in ultra-short read data sets from high-throughput DNA sequencing. Nucleic Acids Res 36: e105.

15. Alani E, Kleckner N (1987) A new type of fusion analysis applicable to many organisms: protein fusions to the URA3 gene of yeast. Genetics 117: 5-12.

16. Rose MD, Winston F, Hieter P (1990) Methods in yeast genetics. Cold Spring Harbor Laboratory Press, Cold Spring Harbor, N.Y.

17. Ho SN, Hunt HD, Horton RM, Pullen JK, Pease LR (1989) Site-directed mutagenesis by overlap extension using the polymerase chain reaction. Gene 77: 51-9.

18. Gietz RD, Schiestl RH (2007) Quick and easy yeast transformation using the LiAc/SS carrier DNA/PEG method. Nat Protoc 2: 35-7.

19. Winston F, Dollard C, Ricupero-Hovasse SL (1995) Construction of a set of convenient Saccharomyces cerevisiae strains that are isogenic to S288C. Yeast 11: 53-5.

20. Lea DE, Coulson CA (1949) The distribution of the numbers of mutants in bacterial populations. J. Genet. 49: 264-285.

21. Lynch M, Sung W, Morris K, Coffey N, Landry CR, et al. (2008) A genome-wide view of the spectrum of spontaneous mutations in yeast. Proc Natl Acad Sci U S A 105: 9272-7.

22. Tran HT, Keen JD, Kricker M, Resnick MA, Gordenin DA (1997) Hypermutability of homonucleotide runs in mismatch repair and DNA polymerase proofreading yeast mutants. Mol Cell Biol 17: 2859-65.

23. Tran PT, Simon JA, Liskay RM (2001) Interactions of Exo1p with components of MutLalpha in Saccharomyces cerevisiae. Proc Natl Acad Sci U S A 98: 9760-5.

24. Marsischky GT, Filosi N, Kane MF, Kolodner R (1996) Redundancy of Saccharomyces cerevisiae MSH3 and MSH6 in MSH2-dependent mismatch repair. Genes Dev 10: 407-20.

25. Gragg H, Harfe BD, Jinks-Robertson S (2002) Base composition of mononucleotide runs affects DNA polymerase slippage and removal of frameshift intermediates by mismatch repair in Saccharomyces cerevisiae. Mol Cell Biol 22: 8756-62.

26. Keightley PD, Trivedi U, Thomson M, Oliver F, Kumar S, et al. (2009) Analysis of the genome sequences of three Drosophila melanogaster spontaneous mutation accumulation lines. Genome Res 19: 1195-201.

27. Denver DR, Dolan PC, Wilhelm LJ, Sung W, Lucas-Lledo JI, et al. (2009) A genome-wide view of Caenorhabditis elegans base-substitution mutation processes. Proc Natl Acad Sci U S A 106: 16310-4.

28. Giaever G, Chu AM, Ni L, Connelly C, Riles L, et al. (2002) Functional profiling of the Saccharomyces cerevisiae genome. Nature 418: 387-91.

29. Tian D, Wang Q, Zhang P, Araki H, Yang S, et al. (2008) Single-nucleotide mutation rate increases close to insertions/deletions in eukaryotes. Nature 455: 105-8.

30. Streisinger G, Okada Y, Emrich J, Newton J, Tsugita A, et al. (1966) Frameshift mutations and the genetic code. This paper is dedicated to Professor Theodosius Dobzhansky on the occasion of his 66th birthday. Cold Spring Harb Symp Quant Biol 31: 77-84.

31. Sia EA, Kokoska RJ, Dominska M, Greenwell P, Petes TD (1997) Microsatellite instability in yeast: dependence on repeat unit size and DNA mismatch repair genes. Mol Cell Biol 17: 2851-8.

32. Hile SE, Eckert KA (2008) DNA polymerase kappa produces interrupted mutations and displays polar pausing within mononucleotide microsatellite sequences. Nucleic Acids Res 36: 688-96.

33. Snyder M, Buchman AR, Davis RW (1986) Bent DNA at a yeast autonomously replicating sequence. Nature 324: 87-9.

34. Lovett ST (2007) Polymerase switching in DNA replication. Mol Cell 27: 523-6.

35. Kim N, Abdulovic AL, Gealy R, Lippert MJ, Jinks-Robertson S (2007) Transcription-associated mutagenesis in yeast is directly proportional to the level of gene expression and influenced by the direction of DNA replication. DNA Repair (Amst) 6: 1285-96.

36. Struhl K (1985) Naturally occurring poly(dA-dT) sequences are upstream promoter elements for constitutive transcription in yeast. Proc Natl Acad Sci U S A 82: 8419-23.

37. Iyer V, Struhl K (1995) Poly(dA:dT), a ubiquitous promoter element that stimulates transcription via its intrinsic DNA structure. Embo J 14: 2570-9.

38. Segal E, Widom J (2009) Poly(dA:dT) tracts: major determinants of nucleosome organization. Curr Opin Struct Biol 19: 65-71.

39. Wierdl M, Greene CN, Datta A, Jinks-Robertson S, Petes TD (1996) Destabilization of simple repetitive DNA sequences by transcription in yeast. Genetics 143: 713-21.

40. Kim N, Jinks-Robertson S (2010) Abasic sites in the transcribed strand of yeast DNA are removed by transcription-coupled nucleotide excision repair. Mol Cell Biol. Apr 26, Epub ahead of print.

41. Wei W, McCusker JH, Hyman RW, Jones T, Ning Y, et al. (2007) Genome sequencing and comparative analysis of Saccharomyces cerevisiae strain YJM789. Proc Natl Acad Sci U S A 104: 12825-30.

42. Liti G, Carter DM, Moses AM, Warringer J, Parts L, et al. (2009) Population genomics of domestic and wild yeasts. Nature 458: 337-41.